

2021

Verification of Gynaecological Brachytherapy Treatments Using an End-to-End Phantom

Yashiv Dookie
University of Wollongong

Follow this and additional works at: <https://ro.uow.edu.au/theses1>

University of Wollongong

Copyright Warning

You may print or download ONE copy of this document for the purpose of your own research or study. The University does not authorise you to copy, communicate or otherwise make available electronically to any other person any copyright material contained on this site.

You are reminded of the following: This work is copyright. Apart from any use permitted under the Copyright Act 1968, no part of this work may be reproduced by any process, nor may any other exclusive right be exercised, without the permission of the author. Copyright owners are entitled to take legal action against persons who infringe their copyright. A reproduction of material that is protected by copyright may be a copyright infringement. A court may impose penalties and award damages in relation to offences and infringements relating to copyright material.

Higher penalties may apply, and higher damages may be awarded, for offences and infringements involving the conversion of material into digital or electronic form.

Unless otherwise indicated, the views expressed in this thesis are those of the author and do not necessarily represent the views of the University of Wollongong.

Recommended Citation

Dookie, Yashiv, Verification of Gynaecological Brachytherapy Treatments Using an End-to-End Phantom, Master of Research - Medical Radiation Physics thesis, School of Physics, University of Wollongong, 2021. <https://ro.uow.edu.au/theses1/1353>

Research Online is the open access institutional repository for the University of Wollongong. For further information contact the UOW Library: research-pubs@uow.edu.au

Verification of Gynaecological Brachytherapy Treatments Using an End-to-End Phantom

A research report submitted in fulfilment of the requirements for the award of the degree

Master of Research - Medical Radiation Physics

from

University of Wollongong

by

Yashiv Dookie

School of Physics

2021

Certificate

I certify that this thesis has not previously been submitted for any degree and is not being submitted as part of candidature for any degree.

I also certify that the thesis has been written by me and any help that I have received in preparing this thesis, and all sources used, have been acknowledged in this thesis.

Signature of candidate:

.....

Yashiv Dookie

Acknowledgements

I would like to thank the multitude of people who have supported and me throughout my Masters. First foremost, I would like to thank my friends and family for supporting me throughout my studies. Thank you to my father, brother and partner for proof reading my thesis and constantly keeping me sane. A special thank you to Nicholas Ambrosi for his constant support and “never say die” attitude. I am appreciative of Dean Cutajar for his help and support, for without him none of this would be possible. I would also like to thank Joel Poder for his infectious enthusiasm for research and contributions to the applicator displacement study. I am grateful to St George Cancer Care Centre for their consistent efforts to facilitate these experiments. Thank you to Simon Downes and the physics team at Prince of Wales Hospital for providing advice and assistance. Finally, thank you to Owen Brace, Marco Petasecca, Anatoly Rosenfeld and the CMRP team for delivering the MP987 when we needed it most.

Contents

Acknowledgements	ii
List of Figures	xi
1 Introduction	1
2 Literature Review	4
2.1 Treating Gynaecological Cancer	4
2.1.1 External Beam Radiotherapy	6
2.1.2 Brachytherapy	7
2.2 Treatment Planning	9
2.2.1 AAPM Task Group 43	13
2.3 Gynaecological Brachytherapy Applicators	17
2.4 Dosimeters	19
2.5 Uncertainty and Error Within HDR Brachytherapy	22
2.5.1 Failure Mode and Effect Analysis	24
2.6 The Impact of Catheter and Applicator Displacement	25
2.7 Quality Assurance	29
2.7.1 AAPM Task Group 56	29
2.7.2 The Gamma Index	31
2.7.3 Developments in QA	31

2.8	The Magic Plate	36
2.8.1	Localisation Algorithm	39
2.9	End-to-end Verification of HDR Gynaecological Brachytherapy	42
3	Materials	47
3.1	Iridium-192	47
3.2	Afterloader	49
3.3	Gynaecological Applicators	49
4	Determining The Impact of Applicator Displacement for HDR Gynaecological Brachytherapy	52
4.1	Introduction	52
4.2	Method	54
4.3	Results	61
4.3.1	Intracavity Treatments	64
4.3.2	Interstitial Treatments	71
4.3.3	Outliers	75
4.4	Conclusion	76
5	Characterisation of the MP987 for High Dose-rate Source Tracking	78
5.1	The MP987	78
5.1.1	The Data Acquisition System	79
5.2	Frame Processing	80
5.3	Source Tracking Methodology	83
5.4	Temporal Resolution	88
5.4.1	Method	88

5.4.2	Results	90
5.4.3	Discussion	95
5.5	Source Localisation	97
5.5.1	Method	97
5.5.2	Results	98
5.5.3	Discussion	100
5.6	Source Tracking at Different Depths	101
5.6.1	Method	101
5.6.2	Results	102
5.6.3	Discussion	103
5.7	Preliminary Source Tracking	104
5.7.1	Method	104
5.7.2	Results	106
5.7.3	Discussion	108
5.8	Conclusion	110
6	Validation of the End-to-end Verification Phantom	113
6.1	Validation of the End-to-end Phantom for a Vaginal Brachytherapy Treatment	114
6.1.1	Method	114
6.1.2	Results	117
6.1.3	Discussion	119
6.2	Validation of the End-to-end Phantom for a Cervical Brachytherapy Treatment . . .	122
6.2.1	Method	122
6.2.2	Results	126
6.2.3	Discussion	127
6.3	Conclusion	129

7 Conclusion	131
7.1 Future Work	134
Bibliography	148

List of Figures

2.1	Definition of target volumes due to cancer cell density [1]	10
2.2	Traverse slice view used for treatment planning, displaying the lunar ovoids of the Venezia applicator, the red HR-CTV and isodose lines.	11
2.3	HR-CTV and OAR reconstruction for gynaecological brachytherapy, with the bladder yellow, HR-CTV red, sigmoid colon magenta and rectum green	12
2.4	Polar co-ordinate system geometry for dose calculation used in TG-43 formalism [2] .	13
2.6	Inverse square reduction in dose, normalised to 6 cm. [3]	14
2.5	The radial dose function normalised to 6 cm.[3]	14
2.7	Anisotropy function at different depths.[3]	15
2.8	Multichannel applicator loading configurations [4]	18
2.9	Farmer ionisation chamber	20
2.10	Semiconductor doping	21
2.11	MOSFET	22
2.12	The workflow of gynaecological brachytherapy for cervical cancer and potential applicator displacement	26
2.13	Elekta Source Position Check Ruler	30
3.1	Decay scheme of Ir-192 [5]	48
3.2	A dummy source from the Flexitron afterloader	48
3.3	Elekta Flexitron HDR brachytherapy afterloader at St George Cancer Care Centre . .	49

3.4	30 mm Multichannel vaginal applicator (Elekta Brachytherapy, Venendaal, Netherlands). [6]	50
3.5	Fletcher applicator tandem and ovoid set (Elekta Brachytherapy, Venendaal, Netherlands) [6]	50
3.6	Venezia applicator, with added perineal template (Elekta Brachytherapy, Venendaal, Netherlands) [6]	51
4.1	A treatment structure set DICOM visualised in RadCalc, a secondary check program (Lifeline Software, Austin, USA). The contour of each slice is displayed, with the rectum on the left in dark yellow, the HR-CTV a purple structure in the middle and the bright yellow structure to the right a bladder. The channels of a Fletcher applicator is seen with the tandem in bold blue within the HR-CTV and the ovoid channels in red and yellow.	55
4.2	Definition of the axes used in relation to the anatomy	56
4.3	The Python displacement script created to simulate applicator displacement demonstrates its function to change dwell positions, shifting a maximum of ± 7 mm along each axis.	58
4.4	The two treatment types used within the study demonstrated with the HR-CTV being treated in red	60
4.5	Fletcher applicator treatment plan rotated 20°	61
4.6	Isodose volume position in relation to the bladder, rectum and HR-CTV. The isodose volume is blue, HR-CTV red, bladder yellow and rectum a dark yellow.	61
4.7	Prescribed D_{2cc} for the Organs At Risk	63
4.8	Prescribed D_{90} for the High Risk Clinical Treatment Volume	63
4.9	A relative change in dose to the bladder has been calculated for each displaced treatment plan. The red dashed line represents a critical change in dose.	65

4.10	A relative change in dose to the rectum has been calculated for each displaced treatment plan. The red dashed line represents a critical increase in dose.	66
4.11	A relative change in HR-CTV coverage has been calculated for each displaced treatment plan. The red dashed line represents a critical reduction in dose.	69
4.12	A rotation of the applicator about the axis of the tandem and the relative change in dose. A 10% change in dose is denoted by the red dashed line.	70
4.13	A relative change in dose to the bladder has been calculated for each displaced treatment plan. The red dashed line represents a critical change in dose.	72
4.14	A relative change in dose to the rectum has been calculated for each displaced treatment plan. The red dashed line represents a critical change in dose.	73
4.15	A relative change in dose to the HR-CTV has been calculated for each displaced treatment plan. The red dashed line represents a critical change in dose.	74
5.1	The Magic Plate 987 system	79
5.2	Measurements taken at a perpendicular distance of 5.5 cm between the source and magic plate through Solid Water. The frame demonstrates processing which occurs prior to source tracking.	82
5.3	Single frame utilised for source tracking algorithm.	84
5.4	A treatment plan with 5 mm step size and 5 second dwell time.	85
5.5	Measured output of a 5 mm step size, 5 second dwell time treatment plan	86
5.6	A treatment plan with 5 mm step size and 5 second dwell time	87
5.7	The measured histogram used for of 5 mm step size, 5 second dwell time plan	87
5.8	Treatment plan for temporal resolution test	89
5.9	Temporal resolution test without frame averaging.	91
5.10	Temporal resolution test averaging 10 frames.	91
5.11	Catheters processed without frame averaging	92

5.12	Catheters processed averaging 10 frames	93
5.13	Residuals when using single frames.	94
5.14	Residuals for each dwell time when averaging 10 frames.	95
5.15	Set up for source tracking at different depths	97
5.16	A measure of variance in dwell position for different distances between source and MP	98
5.17	A change in mean error with dwell time along the Y axis	99
5.18	A change in mean error with dwell time along the X and Z axes	99
5.19	Measured Z position at different depths	102
5.20	Spatial linearity at different depths	102
5.21	MVC setup for preliminary source tracking	105
5.22	Applicator orientation	106
5.23	Source tracking along the Y axis	106
5.24	Difference in dwell times from treatment plan	107
5.25	Difference in step size	107
5.26	Source tracking along the Z axis	108
6.1	Prepared applicator for end-to-end test.	115
6.2	MVC end-to-end phantom	115
6.3	PTV drawn for vaginal wall treatment and reconstructed channels shown in the TPS co-ordinate system.	116
6.4	Measurement of vaginal treatment plan. Undetected dwell position highlighted by the red arrow.	117
6.5	A view of the measurement and treatment plan in the Z direction.	118
6.6	Residuals for catheter swap error	118
6.7	Residuals for incorrect indexer lengths	119
6.8	Ovoid and tandem channels.	122

6.9	Fletcher applicator constructed and attached to ring-clamp with thermoplastic.	123
6.10	The End-to-end phantom, with fletcher applicator positioned in the water tank. The red arrow demonstrates a ball bearing, which is used for co-registration.	124
6.11	Cervical point-based treatment plan	125
6.12	Measurement of cervical treatment plan in XY plane	126
6.13	Measurement of cervical treatment plan in ZX plane	126
1	Radiotherapy consent form submitted NRA ethics application for retrospective treatment planning study with anonymised patient data.	149

Abbreviations

OAR: Organs at risk

DSB: Double strand break

GTV: Gross target volume

CTV: Clinical target volume

PTV: Planning target volume

HR-CTV: High risk clinical treatment volume

SDD: Source-to-detector distance

MP: Magic Plate

QA: Quality assurance

HU: Hounsfield Unit

PLA: Polylactic acid

ABS: Acrylonitrile butadiene styrene

MOSFET: Metal oxide field effect transistor

TLD: Thermoluminescent dosimeter

DTA: Distance to agreement

DD: Dose difference

MBDCA: Model-based dose calculation algorithm

LBTE: Linear Boltzmann transport equation

DICOM: Digital imaging and communications in medicine

MVC: Multichannel vaginal applicator

IGABT: Image Guided Adaptive Brachytherapy

EMBRACE: Image guided intensity modulated External beam radiochemotherapy and MRI based adaptive BRACHytherapy in locally advanced CErvical cancer

Abstract

High dose rate brachytherapy allows the delivery of radiation internally, with high-dose gradients creating a conformal distribution. The inherent drawback of this treatment exists within small uncertainties producing a large impact on safety and efficacy. Applicator displacement was retrospectively simulated for 29 cervical cancer treatments to determine a critical shift in applicator position. A 2 mm shift in the anterior and posterior directions was detrimental to the bladder and rectum, respectively and a 4 mm shift in all directions caused a critical reduction in HR-CTV coverage. These findings indicate the importance of quality assurance practices that mitigate applicator displacement. Furthermore, the source localisation accuracy required for cervical brachytherapy was quantified. HDR gynaecological brachytherapy relies on 3D imaging, contouring, precise reconstruction of applicator position and transfer of data to the afterloading device. To evaluate this process an end-to-end phantom was developed, which consists of a component that houses gynaecological applicators and the Magic Plate 987 (MP987), created by the Centre of Medical and Radiation Physics, University of Wollongong. The $21 \times 22.5 \text{ cm}^2$ silicon diode array facilitates source tracking at clinically relevant depths. A characterisation of the MP987 for HDR source tracking has been performed, producing an error in dwell time and position of 0.1s and 0.25 mm respectively, for dwell times greater than 5 s. Source tracking accuracy is a function of both dwell time and distance from detector to source.

The End-to-end phantom has verified both vaginal and cervical treatments. For a vaginal treatment, the mean residual in dwell position is within (0.24 ± 0.01) mm for all directions, with the difference in dwell time being (0.10 ± 0.01) s. Catheter swap, indexer length and activity miscalibra-

tion errors were all detected within the vaginal therapy end-to-end test. Validation of the End-to-end phantom for a cervical brachytherapy treatment produced a mean difference of (3.49 ± 0.57) mm, (4.74 ± 0.77) mm, (6.14 ± 1) mm in the X, Y and Z directions respectively, with a dwell time difference of (0.19 ± 0.03) s. The localisation accuracy achieved is below the critical displacement value established within the treatment planning study. Improvement in co-registration and Z localisation methodologies will provide better outcomes for cervical cases. The End-to-end phantom successfully verifies the procedure for HDR gynaecological brachytherapy treatments, enabling safe and effective patient care.

Chapter 1

Introduction

Gynaecological cancer refers to cancer of the female reproductive system and is the 3rd most prevalent cancer affecting females in Australia.[7] Treatment for gynaecological cancers generally requires a combination of chemotherapy and radiotherapy, and/or surgery if possible. Early-stage lesions in the lower genitalia can be removed surgically, however, analysis on a cellular level might still suggest a high probability of local recurrence. The combination of surgery, external beam radiotherapy, chemotherapy and brachytherapy utilised is defined by the stage, grade and type of disease. Brachytherapy is a type of radiotherapy used to treat a range of cancers. The radiation is delivered to the clinical target volume from within, via the implantation of radioactive sources. Administering dose internally allows for a short-range dose, facilitating the conformity required. Dose conforming to the treatment volume is extremely important as it minimises irradiating organs at risk (OAR). [8] Gynaecological brachytherapy is performed with the use of applicators, which assist in transporting the brachytherapy source to the right locations. Applicator selection depends on the specific type of gynaecological cancer being treated.[8] Careful treatment planning and quality assurance are integral to a positive patient outcome since brachytherapy administers a large dose gradient. Clinical errors such as a shift in applicator position, uncertainties in applicator reconstruction or an activity miscalibration can cause incongruencies between the treatment plan and delivered radiation distribution.[9] Dose applied outside the planned treatment volume will result in tissue damage.

The shortcomings in gynaecological brachytherapy's lay within the detriment small errors or uncertainties have on the treatment due to large dose gradients. The impact a shift in dose distribution can have on treatment quality is evaluated in a retrospective treatment planning study. Within this study, the dose distribution is shifted, and its impact is calculated. This provides insight into the change in dose to organs at risk and quantifies a clinically relevant objective for source tracking accuracy.

Quality assurance needs to be performed for new and existing aspects of a treatment workflow to ensure patient safety and treatment efficacy. To accomplish this an end-to-end test is proposed to test a complete clinical workflow and compare the intended treatment to what is delivered. Clinical errors, applicator construction and use and data transfer protocols are all tested to determine if the intended treatment is delivered. This is especially important when introducing new equipment, software or protocols.

We propose the construction of a phantom to provide end-to-end testing of gynaecological brachytherapy treatments. Establishing a means of examining imaging, planning and treatment delivery. The End-to-end phantom consists of a component that can house gynaecological applicators for treatment planning and imaging as well as a novel silicon diode array used for HDR source tracking. The Magic Plate 987 is a novel diode array with 987 silicon diodes and a 21 cm by 22.5 cm field of view. A characterisation for HDR source tracking will be completed within this thesis. A. Espinoza et al, produced a source tracking system with the Magic Plate-121, providing submillimeter localisation and dwell times within 1 ms. The plan verification "Magic Phantom" accomplished source tracking with catheters at a distance of 6 mm. [10] The MP987's large field of view will allow source tracking at greater distances enabling the evaluation of different treatment configurations. The following thesis develops a methodology to facilitate tracking within the End-to-end phantom, providing source location and timing information. Performing a full treatment on the proposed phantom will allow a comparison between the treatment planning system's intended and implemented treatment.

This thesis will serve as a validation of the End-to-end phantom. The Centre of Medical and

Radiation Physics at the University of Wollongong has developed the MP987, which will be characterised for HDR source tracking. Practical components were carried out at St. George Cancer Care Centre and Prince of Wales Hospital, Nelune Cancer Care Centre.

Project Goals:

- Provide a clinical benchmark for the End-to-end source tracking phantom by establishing a deviation from the planned dwell position which causes a critical deterioration in treatment efficacy and safety
- Inform on the clinical importance of protocols that mitigate the risk of a physical displacement in applicator position and reconstruction uncertainty
- Develop an HDR source tracking methodology for its use in the End-to-end phantom. Determining dwell times and positions.
- Outline optimal processing parameters and define source localisation and temporal accuracy
- Construct End-to-end phantom for vaginal and cervical brachytherapy
- Image and develop treatment plan on the End-to-end phantom for vaginal and cervical brachytherapy
- Deliver full clinical plans for the applicators within the End-to-end phantom. Compare dwell times and positions with a treatment plan to determine discrepancies.
- Determine if the End-to-end phantom can detect the following clinical errors: catheter swap, indexer length error and an activity miscalibration

Chapter 2

Literature Review

2.1 Treating Gynaecological Cancer

Gynaecological cancer is an umbrella term which encompasses many cancers of the female reproductive system and is the 3rd most prevalent cancer affecting females, as per the Australian Institute of Health and Welfare in 2018. [7] A combination of treatments are required for gynaecological cancer depending on the type and extent. These treatments can include a combination of surgery, chemotherapy and radiation therapies. The stage of cancer is classified via the FIGO (International Federation of Gynecology and Obstetrics) system or the AJCC (American Joint Committee on Cancer) “TNM” staging system, both are extremely similar. Both systems classify the stage depending on 3 factors, (TNM):

- Tumour size(T)- The size of main/primary tumour
- Lymph nodes (N)- Extent of cancer development into nearby lymphatics
- Metastasis (M)- The spread of the primary tumour to distant tissues.[11]

Surgery entails the removal of tumours and effected tissue, and is dictated by the stage of the disease. In the case of cervical cancer, removal of the uterus and cervix is known as a hysterectomy

and is sometimes prescribed. In the case of a radical hysterectomy the removal of the ovaries, fallopian tubes, uterus, cervix, soft tissues around the cervix and top of the vagina may be required.[12]

Chemotherapy is a drug based treatment which damages cells that replicate at a rapid pace. It can be applied before or after surgery, which is known as neoadjuvant or adjuvant therapy respectively. A chemotherapy plan is prescribed in cycles to allow healthy cells effected by the drugs to recover. The medicine can be administered orally, via intravenous or injected into the tissue. Chemotherapy is effective in destroying cancer cells since they divide quickly. However, this causes certain normal cells such as nail, mouth, digestive tract, bone marrow and hair follicle tissues to also sustain damage. The cytotoxic effect on normal cells is largely responsible for the associated side effects.[13] A review of radiosensitisers in cervical cancer has determined that cytotoxic agents which are widely used clinically are also generally radiosensitisers. The chemotherapy drug while cytotoxic also prevents the DNA repair of a cell, allowing a sub-fatal amount of radiation to cause cell apoptosis, making adjuvant radiation treatment more effective.[14]

Radiation therapy functions by causing lethal damage to cancer cells in a manner which conserves normal tissue. The main mechanism by which ionising radiation causes cellular damage is via double-strand breaks (DSB), where both strands of DNA have been broken within proximity of each other to inhibit repair.[15] DSBs can occur via direct or indirect methods. Direct breaks are the result of ionisation electron tracks breaking each strand, while indirect breaks occur due to radiation-producing free radicals such as a hydroxyl group which damages DNA.[16] T.J McMillan et al demonstrated the importance of DSBs when determining if there is a use for the quantification of DSBs in radiotherapy. It is clear that DSBs are pivotal, however, other damage types aid in triggering cell death pathways.

For patients where surgery is of high risk such as the morbidly obese or elderly, primary radiotherapy can be a good alternative. In a review, Elzbieta van der Steen-Banasik found brachytherapy for endometrical cancer to be a well tolerated treatment approach with outcomes comparable to surgery.[17] Alternatively, Sedlis et al demonstrated the benefit of postoperative radiotherapy in early-stage cervical cancer treatments with a study of 277 cervical cancer patients who had under-

gone surgery. 137 of whom have been treated with pelvic radiotherapy and 140 received no further treatment. This concluded a statistically significant 47% reduction in risk of recurrence but did induce a 6% increase in toxicity and one death following adverse GI effects. The use of postoperative radiotherapy is beneficial in most stages across multiple gynaecological cancers.[18] A combination of external beam therapy and brachytherapy is utilised with or without surgery to constitute a complete radiotherapy regime.

2.1.1 External Beam Radiotherapy

External beam radiotherapy (EBRT) consists of a carefully constructed conformal beam of photons incident on a specific region to administer a tumoricidal radiation dose with the aim of destroying cancer cells while sparing normal tissue. The consequences of normal tissue damage consist of both the long term risk of secondary cancers and organ damage.[19] A case of this was demonstrated by Devarati Mitra et al, where 212 endometrial cancer patients received a combination of EBRT and intracavitary brachytherapy of which 17% experienced rectal bleeding.[20] Fortunately the treatment's subsequent organ damage is present only within a subset of patients due to the heavy optimisation of EBRT. A unanimous goal sought within radiotherapy is the isolation of dose to cancer cells. This has motivated the development of highly conformal methods of treatment such as intensity-modulated beam therapy, which is the result of multi-leaf collimator adjusting the specific shape of the beam and thus a tailored resulting dose profile.[21] This combined with the use of multiple beams enables three-dimensional tumour conformity. The treatments are performed based on a treatment planning system(TPS), where computed tomography (CT) and/or magnetic resonance imaging (MRI) data is input into the planning system to carefully construct a treatment volume. The final target volume considers various characteristics such as organs at risk (OAR) and organ motion based on the individuals anatomy. Quality assurance is then conducted on the treatment plan using dosimetry methods before the treatment is carried out.[22] An example of the importance of treatment planning considerations is given by John Ng et al, Columbia University Medical Center, where the treatment

plans for 15 patients with early-stage breast cancer were retrospectively assessed by an institutional review board. Finding that treatment in a prone position produces substantially lower risk of secondary lung cancer when compared to the supine position.[23] The need for meticulously thought out and accurate treatment planning is paramount to positive patient outcomes.

The treatment planning system optimises conformity of each treatment, an example of which is the use of an multi-leaf collimator, a collimator which has multiple motorised segments, attenuating and contouring the beam into different profiles. Planning with such complexity via the use of a treatment planning system enables a designed dose tailored to the target volume. This has been demonstrated by Vivian et al, using a micro multi-leaf collimator and BrainSCAN v3.5 stereotactic treatment planning system. Leaf transmission, penumbra and multiple fixed field dose distributions are measured. Beam data was acquired using a water tank and diamond detector with the planned dose distributions verified using LiF, TLDs and film. Vivian et al concluded that the micro-multi leaf/treatment plan system set-up is stable and accurate enough for small field applications. [24]

External beam therapy is generally standard practice for gynaecological cancers, with brachytherapy implemented to provide a local dose boost. 45 Gy in 25 fractions over 5 weeks of EBRT is recommended by the EMBRACE collaborative group and a brachytherapy course is prescribed according to dose volume constraints.[25]

2.1.2 Brachytherapy

Brachytherapy is a type of radiotherapy used to provide a local dose to a range of cancers. The radiation is delivered to the clinical target volume from within, via the implantation of radioactive sources. The source position within the patient, strength and amount of time at this position defines the applied dose distribution. A large dose gradient localised around the source allows the treatment to have more of a conformal approach. Specific protocols which govern the use of brachytherapy were developed relatively early, with the Stockholm and Paris methods for intracavitary treatments prescribed in 1914 and 1919 respectively. Historically Ra-226 was used followed by the implementation

of other radionuclides such as Co-60, Cs-137 and Au-198 before Henschke first used Ir-192. Developments in the 1950s and 1960s provided the application of afterloading devices, initially to minimise exposure to medical professionals[26]. The function of these afterloaders has since evolved to mechanically drive sources into implanted applicators or catheters. Enabling a computerised execution of source dwell position and time, creating the required dose distribution.

Brachytherapy is used on its own or in conjunction with other treatments. The treatment can achieve high levels of local precision given the introduction of 3D aspects to treatment planning; utilising MRI and/or CT. Such precision is important to ensure coverage of the target volume as well as conservation of healthy tissue. Brachytherapy is useful for gynaecological cancers to provide a radiation boost as there are many organs at risk in this pelvic region. The current standard of care to treat locally advanced cervical cancer has progressed from solely external beam therapy to external beam therapy, brachytherapy and chemotherapy combined. Brachytherapy provides an extra dose to the gross tumour while the chemotherapy also serves as a radio-sensitiser and kills fast-growing cells. [8]

Low dose rate treatments refer to the implanting of low activity sources within the patient for 1-3 days or permanently, with a dose rate of under 0.4 Gy/hour.[8] The disadvantages of LDR treatment in gynaecological brachytherapy includes possible radiation exposure to staff, hospitalisation, long-term discomfort from applicators and the possible displacement of applicators.[27] The high dose rate (HDR) alternative uses a small, highly active source inserted via remote afterloading; where a mechanically driven cable with a radioisotope at the tip allows travel via a catheter into the body. The source spends specific amounts of time at predetermined locations, creating the required dose profile. HDR treatment lasts a few minutes as opposed to the large treatment time of LDR brachytherapy.[8]

Sonali S. Patankar et al compared low and high dose rate brachytherapy for cervical cancer within the National Cancer Database in the United States in which contains 10,564 women across 900 hospitals determining an increase of HDR brachytherapy and a decrease of the use of LDR.

However, the overall survival is the same for both HDR and LDR.[28] Additionally, HDR therapies allow dose optimisation when treatment planning after surgical insertion has occurred. Minimising the effect of suboptimal needle placement. Discomfort to the patient when considering LDR implants and the longer treatment time affecting hospital throughput has seen a HDR implementation of gynaecological brachytherapy be more prevalent and thus has become more appropriate to research.

Brachytherapy allows a large conformal dose distribution making it an attractive treatment option, with the down-side being costly repercussions for uncertainties and error within the treatment.

2.2 Treatment Planning

Treatment planning requires imaging of the region being treated to identify the extent and location of the disease. As methods have become more sophisticated the assignment of treatment specifications within the plan requires dosimetry to predict the applied dose distribution. Early brachytherapy planning used orthogonal x-rays to localise non-radioactive dummy sources or implants and superimposed each source's dose distribution to determine the applied dose. Previous systems prescribed dose, based upon dose-rates at specific distances from the implanted applicator and not the patient's anatomy (Point A prescription).[26] Currently, 3D imaging is utilised to plan according to anatomic volumes, with organs at risk and tumour volumes identified. This well-established treatment planning approach has seen the development of the gross target volume (GTV), clinical target volume (CTV) and planning target volume (PTV) quantities. The GTV is the macroscopic tumour volume which is visible in the imaging, where the CTV is the microscopic spread and includes margin for the associated lymphatics. The PTV accounts for organ motion and treatment uncertainty. The GTV exists within the CTV which is contained within the PTV.[29]

The GYN GEC-ESTRO group have compiled the protocols from many contributing physicists, to delineate important protocols which allow effective, 3D volume-based, treatment planning. When treating cervical cancer, prescription is required which priorities complete remission. The terminology

which allows this is the High-Risk CTV (HR-CTV) and Intermediate Risk CTV (IR-CTV). The HR-CTV is defined to have a major risk of local recurrence because of residual macroscopic disease and requires clear definition by a radiation oncologist when treatment planning. The IR-CTV contains significant microscopic disease and also poses a risk of local recurrence. HR-CTVs receive as much dose as possible to achieve eradication of all residual macroscopic tumour. Prescription is also made with the intent of curing the microscopic disease which typically results in a total dose of at least 60 Gy to the IR-CTV. The target volumes are contained by anatomical structures demonstrated in figure 2.1, where the pelvic wall serves as a border of which target definition is not crossed without justification. [1]

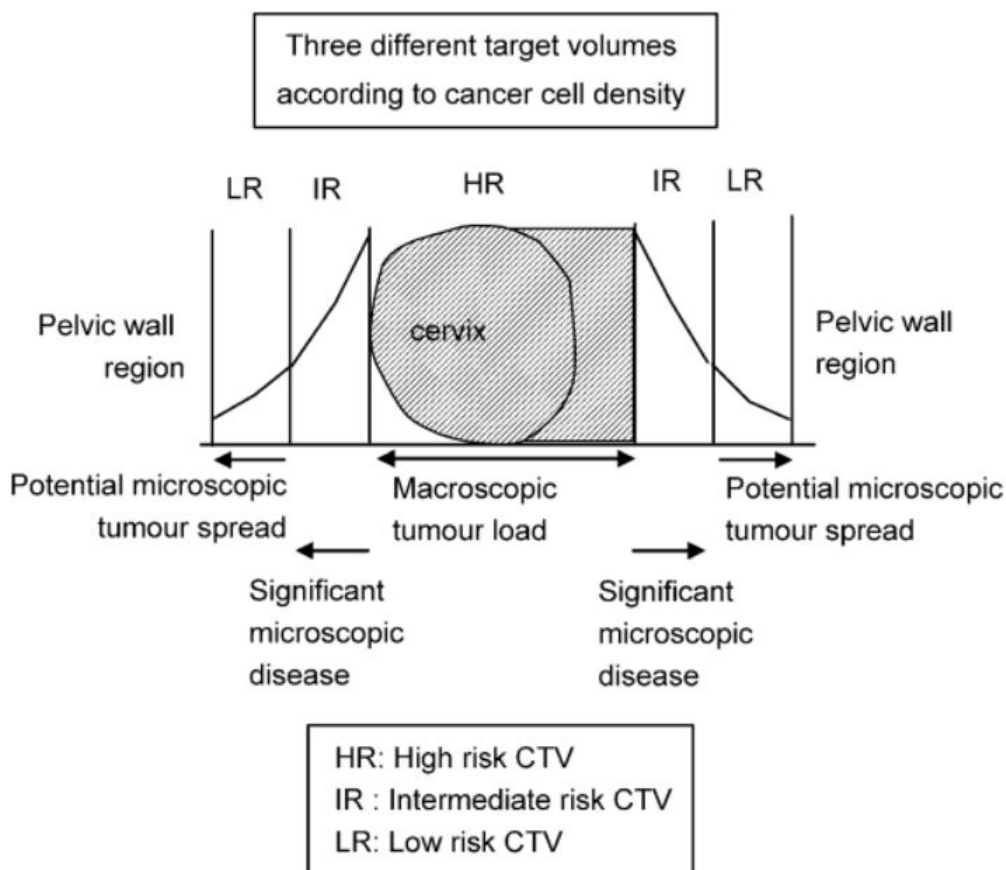


Figure 2.1: Definition of target volumes due to cancer cell density [1]

An example of 3D data motivated treatment planning can be seen in figure 2.3, where isodose lines can be seen overlaying the CT images. Historically dose prescription is completed utilising specific dose points. This is known as the Manchester system, where the dose is considered at points “A”

which is 2 cm superior and 2 cm lateral to the cervical os. Point B is 3 cm lateral from point A and a dose points on the bladder and rectum are considered.[30] The International Commission on Radiation Units and Measurements (ICRU) recommend dose to volume specification instead, this is accepted clinically as advances in 3D imaging has enabled the treatments to progress.[31] A comparison between point dose planning and treatment planning using 3D data by Yasur A. Bahadur et al demonstrates that without volumetric treatment planning, the target volume is underdosed and OAR such as the bladder and rectum receive more dose.[32]

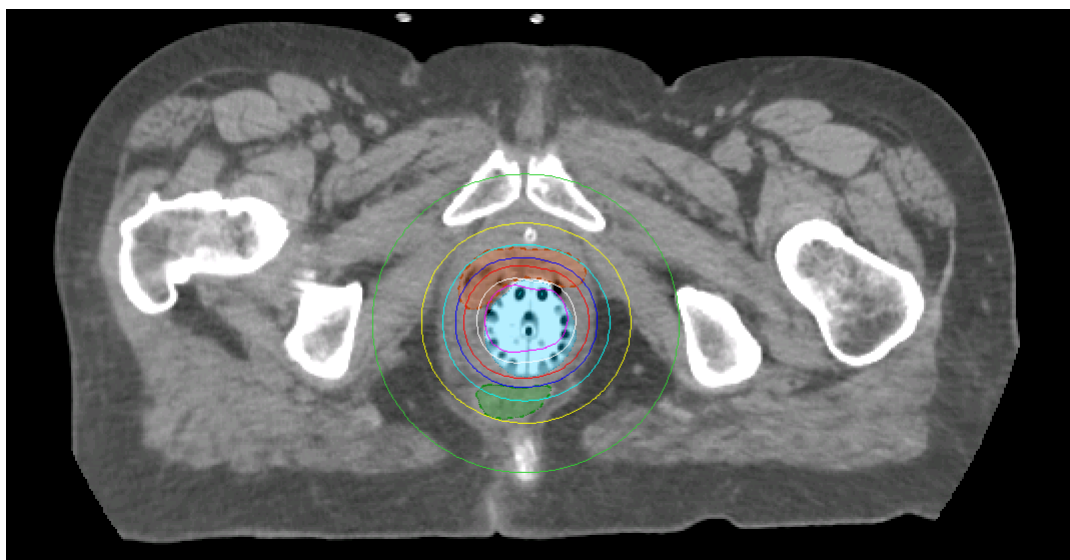


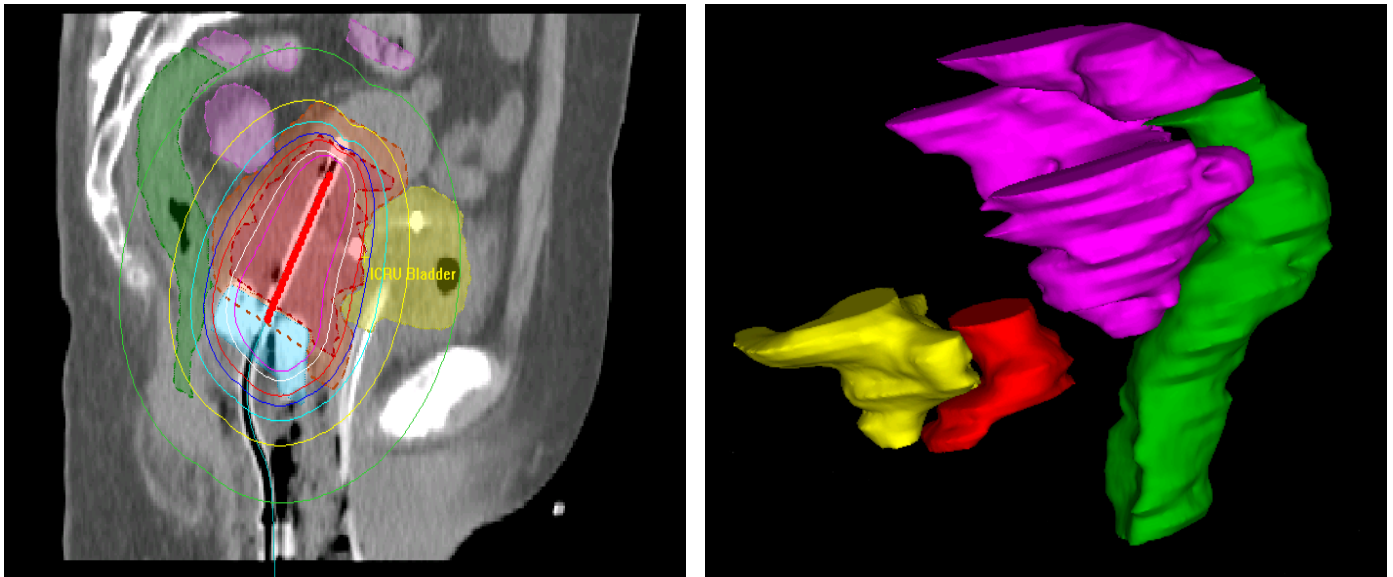
Figure 2.2: Traverse slice view used for treatment planning, displaying the lunar ovoids of the Venezia applicator, the red HR-CTV and isodose lines.

Contouring of critical volumes such as the CTV, and OARs are conducted on the planning image. Structures of interest are outlined by a clinician in each 2D slice, an example of which is illustrated in figure 2.2. All transverse slices are combined to reconstruct the clinical volumes. The bladder, HR-CTV, sigmoid colon and rectum are displayed in a sagittal view within the anatomy and as reconstructed volumes from a cervical brachytherapy treatment in figure 2.3. Similarly catheters are localised within each slice, isolating the path the source will take. The treatment plan is created by determining the dwell time and position of the source will take relative to the reconstructed volumes.

Dose optimisation occurs by determining the optimal weighting of each dwell position to provide the required CTV coverage and OAR dose limits. Accomplished by manual adjustment or using

inverse planning methods. Inverse treatment planning requires a set dose prescription to the clinical volumes (CTV, OARs) and calculates dwell times and positions which accomplish the prescribed dose distribution.

The EMBRACE publication is a commonly used recommendation for image-guided brachytherapy. The study is an interventional and observational multicentre study by the GEC-ESTRO GYN working group. EMBRACE stands for Image guided intensity modulated external beam radiochemotherapy and MRI based adaptive brachytherapy in locally advanced cervical cancer. The study aims to establish a high level of tumour control while limiting morbidity. Previous RetroEMBRACE and EMBRACE I studies have indicated that positive patient outcomes stem from the evidence-based specification of dose prescription and technique.[33][34] EMBRACE II proposes an advanced target volume selection and contouring protocol for brachytherapy and EBRT. The protocol also consists of weekly chemotherapy and a bio-imaging sub-study of MR biomarkers to assist risk of local recurrence. The protocol specifies a multifaceted approach of dose and volume end-points, as well as dose escalation and de-escalation for image-guided adaptive brachytherapy (IGABT). [25]



(i) Sagittal view of critical volumes within anatomy

(ii) Reconstructed volumes

Figure 2.3: HR-CTV and OAR reconstruction for gynaecological brachytherapy, with the bladder yellow, HR-CTV red, sigmoid colon magenta and rectum green

2.2.1 AAPM Task Group 43

The American Association of Physicists in Medicine (AAPM) task group reports provide a clinical standard of practice through the construction of specific formalism. The AAPM Task Group 43 updated its report in 2004 and is recognised globally. The formalism exists to provide good practice in determining dosimetric quantities both experimentally and via Monte Carlo methods. The formalism specifies dose calculation from a single source at point $P(r,\theta)$ as shown in figure 2.4. The equations 2.1 and 2.2 provide insight into the factors which the TG-43 formalism uses for calculation of dose rate in 1 dimension and 2 dimensions respectively.[2]

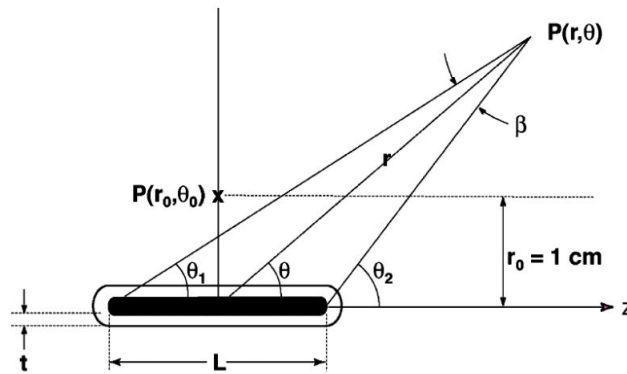


Figure 2.4: Polar co-ordinate system geometry for dose calculation used in TG-43 formalism [2]

$$\dot{D}(r) = S_k \cdot \Lambda \cdot \left(\frac{r_0}{r}\right)^2 \cdot g_p(r) \cdot \phi_{an}(r) \quad (2.1)$$

$$\dot{D}(r) = S_k \cdot \Lambda \cdot \frac{G_L(r, \theta)}{G_L(r_0, \theta_0)} \cdot g_L(r) \cdot F_{an}(r, \theta) \quad (2.2)$$

The air-kerma strength S_k ($1 \text{ U} = 1 \mu\text{Gym}^2\text{h}^{-1}$), is a measure of brachytherapy source strength. S_k is the air kerma rate measured in free-space at a point far enough from the source that it can be considered a point-source, multiplied by that distance squared. $S_k = \dot{K}(d) \cdot d^2$. The dose rate constant Λ is defined in a medium using S_k normalisation. Both equations demonstrate many similar factors, including radial dose functions which consider the scatter and absorption within the medium. Considering the dose-rate fall off is integral to source tracking in three dimensions, as it is used to

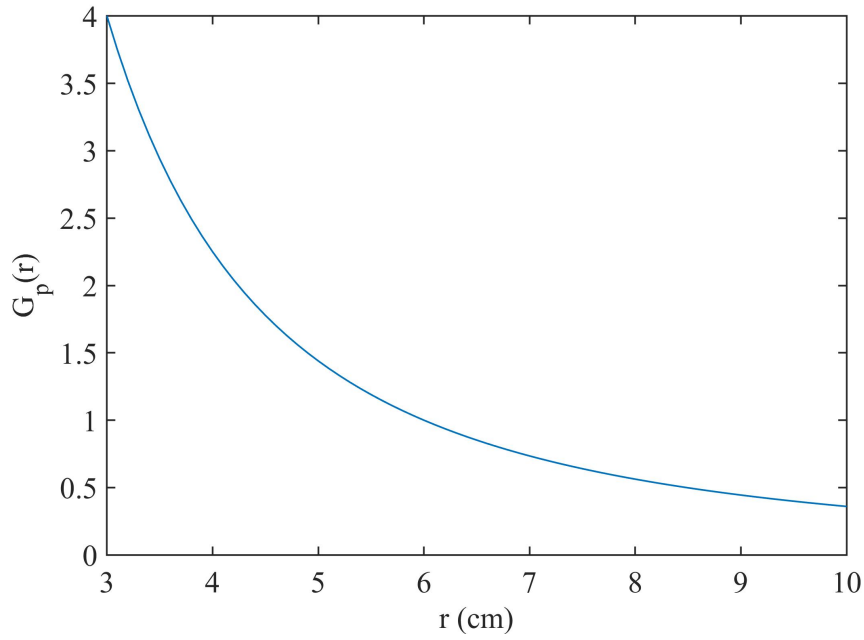


Figure 2.6: Inverse square reduction in dose, normalised to 6 cm. [3]

determine SSD. In the 1 dimensional case, a point-source is considered and so an inverse-square reduction ($G_p(r)$) is applied with the radial dose function $g_p(r)$. Comparing figures 2.6 and 2.5 demonstrates the relative effect each factor has on the dose fall-off with distance. The inverse-square reduction is dominant when comparing the two factors.

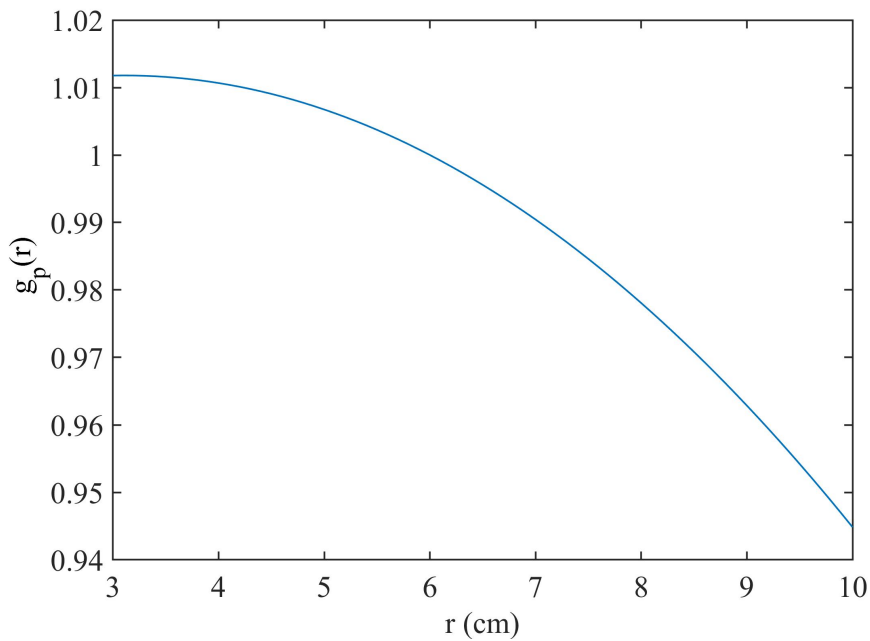


Figure 2.5: The radial dose function normalised to 6 cm.[3]

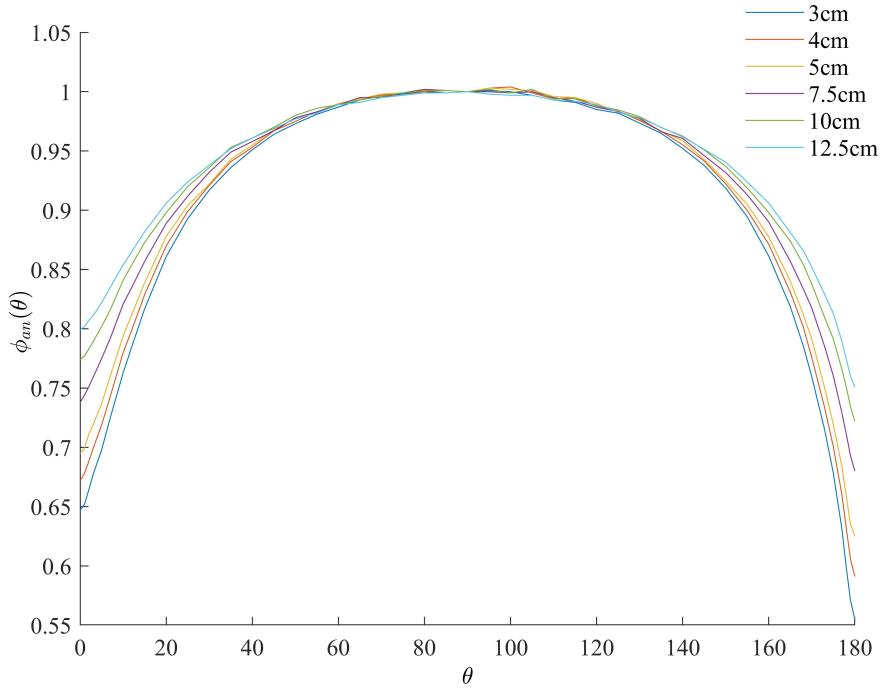


Figure 2.7: Anisotropy function at different depths.[3]

While equation 2.2 considers a line-source, radial dose function $g_L(r)$ and the geometry function $G_L(r, \theta)$ weights the distribution of activity within the source. Both equations address the dose rate's respective angular dependence with functions $\phi_{an}(r)$ for an anisotropic point source model and $F_{an}(r)$. [2]

There are a set of TG-43 assumptions which accompanies its implementation, these are stated as:

- Dose rate contributions from individual sources are summed to give the total dose rate, neglecting source-to-source interactions
- Water equivalence of all material within 30 cm of the calculation point

These assumptions simplify the clinical situation to enable fast standardised calculation and have been implemented widely throughout treatment planning systems. However, this can present limitations which need to be considered on a case by case basis. Rivard et al presents multiple limitations such as the difference in absorbed doses for lower energy photon emitting sources.[26] Secondly, scattering conditions within the treatment need to be considered with Ir-192 presenting a 5% dose

difference over 10 cm. Patients who are undergoing brachytherapy treatments which are closer to the skin will differ dosimetrically from the TG-43 formalism due to the lack of backscatter material. Additionally, a lack of charged particle equilibrium can exist within 2 to 7 millimetres of an HDR source, with a dose/kerma ratio greater than 1.05 occurs. Finally, a difference in non-water equivalent media around the source needs to be considered given possible tissue heterogeneity and/or applicator shielding.[26] Depending on the brachytherapy source used, the effect of neighbouring heterogeneity needs to be considered accordingly.[35]. The AAPM specifies that the medical physicist has to quantitatively evaluate the influence a TG-43 dose calculation method and associated approximations will have on dose delivery. [36]

Model-based dose calculation algorithms (MBDCA) will be able to address the TG-43 formalism limitations by progressing from water geometries by modelling radiation transport in different media, which should correspond to a more accurate representation of the dose distribution patients receive. The Linear Boltzmann Transport Equation (LBTE), which describes the radiation's interaction with media, needs to be solved to model the dose deposited. The equation can be solved by Monte Carlo codes which track a multitude of particles with a set probability of each interaction within the media. Kernel superposition can also be used which is the application of a simpler solution which will be adapted to fit the set-up. A discrete numerical approach to MBDCAs can also be implemented. [37]

In 2012 the TG-186 report created recommendations for the transition from TG-43 formalism to MBDCA, arguing that "clinical dose parameters may vary by at least 5% and by as much as a-factor-of 10 in numerous situations" providing a variability which will be detrimental to patient outcomes.[38] The extent upon which the MBDCA will improve treatment varies, depending on the circumstances of that treatment. Jacob et al., conducted a retrospective study to compare CT based tandem-ring treatment MBDCA plans with TG-43 based dose formalism. Both manual applicator contouring and vendor catalogue applicator models were tested. Finding a $2.1 \pm 0.3\%$ and $3.3 \pm 1.4\%$ reduction in OAR coverage relative to the TG-43 plan for the manual applicator contouring and vendor applicator library respectively. These improvements are met with the corresponding

reduction of $2.4 \pm 0.9\%$ in the target D_{90} dose compared to the TG-43 formalism.[39] The MBDCA is computationally intensive and increases planning time, however, it will improve patient outcomes in most circumstances.

MBDCAs will address the difference in absorbed dose in water and tissue, the radiation's interaction with surrounding sources or applicator as well as a correct dose calculation for all scattering conditions. However, for the algorithm to perform adequately it requires accurate inputs. Applicator and source models are built into the vendor's software and need to be selected. The input of the patient's anatomy via a 3D scan is required with the assigning of media properties such as density and elemental composition of each structure. This can be accomplished assigning these properties from a predefined catalogue or conversion of CT data from Hounsfield Units to density information.[39] The accuracy of mapping HU to mass density can be improved by dual-energy CT.[40] Key areas which determine the clinical success of MBDCAs are the modelling of sources and applicators, CT/MRI data being accurately converted to have the correct material properties and a sufficiently accurate LBTE solver.[41]

Currently, Varian Medical System's BrachyVision has incorporated MBDCA for Ir-192 source and Elekta has done the same with their Oncentra Brachy treatment planning software. With Varian's AcuroTMBV Grid-Based Boltzmann Solvers which directly solves the LBTE via discretization and Elekta's Oncentra functioning on a 3 phase collapse-cone convolution/superposition.[42][37] A model-based formalism is the future of treatment planning and will become more prevalent as computational development continues.

2.3 Gynaecological Brachytherapy Applicators

Accurate placement of brachytherapy sources are an extremely important facet of the treatment. Applicators are medical devices with internal channels which source runs through to provide control, stability and reproducibility in each fraction. A vast array of applicators are available for different

types of brachytherapy treatments to assist interstitial and interactivity use. Applicators can be a surgical insert for gynaecological needs, a surface applicator for skin cancer treatment and even an external grid attachment for the fortification of interstitial catheter position. Applicators can be used for both LDR and HDR applications.[21]

The gynaecological treatment planning process consists of applicator selection depending on the type of cancer. Multiple attachments and configurations enable customisation of the specified applicator type.

Multichannel cylindrical applicators are used to treat vaginal malignancies, as it can deliver dose to the vaginal canal, vaginal cuff and submucosal lymphatics. The cylindrical applicator is also used for the treatment of endometrial cancer post-hysterectomy.[43] Hsiang-Chi Kuo et al investigated the optimisation of the multichannel applicator with loading methods. Plans were generated and evaluated for central loading(CL), peripheral loading(PL), modified peripheral loading(MPL) and middle ring loading(MRL).[4] The configurations are demonstrated in figure 2.8, where the red channels are those being used and the others are unoccupied.

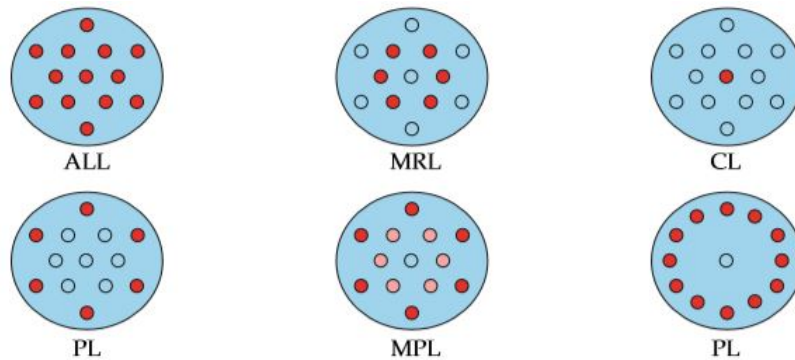


Figure 2.8: Multichannel applicator loading configurations [4]

Hsiang-Chi Kuo et al demonstrated a change in loading plan to suit unique anatomy providing better conformity, reducing dose to normal tissue and inner mucosa.[4]

Air pockets between the cylindrical applicator and vaginal mucosa are common since the tissue is not smooth. An overall reduction in dose is found to be $26.4\% \pm 13.9\%$ by Ashraf Hassouna et al as a result. With an average air-pocket volume of $0.15 \text{ cm}^3 \pm 0.36 \text{ cm}^3$. Vaginal balloons can be

attached to cylinder applicators to reduce this effect, but are not commonly used.[44] Tandem and ovoid applicators are used to treat endometrial and cervical cancer. At the end of the applicator in figure 3.5, is the tip of the tandem, this travels through the cervix providing dose to the uterus. At the base of the tandem sits two ovoids which in the case of the fletcher applicator are more cylindrical. The ovoids are positioned outside the cervix to provide dose for cervical treatment. Multiple types of tandem ovoid applicators are available, some with additional ports for interstitial needles.

2.4 Dosimeters

Dosimetry is the measurement of dose deposited to a certain volume by incident radiation and verification of the dose distribution specified is vital in all forms of radiotherapy. Higher dose gradients require smaller margins for error to minimise toxicity to healthy tissues and ensure the treatment is beneficial. The dosimetric goals within treatment are verified by the calculation of the dose deposited to OAR or the CTV. Dosimetry can evaluate the physical translation of a treatment plan and whether execution within these tolerances is achieved. [45]

The dosimeters used specifically in brachytherapy require a high spatial resolution due to the high dose gradients. Radiochromic films are common dosimeters as they easily provide dose and position without the need for chemical processing. The films can be easily integrated into most set-ups, as the size and shape of the detecting volume can be cut into the required shape. The film operates on a proportional change of opacity to dose. Incident ionising radiation or thermal annealing causes di-acetylenes monomer to undergo polymerisation, this reaction causes the creation of crystalline poly-acetylene resulting in a change of colour.[46]

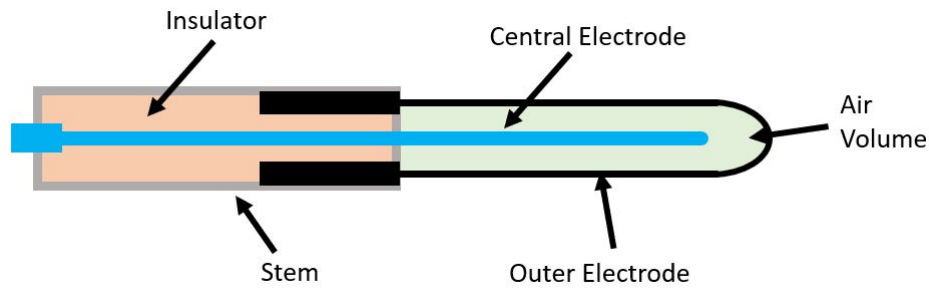


Figure 2.9: Farmer ionisation chamber

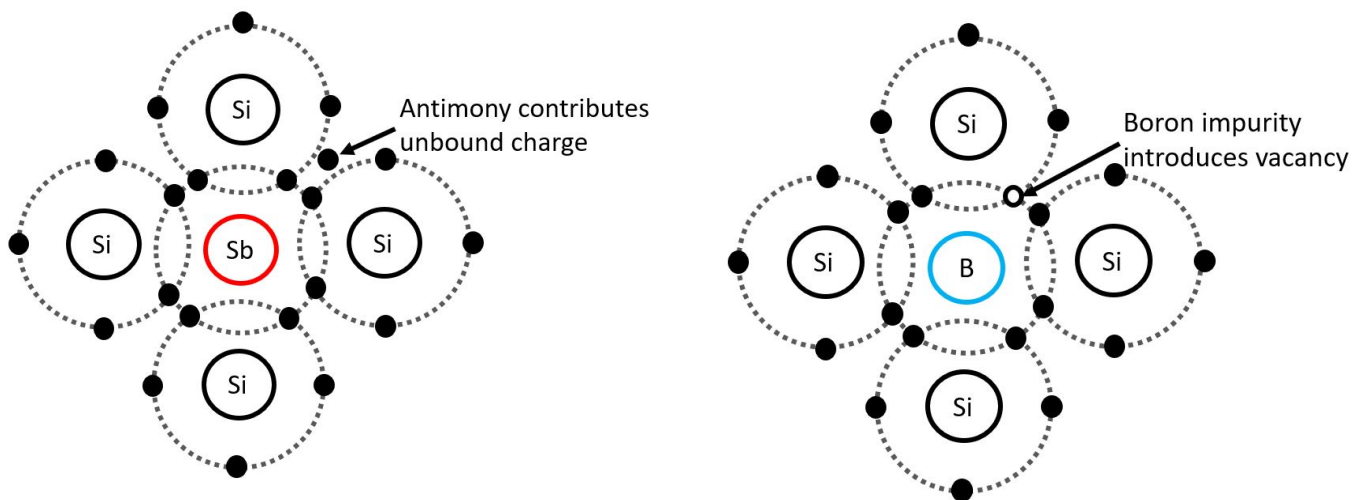
Ionisation chambers are also commonly used for dose verification and are used heavily in water-tank phantom beam calibration. A farmer ionisation chamber can be seen in figure 2.9 and represents the basic design of an ionisation chamber. It is a gas-filled cavity with an outer electrode made from graphite and an aluminium central collecting anode. An insulator separates the two electrodes to prevent current leakage. The electric field is established across the gas between the two electrodes to collect the charge produced by ionisation events from the incident radiation. The ion-pairs created by these events are collected by the oppositely charged electrode and a signal is collected. [47] The signal can be converted into absorbed dose when combined with calibration factors and the water-to-air ratio of mean mass energy-absorption coefficients.[48]

Multiple types of ionisation chambers exist with different shapes and sizes. A well ionisation chamber is generally used for brachytherapy source calibration for example, since it has an almost complete 4π counting geometry. This ionisation chamber allows the source to be placed inside it. The source is surrounded by two layers when placed in the well, one the inner electrode and the next the outer electrode.[49] Generally, the brachytherapy source strength quoted by vendors can have an uncertainty of 5%.

Thermoluminescent dosimeters (TLD) can be used for determining surface doses during treatments or in personal monitoring devices for staff. TLDs function through holes in the lattice structure trapping charges which are filled during an ionisation event within the dosimeter. After irradiation, the TLDs go through an annealing process where the dosimeter is heated to provide the trapped charges with enough energy to be released from its potential well. When the charges overcome this

potential, they relax to a lower energy state and release a light photon. The intensity of light produced during annealing is proportional to the dose deposited. Optically stimulated luminescent dosimeters (OSLDs) function similarly but require light, to free trapped charge, instead of heat and so are more stable over time. Although readout is not live, in-vivo and surface monitoring of treatments are ideal for TLDs and OSLDs since the patients do not require wiring during the procedure.[50]

Solid-state dosimetry is ideal for brachytherapy QA applications due to good spatial resolution, on-line readout and little to no bias voltage. The simplest form of solid-state dosimeter is a p-n junction diode made from silicon.[47] A p-type semiconducting material is a semiconductor that has been doped with trace amounts of atoms with one less valence electron, thus its addition to the pre-existing semiconductor lattice will leave a locally positive hole. Similarly, an n-type semiconductor is formed when the dopant has one more valence electron, leaving an unbound negative charge. Both structures are displayed in figure 2.10.



(i) Silicon doped with antimony to create p-type semiconductor (ii) Silicon doped with boron to create n-type semiconductor

Figure 2.10: Semiconductor doping

A p-n junction is formed by an interface of p and n-type material, coupling the two semiconductor types leads to majority charge carrier diffusion across the boundary, where electrons have travelled to the p-type and holes have travelled to the n-type. This creates a depletion region, in this region exists a steady electric field. Electron-hole pairs created by incident ionising radiation will be

collected by the intrinsic electric field in the depletion region, eliminating the need for an external bias.[51] In-vivo dose measurement capitalises on this, making solid-state devices optimal for rectal measurements.[52] Variations utilising solid-state technology have seen the development of multiple types of dosimeter.

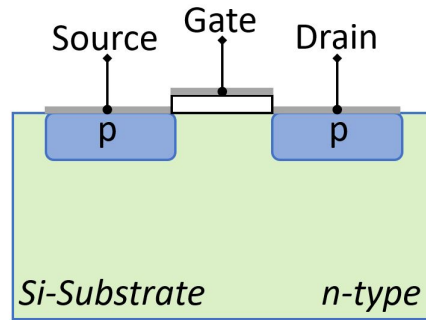


Figure 2.11: MOSFET

An extension of the semiconductor-transistor based dosimeter is the metal oxide field-effect transistor (MOSFET) dosimeter. MOSFETs function via two p-type channels embedded in an n-type base, one of those channels being the source and the other the drain, as displayed in figure 2.11. When a negative voltage is applied to the gate, holes are attracted to the oxide surface. Once the threshold voltage is reached enough holes would have accumulated for a current to flow between source and drain.[53] Upon irradiation, the electron-hole pairs created in the silicon oxide layer move out of the gate causing a shift in threshold voltage. The miniature transistors possess excellent spatial resolution and are perfect for in-vivo measurements[54]. MOSFETs enable real-time or delayed feedback through a shift in threshold-voltage which is linearly proportional to the absorbed dose. MOSFETs are ideal for dose verification and preventing overexposure as direct feedback from a rectal dose measurement can ensure the treatment stays within safe limits. [47]

2.5 Uncertainty and Error Within HDR Brachytherapy

Uncertainties in brachytherapy cause a difference between prescribed dose values in the treatment plan and what is delivered to the patient. There exists systematic uncertainty which is present for

all treatments and will thus have the same influence on each treatment fraction. Some examples of systematic uncertainties include the selection of slice thickness within imaging, as it can limit the accuracy of applicator reconstruction or identifying interstitial needle position. TPS uncertainties exist within interpolations or model simplifications which neglect the effects of applicator material, or dose delivery uncertainties due to catheter curvature and temporal rounding off. The effects of random uncertainties can differ between brachytherapy sessions, such as imaging artifacts, catheter displacement or implant motion.[55]

Applicator reconstruction involves the correct positioning of an applicator within the treatment planning system relative to anatomical structures. While catheter reconstruction can be clear with CT scans, MRI imaging is used to visualise critical soft tissue structure in gynaecological cases. Rigid applicator models or digital reconstruction is used to position the applicator within the TPS. As recommended by the GYN GEC-ESTRO working group a slice thickness must be less than 3 mm for CT images and 5mm for MR sequences .[56] These image data sets are used for reconstruction and contouring, to minimise inaccuracy a smaller slice thickness should be considered. Regulated commissioning and reconstruction methods need to be established to minimise reconstruction uncertainties and errors. Under these conditions, reconstruction uncertainty commonly has less of an impact on treatment than contouring or organ movement uncertainties.[56]

Other factors which inevitably impact every brachytherapy treatment involve. source strength calibration accuracy and correct specification of this source strength within the TPS. Additionally, temporal uncertainty within the afterloader will cause a deviation in dwell times and ultimately uncertainty in dose deposited. A rounding error can be introduced when transferring the treatment plan to the afterloading console. However, when the dose distribution is optimised, and dwell weightings are set, the rounding error is negligible. [55] An adequate, well-maintained quality assurance routine will ensure that these factors will not alter treatment efficacy in any substantial manner.

Treatment planning around heterogeneity and inadequate scattering material need to be considered, especially where calculations are TG-43 based.[2] A large difference in the material composition

and density can introduce attenuation effects and thus implant/applicator effects need to be considered.

The AAPM TG-138 report standardises uncertainty propagation in the source dosimetry data chain and encourages medical physicists to use this data when necessary to enable correct entry and commissioning with the TPS. Uncertainty within the TG-43 formalism, and Monte Carlo recommendations are also demonstrated within the TG-138 report.[57]

2.5.1 Failure Mode and Effect Analysis

Failure modes and effect analysis (FMEA) systematically identifies each possible uncertainty or error within the procedure and defines this as a failure mode. FMEA is a powerful tool that can guide future development within a clinic, highlighting where improvements can be made to provide safer and more effective treatment. FMEA is conducted by mapping out the entire treatment process and possible failure modes are identified at every stage. A committee of practitioners from the clinic, rate each failure mode on a risk priority number (RPN) scale.[58] The RPN is calculated by multiplying together three factors, each a rating between 1 and 10. The factors are; the frequency of occurrence, detectability and severity of the failures consequence. A 10 on each scale means the failure mode occurs several times a day (frequency), is impossible to detect (detectability) and leads to patient death (severity). This allows the failure modes with a higher ranking RPN to receive attention and resources.

J. Mayadev et al conducted an FMEA study on HDR gynaecological brachytherapy analysing a tandem-ring brachytherapy procedure. Evaluation of sub-processes in the treatment workflow was conducted to determine a FM and assign scores by consensus of the group. The failure mode of applicator movement during transportation would change the dose applied relative to the surrounding anatomy, greatly altering the prescribed dose to treatment volumes and organs at risk. Producing a frequency score of 3, but a detectability and severity score of 8. The other failure mode which scored 192 was the treatment planning team not communicating effectively concerning the completion of the

treatment simulation, extending the patient's time under sedation. Evaluated to have a frequency of 4, detectability of 6 and severity of 8. [9]

Some highly rated sub-processes and their failures within the analysis includes:

- Treatment simulation error - external fixation device not adequately tightened or attached to the board and the wrong image dataset transferred
- Treatment planning - not detecting errors in physics, incorrect source activity entered, error within the dwell control window, CTV contouring error and DVH constraints not met or checked
- Treatment delivery - incorrect bladder fill, not removing the rectal tube, incorrect afterloading channel used and therapist not performing verification check-list

Closely monitoring these uncertainties is critical for safe and effective HDR gynaecological brachytherapy. The design of specific QA protocols directed by failure mode effect analysis is required to provide optimal treatment and guide research.

2.6 The Impact of Catheter and Applicator Displacement

High dose-rate (HDR) brachytherapy provides a high dose gradient which is effective in producing a conformal dose. This leads to effective treatment of the clinical target volume (CTV) while sparing surrounding tissues and organs, such as the rectum, bladder, and urethra. The benefit of brachytherapy's high dose gradient is met with the consequence of small inaccuracies having large effects on the treatments potency and safety. The calculated dose distribution depends on the sources position relative to the relevant volumes. During gynaecological brachytherapy, uncertainty in applicator/-catheter reconstruction, tissue swelling and applicator displacement during patient transport can cause the delivery of dose to differ from the treatment plan. This change in position may give an additional dose to organs at risk and inadequately treat the CTV. Toxicity and damage sustained to

organs at risk (OAR) can affect patient quality of life and survival. Dose to these clinical volumes provides the endpoints for which treatments are planned. [59]

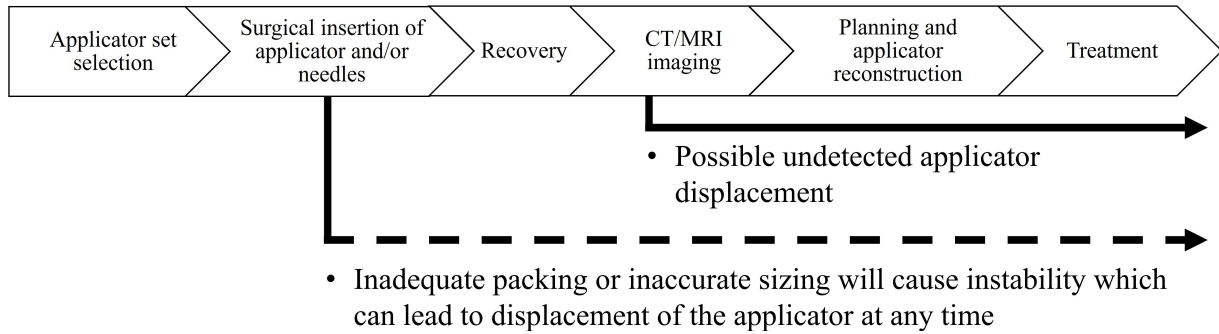


Figure 2.12: The workflow of gynaecological brachytherapy for cervical cancer and potential applicator displacement

Determining the impact of applicator displacement will enable the development of clinical tolerances which allow hospital staff to make informed decisions when evaluating potential uncertainty and patient safety. Failure mode and effect analysis (FMEA) evaluates the likelihood of occurrence, detection, and detriment to the patient a particular failure will cause. FMEA finds applicator shifting to be one of the two highest-ranking failures. The inability to detect this failure demonstrated within the workflow illustrated in figure 2.12 accompanied by the detrimental impact it would have on patient care. The impact of a shift in applicator position due to displacement or reconstruction uncertainty is evaluated in several different instances through retrospective studies. [60] Previously conducted plans are altered through a virtual shift in applicator position within the treatment plan and the resulting change in DVH for critical volumes is calculated via comparison with the initial plan. Tanderup et al, conducted this study to evaluate the consequences of applicator position, using 20 cervical cancer cases with MRI based planning. 10 cases required sole intracavitary, ring-tandem applicators, with the other 10 being treated with an intercavitary-interstitial combination using a modified ring-tandem applicator. Displacement was simulated with applicator translation ± 3 mm in every dimension, and an additional ± 5 mm in the anterior-posterior direction. A $\pm 15^\circ$ rotation is applied to the ring component to simulate applicator rotation. The corresponding change in DVH parameters for the patient population serves as input parameters for a linear model. The model

found a 5-6% per mm change in the rectum and bladder mean DVH parameters, for displacement in the anterior-posterior direction, and a 4% per mm change in all other directions.[61] The study demonstrates the significant impact 2 or 3 mm of shifting can have on a patient population, solidifying the importance of strict quality assurance procedures for both applicator reconstruction, and implant stability during the procedure. Overall, only 20 patient cases were used, a larger population size would provide greater credibility. Tanderup et al., intentionally centred the study around reconstruction uncertainty, without a comprehensive evaluation of applicator displacement failures. This is demonstrated by the model used functioning for minor displacements in the superior-inferior direction. Additionally, applicator rotation was only evaluated through a shifting of dwell positions within the ring and not a rotation of the entire applicator set, which could occur clinically during patient transport or if the implant has not been placed firmly against the vaginal fornices. This could affect the dose to rectum and bladder which are critical OARs and further study is required to evaluate the impact of this failure.

Alternatively Schindel et al., set out to evaluate both, the impact of reconstruction uncertainty and applicator displacement, but evaluate between ± 1.5 mm and ± 20 mm for the superior-inferior direction. Two sets of shifting are completed, moving the entire applicator in the superior-inferior axis to simulate applicator displacement and a shift in dwell position along each channel to simulate reconstruction error.

The tandem-ovoid applicators used, produced a 10% change for a ± 1.5 mm displacement, with a significantly larger impact found for volume-based planning than point A plans. This is most likely due to the optimisation of the conformal distribution for volume-based planning. A ± 3 mm reconstruction-based shift caused a 10% change for both MRI-guided, conformal brachytherapy planning and point A planning.[62] Although applicator displacement was simulated in this retrospective study, only one axis of motion was evaluated (sup-inf). Movement in any dimension is clinically relevant since the specific failure can be caused by sub-optimal vaginal packing, which is used to hold the applicator in place within the vaginal cavity. Shifting of applicator position during patient

transferring to imaging and incorrect applicator size selection can result in applicator displacement in any direction.

Retrospectively evaluating the impact of catheter and applicator displacement through both possible translation and rotation over a larger patient population will build on the existing literature. Comprehensively determining the dosimetric risk of applicator displacement and reconstruction uncertainty will enable specific guidelines to be determined and establish the importance of quality control measures for reconstruction and applicator insertion.

2.7 Quality Assurance

Brachytherapy enforces a localised dose to a tumour volume through the application of large dose gradients. Whether the radiative source is implanted for low dose rate therapies or with a remote after-loading device for high dose rate treatments, the precise implementation of a patient-tailored treatment plan is paramount to positive patient outcomes. The advantage of large dose gradients presents with the associated drawback of any deviation from the treatment plan causing toxicity in nearby OAR and/or render the treatment ineffective. For the safety of staff and patients, quality assurance (QA) procedures are developed to minimise the prevalence of human error, device malfunction and miscommunication.

2.7.1 AAPM Task Group 56

The American Association of Physicists in Medicine developed a task group to devise the “Code of Practice for Brachytherapy Physics: Report of the AAPM Radiation Therapy Committee Task Group No. 56” which outlines the complete design and implementation of a QA program for brachytherapy facilities. The report dictates an adequate quality assurance program addresses the following fundamental endpoints.

Radiation Safety

The facility needs to address the safety of the patient, staff and public when considering the consequences of a quality assurance plan. This means controlling exposure to all personnel involved in the procedure through adequate shielding barriers and substantial consideration of treatment workflow. For HDR afterloading sources, this includes verifying the function of error identification features such as interlocks, treatment status indicators, emergency stop button and background measurements. The maintenance of a comprehensive radiation safety QA program mitigates risk to the institution, staff, patient and the public.

Positional Accuracy

Confirmation of the sources dwell position is vital in determining whether the prescribed dose distribution is being given to the patient. The TG-56 report specifies a ± 2 mm relative to the applicator system and ± 1 mm for remote afterloading devices.[63] Positional accuracy can be tested using a source positioning ruler shown in figure 2.13. The afterloader source is programmed to take a specific position within the ruler and this is compared to the ruler's scale viewed from the safety of the treatment console via a monitoring camera. The position can also be denoted by a radiochromic film measurement.

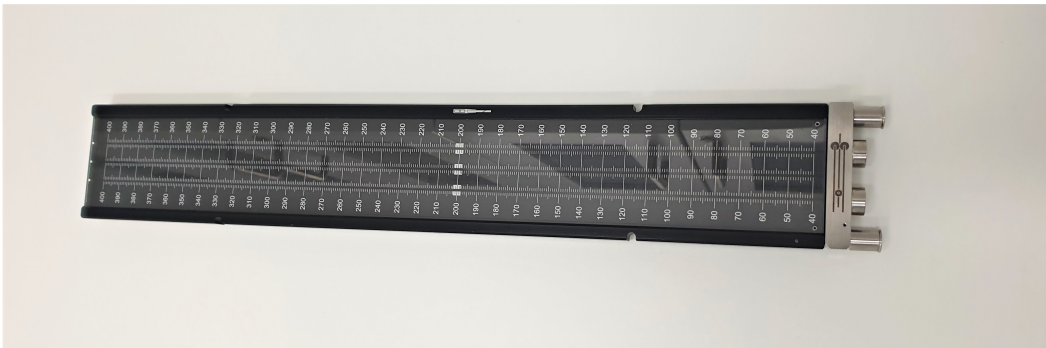


Figure 2.13: Elekta Source Position Check Ruler

Temporal Accuracy

The treatment plan specifies that dwell time each source is required to spend at each location. Dose delivered during the source's motion (transit dose), is accounted for when planning dwell times. Remote afterloading technology has an on-board electronic timer, however, independent tests of the accuracy of the timer need to be done when source calibration is performed. Relative measurements are suitable when the on-board timer is used to control treatment delivery and charge integration during source strength calibration. An accuracy of $\pm 2\%$ is specified [63].

Dose Delivery Accuracy

Perfect delivery of the prescribed plan relies not only on the dwell positions and times being correct but the dose delivery complying with the dose absorbed by the medium. Calculation of applicator attenuation and shielding corrections and accurate calibration of the source in terms of air kerma strength are prime examples of this. Accurate dose delivery is also a function of uncertainties in

treatment planning such as applicator reconstruction and a correct optimisation of uniform dose coverage of the specified volume. A correct definition of the target volume and critical organ margins relative to the implanted applicators will affect dose delivery accuracy.[63]

The TG-56 report intensively characterises the quality assurance of brachytherapy treatments and the creation of a QA plan. These principles have been foundational in the research conducted into treatment verification. Quality assurance techniques have been evolving along with technological development.

2.7.2 The Gamma Index

Dosimetric measurements require an analytical tool that considers a preselected acceptance criteria for each treatment type. This can be accomplished by definition of quantities dose-difference and distance-to-agreement. Dose-difference distributions identify regions where measurements differ from the calculated spatial dose and are expressed as a percentage. The distance-to-agreement (DTA) quantity is defined as the distance between the measured point and the point in the calculated distribution which has the same dose. A combination of dose difference and DTA can be used to characterise the criteria at which the treatment plan in question will be evaluated.[64] The gamma index technique utilises these two quantities to calculate the γ quantity for each point of interest, where $\gamma \leq 1$ passes. The percentage of gamma values that pass is frequently used to compare dose distributions for a given dose difference and DTA tolerance.[65] This analytical apparatus, developed for IMRT evaluation is applied as a measure in some brachytherapy quality assurance studies.

2.7.3 Developments in QA

Quality assurance phantoms and tools are continuously developed to verify brachytherapy practices, determining if the procedure correctly implements the prescribed dose distribution. A wide variety of technologies are utilised in the literature to enable localisation of sources, perform dosimetry and provide a test of congruency between the treatment plan and what is implemented. The literature

establishes developments that range from conceptualising the technology's application in quality assurance to a complete evaluation of clinical workflow. Implementing a comprehensive QA procedure for each type of brachytherapy treatment is extremely important in ensuring positive patient outcomes.

T.Hanada and colleagues developed an HDR remote afterloading QA tool to test the temporal and localisation accuracy of the afterloading system.[66] The tool is made up of a plastic-scintillator coupled with a CCD camera for scintillation photon detection. A straight channel applicator is inserted into the plastic scintillator and with a travel distance of 5 cm and 11 dwell positions programmed. The device can achieve submillimeter localisation and a temporal resolution of one-thirtieth of a second for a stationary source. The specified afterloading positional and temporal accuracy tolerance (1 mm and 1% respectively) fall within these limits, making the device a viable option for HDR afterloader quality assurance. T.Hanada et al, does recognise the devices potential for 2D dosimetry given further development in analytical software. Despite this limitation, the tool demonstrates a capability to perform QA of afterloading cases. The device can evaluate HDR afterloading of straight channel applicators and catheters but the study has not indicated what performance can be expected from curved applicators such as ring-tandem applicators where the source position can vary in three dimensions.[66]

Radiochromic film is widely used for quality assurance, providing a sufficient resolution of the dose deposited. Its application in brachytherapy allows an evaluation of the treatment, which can range from afterloader-applicator checks to phantom studies.[67] The films implementation within current QA is accompanied by an aptitude for complex research applications. I. Gerardy et al, carried out a comparison of in-phantom film measurements and Monte Carlo calculations using the MCNP5 code, in which mesh grids are super-imposed to calculate dose. In both cases, a cylindrical vaginal applicator is used with an intra-uterine tube. The physical phantom allowed the positioning of a calibrated film as well as a small ionisation chamber at specific positions. Isodose curves agreed between the simulation and physical phantom, implying that the simulation is a viable model to estimate

dose [68] I. Gerardy et al, demonstrates congruency between the physical and simulated models. An extension of this concept is evident through the use of radiochromic film to validate model-based dose calculation algorithms. As discussed previously model-based dose calculation algorithms are recommended by TG-186 to improve treatment planning. Gregorz Zwierzchowski et al., uses film dosimetry to verify the TPS calculation algorithm for vaginal applicator shielding. A round hole is cut into the film with a diameter equal to that of the cylindrical applicators tested. The applicator is inserted into the hole, such that the film provides a perpendicular cross-section. Shielding verification is accomplished as the applicator contains several arrangements of internal tungsten inserts which surround the applicator channels. A gamma analysis is conducted to compare the MBDCA and film measured dose distribution with over 90% of the analysed points meeting the 3% / 3 mm criteria. The study determined radiochromic film is suitable for QA of treatment planning systems, revealing shielding leakage which was not calculated. Although this additional dose was not clinically relevant, these findings demonstrate a possible need for shielding leakage checks pretreatment for other configurations. Radiochromic film has been found to provide adequate dosimetry for quality assurance, however, it requires a time-consuming process of calibration and analysis when compared to ionisation chambers or solid-state dosimetry.[69]

Real-time quality assurance for HDR brachytherapy is extremely important to identify errors and uncertainties within the procedure. The need for real-time readout which TLD dosimeters and film measurement do not provide, has inspired the development of multiple dosimeter systems.

Using multiple detectors to localise the brachytherapy source has been outlined by Nakano et al, where three diamond dosimeters are used, combined with the treatment plan timing information to determine the location of the source in three-dimensions. The response as a function of source-to-detector distance, angular dependence, backscatter effect and temperature dependence has been measured to produce a localisation system. This characterisation serves as an appropriate archetype for using multiple detectors to determine source position. HDR brachytherapy source localisation has been achieved with this system within 2 mm. This level of accuracy is accessible for a 10-120 mm

source-to-detector distance, with uncertainty being dominant outside this range.[70] These results were attained within a Perspex, homogenous phantom but provided preliminary research for the development of a 12 diamond detector system that can provide real-time localisation within heterogeneous tissue. A 3 mm positional uncertainty within the system allows the detection of significant errors. [71] Both studies were foundational to the development of utilising multiple detector elements to determine the source position in real-time, enabling superior error identification and establishing the prospect of online quality control during the procedure. GaN radioluminescent probes demonstrate sub-millimetre accuracy in measurements both within gynaecological applicator channels and a PMMA QA phantom. The errors in dwell position are (0.11 ± 0.70) mm and (0.01 ± 0.42) mm for phantom and applicator respectively, with the standard deviation of dwell times less than 100 ms. The system ability to discern errors in dwell position and time were tested through experimentally introduced errors into the phantom protocol. Multiple applications of a 23 position plan were conducted with an implemented position offset which ranged from 0 to 5 mm. 20 positions were run through repeatedly with dwell times adjusted from the planned time to an additional 2.0 s. Using a gamma index pass/fail methodology error detection rates were produced for the system, up to 96% at 1 mm and 100% error detection at 0 s. The QA system performs extremely well when discerning spatial and temporal inaccuracies within an applicator, and can serve as a useful tool for afterloader and applicator checks. The set up did however require, probes to be fairly close to the source and will require modification for the use of different applicator arrangements.[72]

The use of multiple detector elements coupled with a localisation algorithm for HDR source tracking was expanded through the application of two pinholes, pixelated silicon detector units. Each detector contained two pixelated silicon sensors with 256 elements. Despite the large number of elements giving the detectors good spatial resolution, the system's error is largely a function of detector-pinhole alignment. This is demonstrated in the system's limited accuracy of 5 mm for a dwell time of 1 second and the average absolute difference between the reconstructed position and true position of (4.9 ± 2.2) mm for a larger number of measurements. Given the high dose gradients

in HDR brachytherapy the systems ability to perform real-time brachytherapy quality assurance is inadequate.[73] An alternate technology followed, as Manikandan A et al., investigated the use of a commercial ion chamber array, IMatriXX, generally used for LINAC profile checks applied to HDR source tracking. An aptitude for brachytherapy treatment verification is evaluated through comparison with the treatment planning system. The array consists of a 32 by 32 grid arrangement of 0.08 cc active volumes. A maximum error of 1.8 mm has been found for plans with dwell positions greater than or equal to 2 cm apart. Due to the size of each ion chamber, a volume averaging effect causes the output peaks to have a full width half maximum of 5.8 mm, thus a plan with step sizes of 1 cm or less cannot be resolved. The system can provide an adequate solution for plans which have larger step sizes and does well to evaluate the dosimetry against the TPS. [74] Using the IMatriXX for quality assurance of HDR brachytherapy procedures has provided a precedent for the development of array detector devices but performs inadequately for treatment verification.[75][76]

The Magic Plate being a similar application of this concept as it is a 2D array, however uses silicon diode elements to provide three-dimensional sub-millimetre tracking of HDR brachytherapy sources in a TG-43 environment.[77] The Magic Plate detector is superior when compared to other localisation systems with the ability to determine source position within 1 mm and provide a high temporal resolution.[77] Direct comparison with the literature shows a pixelated silicon pinhole system that has a tracking accuracy of 5 mm, or a three diamond detector system with a localisation accuracy of 2 mm.[73][70] The ionisation chamber array IMatriXX provides an uncertainty of 1.8 mm but requires the dwell positions which are more than 2 cm apart due to volume averaging effects.[74] A EPID base system provides a complete evaluation of the treatment plan with 1 mm accuracy similar to the magic plate system, however, requires elaborate commissioning and the use of a robotic arm.[78] The MP possess the advantage of simple setup while achieving adequate pre-treatment verification with the Magic Plate based “Magic Phantom”. [10] Further work is required on the Magic Plate’s phantom to match the EPID setup above which is an end-to-end analysis procedure. It allows water phantom measurements to evaluate any HDR brachytherapy procedure, demonstrating the ability to

house gynaecological applicators as well as interstitial catheters. This discrepancy will be addressed within this thesis, constructing and verifying an Magic Plate end-to-end phantom.

Due to the complexity of HDR brachytherapy planning and the high dose gradients utilised, an accurate quality assurance system is integral to patient, public and institution protection. These developments allow improvements that enable progression towards refined positional, temporal and dose delivery end-points.

2.8 The Magic Plate

The Magic Plate (MP) is a 2D silicon array detector developed for quality assurance by the Centre for Medical and Radiation Physics at UOW and exists in many different generations. Initially, the MP121 is an 11x11 array of thin, $0.5 \times 0.5 \text{ mm}^2$ diodes on a 0.6 mm Kapton substrate that can be used to provide live readings. Wong JH et al performed a large range of characterisations on the novel diode array using a linac. This included a radiation damage study, dose per pulse effect, dose linearity, energy response and angular response, amongst other properties. The results for radiation damage are 2.1% reproducibility following irradiation. The dose rate is measured to be independent at low doses and the response is dampened at higher doses. The dose linearity was excellent with a 10.8% angular dependence at a 180 degrees gantry angle. This is due to the minimal angular dependence of the silicon diode, where a 3.5% difference in response is seen for an incidence 75 degrees in either direction of the normal. [76] The MP121 was initially used for upstream QA, acquiring transmission measurements of linac treatments, as the device offers minimal beam perturbation and a less than 0.5% increase in relative surface dose. The MP's low beam perturbation and skin dose is a result of the detector's "Drop-in" technology, which avoids the use of high Z materials.[79] Additionally, the MP has also demonstrated the ability to function as an in-phantom dosimeter. The IMRT dose profile determined in two dimensions corresponds with ionisation chamber measurements, illustrating the Magic Plate's versatility for low perturbation linac transmission measurements and

dose profile quality assurance.[80] A Magic Plate with higher spatial resolution followed to perform QA for stereotactic radiotherapy, where a large dose 8-24 Gy/fraction is delivered in a low number of fractions (1-5). Small volumes are treated and require precise margins with specific small field quality assurance tools. Volume averaging effects of ionisations chambers and some diodes can be detrimental to the treatment, finding large small-field variations. The monolithic-silicon based MP512 is a Magic Plate that contains 512 pixels, with a pixel size of $0.5 \times 0.5 \text{ mm}^2$. The detector is a viable alternative for stereotactic radiosurgery (single fraction) and stereotactic body radiation therapy, given it's high spatial and temporal resolution. The MP512's spatial and temporal resolution proves the ability to evaluate treatment motion and the intended solutions. The electromagnetic tracking system Calypso enables dynamic MLC compensation in response to motion and the MP512 is suitable for quality assurance of this system, demonstrated by M. Petasecca and M.K. Newall et al.,[81][82]

The Magic Plate-121 spatial and temporal resolution is pivotal for quality assurance of HDR brachytherapy due to its ability to determine both dwell positions and times enabling the complete evaluation of a treatment plan. A. Espinoza et al conducted a feasibility study that validates the Magic Plates use within HDR brachytherapy through the development of a four-dimensional localisation system.[77] Measurements of the angular dependence of a single diode were measured by stepping a source in 15° increments around an arc of 180° about a single diode element. Furthermore, the source-to-detector distance dose (SDD) function was measured for the Magic Plate diode in solid water. These results are used to calculate the radial dose function. Measurements over 71 mm were not obtained due to low signal. The TG-43 calculated radiation dose function differs by 8% at 30 mm and 40% at 70 mm. There exists a substantial deviation from the TG-43 protocol due to the diodes over-response to low energy scatter at these distances. All MP detector elements are coupled with an electronics system (AFE DAQ) and field programmable gate arrays FPGA designed by the Center of Medical and Radiation Physics (CMRP). Due to the X-Tream unit which has also been designed by CMRP, the system can acquire data at a rate of 1 MHz, however, sample averaging is often required to mitigate both thermal and electrical noise. The electronics and detector combination is connected

to a PC via USB for analysis and live readout. Custom C++ based interface software was developed by the CMRP research group to enable real-time source tracking and post-processing, gamma analysis and TG-43U1 protocol dose calculation for evaluation of a treatment plan. The proficiency of this complete quality assurance system is evident through the construction of a brachytherapy phantom known as the Magic Phantom, where the MP is in the middle of a PMMA phantom, which houses 10 catheters above and below the MP at a fixed perpendicular distance of 6 mm. A CT scanner was used to image the Magic Phantom and a treatment plan is created, setting a specified dose to each detector element. A variation of dwell positions and times were programmed for each catheter. A second plan was created with altered dwell times and positions to simulate errors to evaluate the magic plates ability to differentiate these errors from the original plan. The Magic Plate measured source position within 0.5 mm of 75% of measurements. The system's ability to provide sub-millimetre accuracy is undoubtedly impressive when compared to other quality assurance tools in the literature. The device's compatibility and ease of use make it an exciting prospect for integration into future developments. [77][10]

The MP's capacity to be utilised for source tracking is further demonstrated for verification in brachytherapy where Joel Pöder et al tested the accuracy in which this can be achieved via a Monte Carlo study. 12 source positions were simulated from an HDR prostate brachytherapy treatment using a Geant 4 toolkit. This was accomplished via simulation of a Ir-192 Flexisource within a voxelised patient geometry. The magic plate was also inserted into the simulation and the dose deposited in the detector is determined. Joel Pöder et al., found a mean difference between the known and measured source positions to be (2.1 ± 0.8) mm. This was determined to be due to inhomogeneity in the simulated tissues. A calculation with the patient voxels set to be water equivalent enabled a localisation accuracy of 1 mm. CT data integrated into the localisation algorithm to account for inhomogeneity will improve the Magic Plate's accuracy.[83] Presently this study determined that the Magic Plate system requires adjustment to accomplish *invivo* tracking, however, its superior localisation accuracy enables the device to be useful for in phantom quality assurance.

2.8.1 Localisation Algorithm

An iterative localisation algorithm is used to track the source position and compare this dwell position to the treatment planning system. The algorithm uses the position of the diode with the largest response and those around it. The measurement of angular dependence, energy dependence for the Ir-192 spectra and radial dose function has been performed by Espinoza et al[77]. The diode's response and its SDD function are compared to the geometrically calculated distance between the diode and estimate to localise the source.

The initial source position is determined using the detector with the largest response and its nearest neighbours. Given the element $D(x_1, y_1, z_1)$ has the highest response, it serves as an adequate initial estimation of the sources x and y position. The response of the i th diode is a function of its distance to the source $I_i = f(r_i)$, determined via SDD measurement. Using the inverse function we can calculate the distance $r_i = f^{-1}(I_i)$, where r_1 is calculated for element $D(x_1, y_1, z_1)$. Angular dependence is neglected in the first iteration and is incorporated within the algorithm in later iterations. Using the detector element position $D(x_1, y_1, z_1)$ and r_1 , the initial source position estimate $S(x_s, y_s, z_s)$ is $S(x_1, y_1, r_1)$. The detector response combined with a previously determined SDD can establish an initial estimate of source position.

d_i , the distance between the i th diode and the estimated position $S(x_s, y_s, z_s)$ and is calculated geometrically with equation 2.3.

$$d_i(x_s, y_s, z_s) = \sqrt{(x_s - x_i)^2 + (y_s - y_i)^2 + (z_s - r_i)^2} \quad (2.3)$$

A non-linear least-squares fit is used, which is a mathematical procedure for minimizing the sum of the squares of the residuals. The residuals in this case being the relative difference between the geometrically calculated estimate d_i and the quantity r_i , which has been derived from the response and SDD measurements. The relative residual error to be minimised is thus given by equation 2.4.

$$R^2(x_s, y_s, z_s) = \sum_{i=1}^n \left(\frac{d_i(x_{s_n}, y_{s_n}, z_{s_n}) - r_i}{r_i} \right)^2 \quad (2.4)$$

The estimated source position will be similar to the actual source position when the sum of squares of the relative residual R^2 is at a minimum. To find minimum values of R^2 in all three dimensions Newton's Method for optimization is required. Newton's Method is used to find roots of a curve and subsequently can be utilized to perform the optimisation required for the minimisation of R^2 . Considering a one dimensional function $f(x)$, and estimation point x^k . Newton's Method uses a linear approximation to find the roots of a function ($f(x) = 0$) through iteration of δ .

$$\delta_x = \frac{f(x^{k-1})}{f'(x^{k-1})} = x^{k-1} - x^k \quad (2.5)$$

$$x^k = x^{k-1} - \frac{f(x^{k-1})}{f'(x^{k-1})} \quad (2.6)$$

By analogy finding the roots of the derivative function $f'(x) = 0$ for optimisation will yield equation 2.7.

$$x^k = x^{k-1} - \frac{f'(x^{k-1})}{f''(x^{k-1})} \quad (2.7)$$

Applying this method to minimise the three dimensional quantity $R^2(x_s, y_s, z_s)$ requires the differentials taken in 3-dimensions and iteration performed in each dimension.

$$\begin{aligned} x_s^k &= x_s^{k-1} - \delta_x^{k-1} \\ y_s^k &= y_s^{k-1} - \delta_y^{k-1} \\ z_s^k &= z_s^{k-1} - \delta_z^{k-1} \end{aligned} \quad (2.8)$$

$$\nabla \mathbf{R}^2 - \nabla^2 \mathbf{R}^2 \vec{\delta} = 0 \quad (2.9)$$

Calculation of δ in 3-dimensions is accomplished through solving the set of linear equations arranged in the matrix below.

$$\begin{bmatrix} \frac{\partial^2 R^2}{\partial x_s^2} & \frac{\partial^2 R^2}{\partial x_s \partial y_s} & \frac{\partial^2 R^2}{\partial x_s \partial z_s} \\ \frac{\partial^2 R^2}{\partial y_s \partial x_s} & \frac{\partial^2 R^2}{\partial y_s^2} & \frac{\partial^2 R^2}{\partial y_s \partial z_s} \\ \frac{\partial^2 R^2}{\partial z_s \partial x_s} & \frac{\partial^2 R^2}{\partial z_s \partial y_s} & \frac{\partial^2 R^2}{\partial z_s^2} \end{bmatrix} \begin{bmatrix} \delta x \\ \delta y \\ \delta z \end{bmatrix} = \begin{bmatrix} \frac{\partial R^2}{\partial x_s} \\ \frac{\partial R^2}{\partial y_s} \\ \frac{\partial R^2}{\partial z_s} \end{bmatrix}$$

All three coordinates of the source estimate $S(x_s, y_s, z_s)$ are modified in each iteration. The algorithm converges and stops when delta becomes small or the following estimation fails to reduce R^2 . The source position is continuously re-estimated using this method, however, the initial estimate is set as the source position determined in the previous calculation.[83] T Nakano et al.,. used the same algorithm to localise Ir-192, HDR source with 12 diamond detectors within an inhomogeneous phantom. The algorithm described above was used with the addition of weighting parameters accounting for the attenuation through different tissues. The algorithm and detector achieved a real-time localisation of the source within 3 mm. The methodology used serves as an important archetype for source localisation, however, a 3 mm accuracy is not sufficient for HDR brachytherapy but the system will be able to detect large errors. [71] Joel Poder et al.,. also investigated adjustment of the non-linear least squares algorithm to overcome the effect of the TRUS probe for the Magic Plate 900, a 30x30 diode array. Because of the positioning of the TRUS probe, primary radiation from the HDR source during prostate treatment would be blocked affecting the algorithm's source tracking accuracy. Monte Carlo simulations using the Geant4 toolkit were used to create source positions within a voxelised patient geometry and the MP900. Reconstruction of the source position differed from 11.9 ± 2.4 mm and 1.5 ± 0.3 mm with and without the TRUS probe inserted. This demonstrates the degrading effect the TRUS probe has on the system's source localisation accuracy. To mitigate this effect a signal threshold was implemented within the algorithm. Any dose deposited below this threshold was not used for the localisation calculation. A threshold of 70% of the maximum dose deposited demonstrated the least error, achieving a tracking accuracy of 1.8 ± 0.4 mm with the TRUS present.[84]

The iterative algorithm has provided adequate source localisation through homogeneous media for quality assurance and adjustment has allowed for solutions in inhomogeneous source tracking.

The optimisation of these localisation algorithms in each case has utilised signals which originate from multiple detector elements to determine the position and timing information of HDR brachytherapy sources. The algorithm is effective as it allows the incorporation of factors such as weighting for inhomogeneity or angular dependence. The MP121's use in HDR source tracking is indicative of a localisation algorithm that provides the spatial and temporal resolution which is critical for the evaluation of HDR brachytherapy, due to its large dose gradients and high dose rates.

2.9 End-to-end Verification of HDR Gynaecological Brachytherapy

The complexity which accompanies modern imaging-based HDR brachytherapy requires advanced quality assurance to maintain the safety and efficacy of the treatment. The ideal testing procedure will command an evaluation of the complete process. End-to-end testing assesses the entire procedure to determine faults that will present as an incongruency between the prescribed treatment plan and what is implemented. All end-to-end phantoms have a component that houses the gynaecological applicator for treatment planning and detector type that allows HDR source localisation to monitor the treatment. This ranges from Radiochromic film, ion chambers or an EPID panel. An end-to-end phantom is the gold standard of quality assurance as it serves multiple clinical failures within one test, evaluating planning procedure, catheter reconstruction, imaging procedure and a host of treatment delivery errors/uncertainties. The ability to evaluate the entire workflow enables an opportunity to seek improvement within the current treatments or assess the impact of a newly commissioned device. Both are extremely important to achieve optimal patient outcomes.

There are multiple approaches to creating an end-to-end quality assurance system using different technologies. Hiroyuki Okamoto et al, produced a phantom that houses both a tandem-ovoid

applicator and Radiochromic film. Enabling the prescription, imaging, planning and treatment to be performed on the phantom. Three tests were conducted; the reproducibility of 5 source positions, source movements within the catheters and the subsequent change in source position given a curve in the transfer tube. As a trial study, the phantom was mailed to 12 institutions and 2 sets of data were obtained and analysed. Reproducibility of source position fell within 1 mm, movement within the interstitial needles was small at 0.1 mm and curving of the transfer tube resulted in a source position disparity of under 1 mm for all degrees of curvature. The study demonstrates the end-to-end phantom's competence in performing in-depth quality assurance (QA) of the treatment process. [85] The study is extremely important as it provides the potential to use a standard end-to-end apparatus to effectively audit the treatment planning and implementation accuracy of multiple institutions. However, the use of film for these measurements is time-consuming in a clinical setting and diode-based source tracking would provide a practical solution to including the use of an end-to-end phantom for routine QA. An end-to-end test is integral in gynaecological brachytherapy, in contrast with QA techniques such as those conducted by Gerardy et al., which cannot be considered a clinical gold standard as an assessment of both treatment planning and treatment delivery are not accomplished.[68]

Antony et al, also outlined an end-to-end QA approach, describing the study as a full system dosimetric audit comparing the planned and delivered HDR gynaecological brachytherapy dose distributions. The phantom used is a water tank with film and applicator holders made from Solid Water.[86] Solid Water is an epoxy resin-based substitute that has radiation characteristics similar to that of water, Constantinou C, Attix FH, Paliwal BR found it to have only a 0.2% difference in the transmission of X and gamma rays when comparing 10 cm of water and Solid Water. [87] Films are positioned to bisect at high-risk clinical volumes. CT data is taken to conduct the treatment plan involving applicator reconstruction. Gamma analysis is conducted to compare the multichannel dose maps and the TPS dose distributions. Antony et al ran two pilot audits with the prior mentioned set-up using Ir-192 and Co-60 sources resulting in a mean gamma passing rate of 98.6% with 3% /

3 mm (Dose Difference/DTA). An end-to-end study used to evaluate an institutions treatment has been achieved, a method which systematically assess clinical treatment workflow.[86]

End-to-end systems have recently undergone significant development incorporating sophisticated technologies to address QA needs of 3D imaging centred gynaecological brachytherapy. Fabian Krause et al., in 2018 developed a water phantom with a specialised PMMA applicator and ion chamber holders developed to fix the clinical geometry in place within the phantom. A full clinical workflow including CT imaging of the phantom and BrachyVision v.13.7., a treatment planning with the TG-43 based dose calculation. Reference dose points are calculated on this TPS and compared to the PinPoint 3D ion chamber, which is fixed 6.5 cm from the vaginal cylindrical applicator. An MBDCATPS is also used for comparison measurements for a shielded vaginal cylindrical applicator. The end-to-end phantom evaluated the computed doses and found a deviation of less than 5% between the computed and measured dose points. As expected the MBDCATPS calculated dose showed little deviation from the ion chamber measurements when performing end-to-end analysis for the shielded vaginal cylinder applicator. Alternatively, the TG-43 based TPS experienced a large deviation due to the tungsten shielding used. This illustrates an end-to-end phantom's ability to evaluate new technologies and treatment techniques. Error simulation is often tested in an end-to-end system to assess the phantoms ability to detect common clinical errors, Fabian Krause et al., implements this in two tests. One of which examines the systems ability to detect applicator displacement, by shifting the position of the applicator relative to the ion chamber by 1 cm and the second, a switching of dwell weightings within the treatment plan. The ion chamber/water-based phantom detected a deviation of 9.4% for the applicator shift and 1.1% for the dwell positions switching. Although this end-to-end system can evaluate planning and treatment discrepancies it will require a large number of measurements and troubleshooting to identify specific errors such as applicator/catheter reconstruction or multichannel systems being assigned to the incorrect after loader channel. The study does provide an adequate archetype for an end-to-end quality assurance system but lacks the timing and spatial acquisition data when compared to other sophisticated systems, which use 3D source tracking that

the Magic Plate or an electronic portal imaging device (EPID) will provide.[77][88] Gabriel P Fonseca et al, demonstrates a significant improvement of the end-to-end phantom as the study utilises this EPID technology coupled with a water phantom which houses a multichannel vaginal cylindrical applicator to create an end-to-end phantom. However, the added complexity of using an EPID panel means a range of calibrations such as darkfield correction, pixel sensitivity, energy dependence and non-linearity which need to be applied. These systems also enable 3D source tracking which requires the application of additional analysis, similar to what is outlined in the Magic Plate, Localisation Algorithm section. Unlike previous end-to-end systems, Gabriel P Fonseca et al, alters the workflow of the original treatment as the applicator and water phantom are imaged separately with the two image sets fused before planning.[89] A robotic arm is used to accurately position the applicator within the phantom, according to the CT coordinate system. This does introduce the potential of fusion/co-registration uncertainties as well as the intricacy of using a robotic arm but produces sophisticated error detection and a source localisation uncertainty of 2 mm or less. Three errors were simulated; 1) certain dwell positions were set to zero, simulating a missing dwell position, 2) all dwell positions were shifted, each catheter by different amounts and 3) two channels were swapped. Each error was not only identifiable but distinguishable, there were specific characteristics in the positional and temporal data which enabled error identification. A feature that was not present in the Krause et al, ion chamber setup.[88] The use of an EPID panel for HDR source tracking is a sophisticated end-to-end system that accurately performs QA for the treatment procedure and identifies potential failures and errors. However, the availability of a robotic arm within the setup and the EPIDs elaborate calibration requirements will be laborious within a clinical setting. The end-to-end system should be capable of fitting into an MRI based workflow which is common for these gynaecological treatments although this is not tested within the study. This is the most complete end-to-end, HDR brachytherapy phantom within the literature, enabling an efficient review of the planning and treatment errors to ensure optimal treatment quality.[89]

The development of an end-to-end testing system in each case has allowed a progression of error

detection and quality assurance within the HDR brachytherapy procedure. 3D imaging, applicator reconstruction, planning and after-loading uncertainty largely impacts the safety and effectiveness of the treatment. The end-to-end QA approach enables a complete view of treatment quality as well as data transfer methods and evaluating the function of new devices or software within the workflow. The application of the Magic Plate into an end-to-end phantom enables HDR tracking capable of localisation and treatment timing properties to detect and distinguish clinical uncertainties and failures for gynaecological brachytherapy.

Chapter 3

Materials

3.1 Iridium-192

HDR brachytherapy involves the insertion of a radioactive source internally. The small size of Ir-192 enables more flexibility in the treatment plan. The radioisotope has a half-life of 73.8 days, meaning the source has to be changed every 3-4 months.[5]. Source tracking relies on the detection of photons that the source emits. The complex decay pattern of Ir-192 results in twenty-nine gamma emissions, with a minimum energy of 110keV and maximum energy of 1.378MeV. Most notably, gamma emissions are 296keV, 309keV, 317keV and 468keV with probabilities ranging from 29% to 83% respectively. Electron emissions are mostly absorbed by the encapsulation of the source.

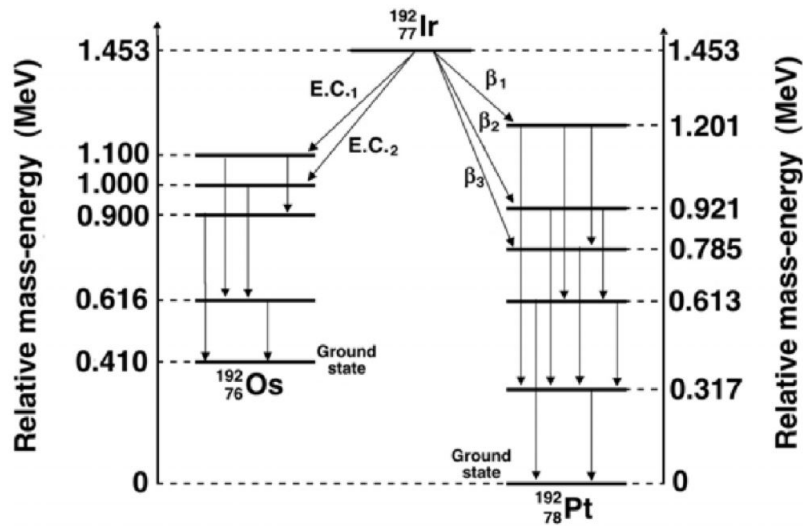


Figure 3.1: Decay scheme of Ir-192 [5]

As seen in figure 3.1 Ir-192 decays with a total of 95.6% probability of β^- decay and 4.4% electron capture.[5] Ir-192 is a common brachytherapy source, encased in stainless steel and attached to a stainless steel cable. The Ir-192 source within the afterloader has an active length of 3.5 mm and a diameter of 0.6 mm. The source is encased within a capsule that has a diameter of 1.1 mm and a length of 5 mm. [90] A dummy source is displayed in figure 3.2 and has the same physical dimensions as the active source. This test source is sent out by the afterloader to check if there are any blockages in the catheter.

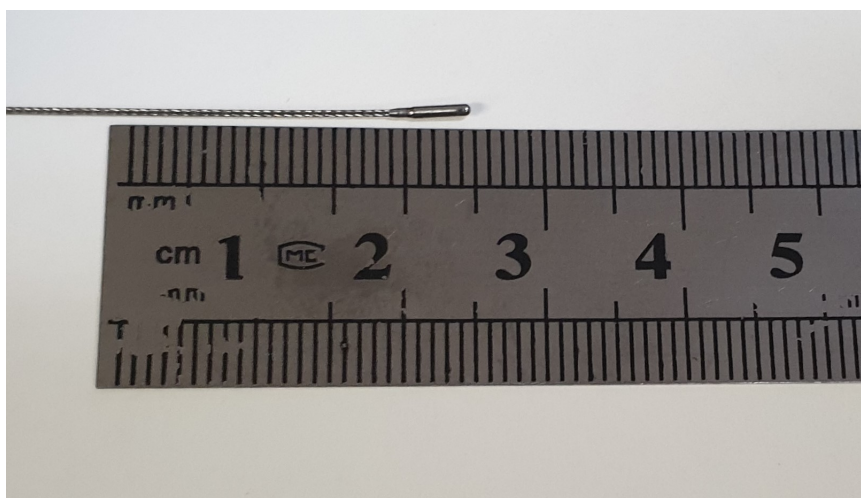


Figure 3.2: A dummy source from the Flexitron afterloader

3.2 Afterloader

The HDR Ir-192 source is controlled by an afterloading machine which sends the source out to pre-determine positions for specific dwell times. The remote afterloading device used within the following experiments is the Elekta Flexitron displayed in figure 3.3. The afterloader also enables safe storage of the source and a mechanism to retract and store the source during emergencies, such as power failures, or other interlocks.[91]



Figure 3.3: Elekta Flexitron HDR brachytherapy afterloader at St George Cancer Care Centre

3.3 Gynaecological Applicators

Gynaecological applicators are medical devices that are inserted into patients to provide a path for the source to travel. Transfer tubes are used to connect the afterloader to catheters or the applicator. The applicators used within this study are CT and MRI safe. This enables patient imaging after insertion without distortions and artifact. As previously described the Multichannel Vaginal Applicator displayed in figure 3.4 is used for vaginal brachytherapy. The applicator can be used with a balloon and inter-uterine tube attachments. Specialised catheters with rubber cuffs placed into the channels and locked in place. The Fletcher applicator with 30 degree tandem is

used for the cervical end-to-end test. The applicator has three channels when used for intracavitary treatments. The Venezia applicator has two lunar ovoids which click together to form a ring-like structure. The applicator can be used in an intracavitary or interstitial capacity, with holes in the ovoids to guide any required needles. All gynaecological applicators used within this study have been provided by Prince of Wales Hospital, Nelune Cancer Care Centre.



Figure 3.4: 30 mm Multichannel vaginal applicator (Elekta Brachytherapy, Venendaal, Netherlands).[6]



Figure 3.5: Fletcher applicator tandem and ovoid set (Elekta Brachytherapy, Venendaal, Netherlands) [6]



Figure 3.6: Venezia applicator, with added perineal template (Elekta Brachytherapy, Venendaal, Netherlands) [6]

Chapter 4

Determining The Impact of Applicator Displacement for HDR Gynaecological Brachytherapy

4.1 Introduction

A shift in the delivered dose distribution can occur due to a physical displacement of the applicator or catheter within the patient or uncertainty in the reconstruction of needle and applicator position within treatment planning[62][61]. A physical displacement of the applicator and/or needles after imaging has occurred in the workflow demonstrated in figure 2.12 will evoke a shift in the applied dose distribution. This physical shift can occur due to tissue swelling (oedema), while moving the patient on and off imaging equipment and during patient transport. Inaccuracies in applicator reconstruction can transpire due to imaging artifact such as volume averaging or uncertainty in applicator model alignment. Both forms of applicator displacement introduce uncertainty in the relative position between the applicator set and critical volumes. Within the treatment planning procedure optimisation occurs once all source channels, OAR and CTVs are reconstructed. This optimisation is done by hand or via an inverse algorithm and enables the clinician to establish the

required CTV-OAR dose compromise, ensuring both the adequate treatment of CTVs and OAR protection. However, the robustness of each plan needs to be considered as the impact of applicator displacement due to reconstruction uncertainty or physical displacement can be dangerous if the plan is overly optimised.[60] Retrospectively, finding critical limits of applicator displacement using optimised patient treatment plans will help practitioners make decisions that mitigate the risk of applicator shifting when optimising treatment plans, maintaining imaging and applicator quality control and creating implant insertion protocols.

In this section, the impact of applicator displacement will be determined and a distinct limitation will be developed to determine the “in vivo source tracking error threshold”. Initially derived for prostate treatments, the in vivo source tracking error threshold is the difference in dwell position from the original plan that requires the treatment to be stopped.[92] Similarly the in vivo source tracking error threshold can serve as a benchmark to which an HDR source tracking system will need to perform. If a discrepancy in source position which is clinically unacceptable is established then a source tracking system must be able to localise the source within this margin.

The impact of applicator displacement will be determined for two purposes:

- Demonstrated the importance of protocols that mitigate the risk of a physical displacement in applicator position and reconstruction uncertainty
- To provide a clinical benchmark for the End-to-end source tracking phantom by establishing a deviation from the planned dwell position which causes a critical deterioration in treatment efficacy and safety

4.2 Method

Applicator displacement will be simulated retrospectively using patient treatment plans and contoured structure sets to calculate a critical limit of displacement. The study will retrospectively calculate treatment plans after a shift in dwell position has been implemented on each plan. The dose to organs at risk and the HR-CTV will be calculated for the shifted plan without re-optimisation to simulate clinical applicator displacement and determine what impact this displacement of dwell positions will have on treatment end-points. Patient data has been extracted from Prince of Wales Hospital, Nelune Comprehensive Cancer Care Centre. Patients have been selected for the study if 18 years of age or over and have undergone brachytherapy for cervical cancer stages IIB, IIIA or IIIB. The patients have had brachytherapy as a local boost to accompany their external beam therapy and chemotherapy treatments. Once patients are selected, all patient data used for the study are anonymised and identified by their assigned unique identification code. The code assigned includes a number and a letter that signifies the applicator or set up used. The required South Eastern Sydney Local Health District Ethics approval has been granted, under the Department of Radiation Oncology Research Authorisation Number, SESLHD-NRA REF: 2021/16.

Two types of digital imaging and communications in medicine (DICOM) files are exported from Oncentra Brachytherapy treatment planning system (Elekta, Stockholm, Sweden) for each patient. While exporting, Oncentra Brachytherapy is set to anonymise the files removing any patient information. A treatment plan file and structure file is exported for each patient. Treatment plan DICOM files contain all dwell positions in 3D space and dwell times for the treatment, as well as the prescription and other relevant set-up specifications. A single fraction of the multi-fraction treatment is considered for each case.

A structure set DICOM file contains the contours which are drawn on each slice of the planning image to outline each OAR, catheters, HR-CTV and IR-CTV. The slice by slice outline of relevant structures within this file can be seen in figure 4.1, these are not all the structures in each file, the

IR-CTV has been removed from the figure to view the HR-CTV well. The reconstructed volumes and positions can be demonstrated in figure 2.3 which are combined with the treatment plan to calculate the dose to each volume.

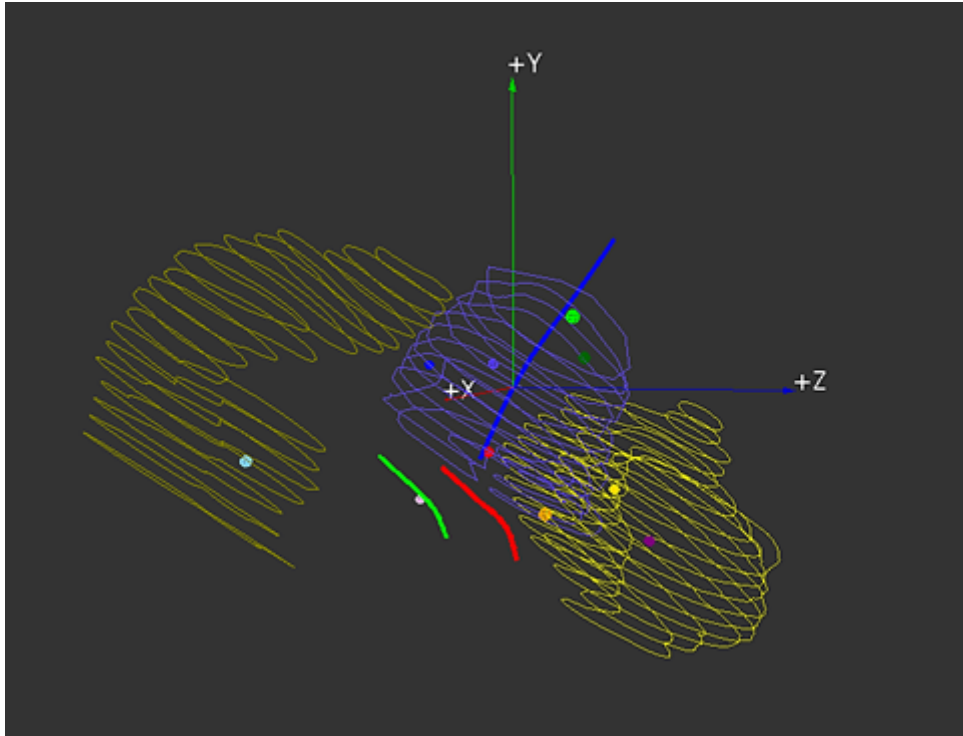


Figure 4.1: A treatment structure set DICOM visualised in RadCalc, a secondary check program (Lifeline Software, Austin, USA). The contour of each slice is displayed, with the rectum on the left in dark yellow, the HR-CTV a purple structure in the middle and the bright yellow structure to the right a bladder. The channels of a Fletcher applicator is seen with the tandem in bold blue within the HR-CTV and the ovoid channels in red and yellow.

A displacement of dwell positions and recalculation of dose to OAR and HR-CTV without re-optimisation enables the simulation of applicator displacement due to both reconstruction uncertainty and physical displacement due to failures within the procedure. To displace the dwell positions a Python script is developed using the Pydicom package, a package that allows the reading and adjusting of many different DICOM file types. The displacement script used loads in a patient treatment plan DICOM and then shifts all catheters along one of the three axes, Anterior-Posterior (Ant-Post), Superior-Inferior (Sup-Inf) or Right-Left demonstrated in figure 4.2. Displacing all dwell positions by a specific displacement value and a new treatment plan file is saved.

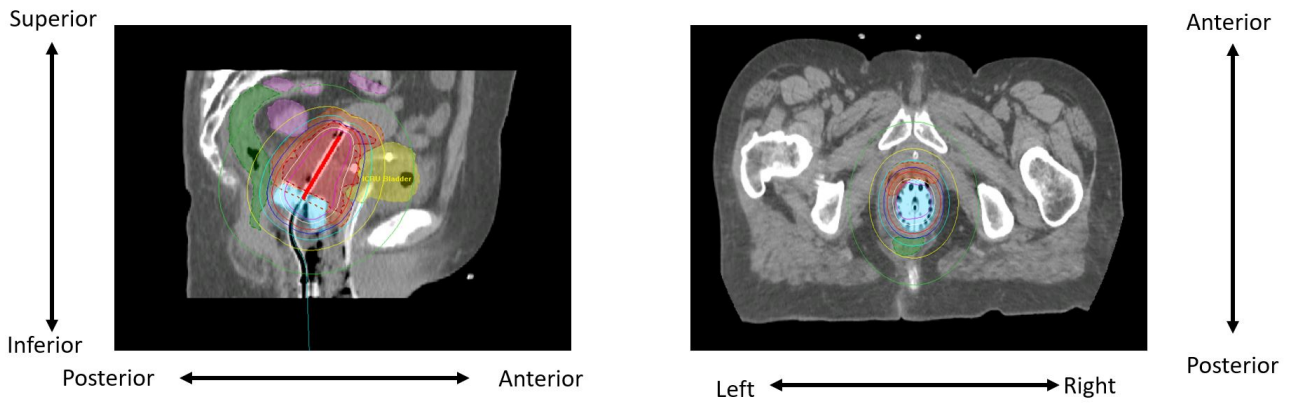
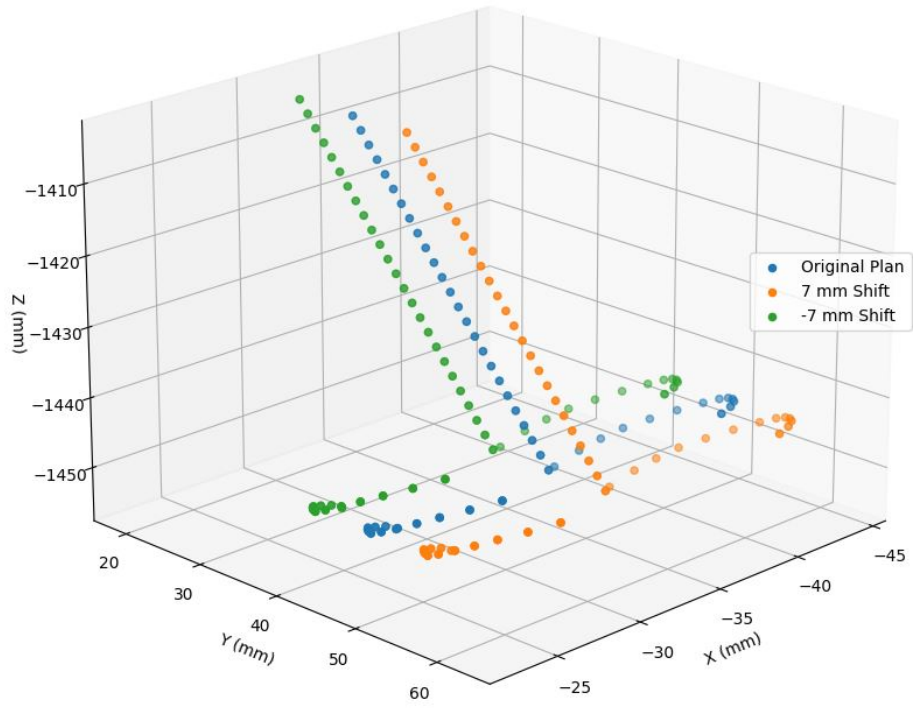
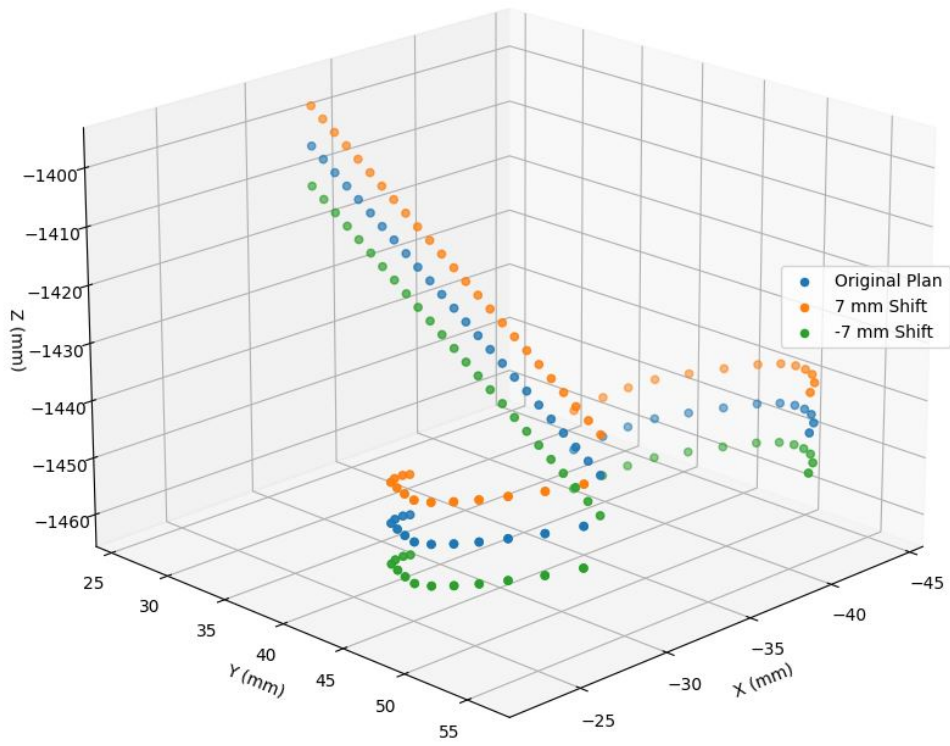


Figure 4.2: Definition of the axes used in relation to the anatomy

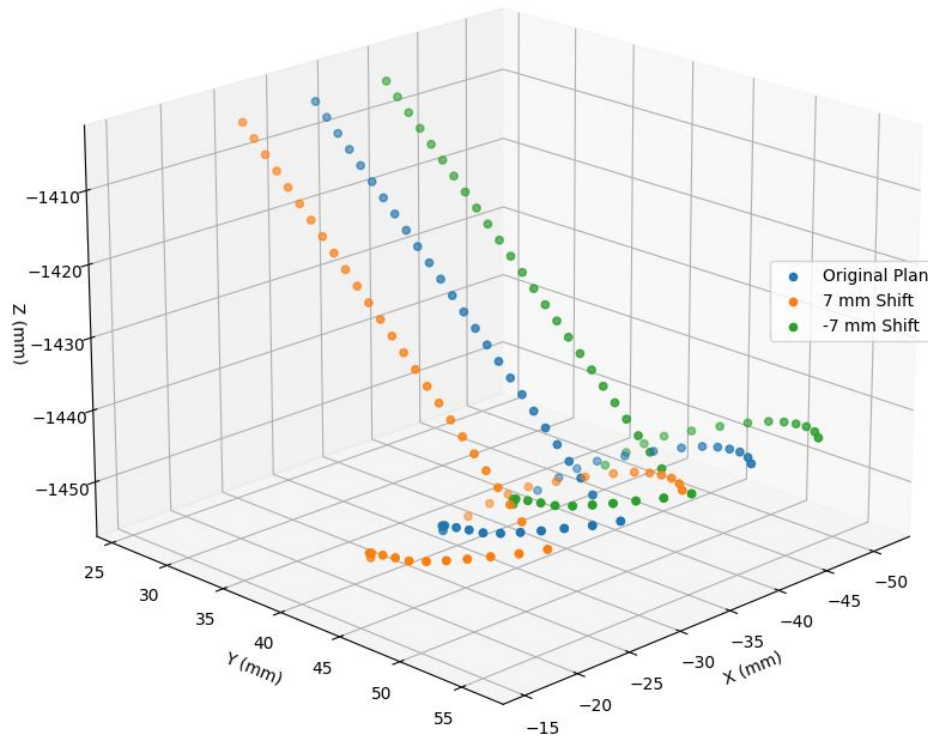
A maximum displacement of ± 7 mm has been calculated in each direction. The current literature investigates maximum shifts of ± 5 mm by Kari Tanderup et al, ± 6 mm by Joel Poder et al, and ± 10 mm and ± 20 mm by Joshua Schindel et al.[61][60][62] These displacements have been investigated as they emulated the possible uncertainty present for the combination of reconstruction and physical displacement uncertainties. A range that is suitable amongst the literature while clinically realistic has been chosen as ± 7 mm which should cover a combination of errors and uncertainties.



(i) Anterior-Posterior shift



(ii) Superior-Inferior shift



(iii) Right-Left shift

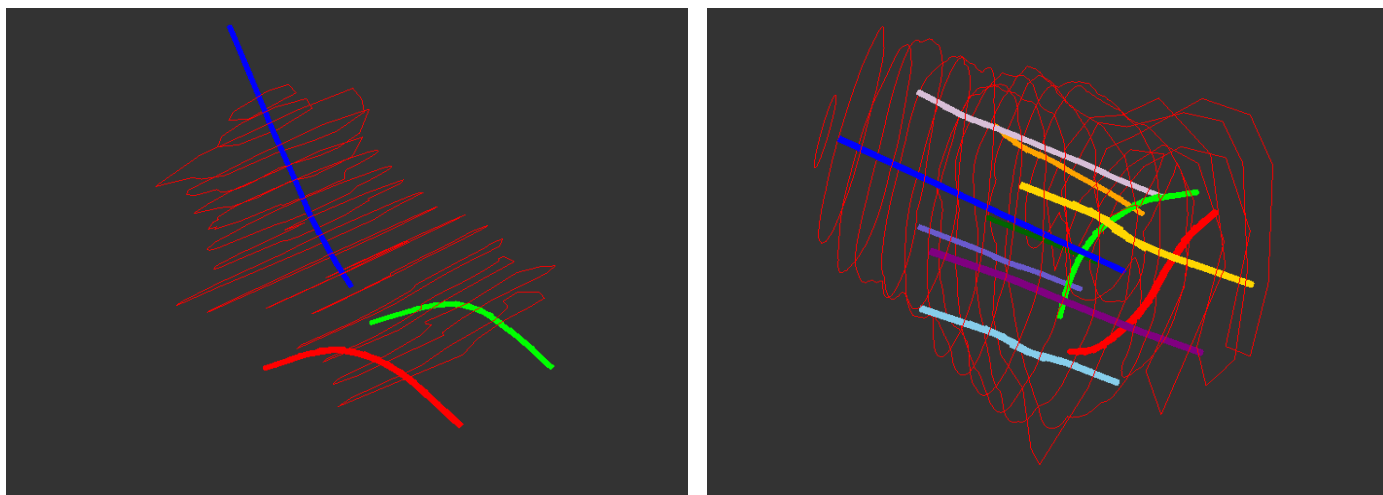
Figure 4.3: The Python displacement script created to simulate applicator displacement demonstrates its function to change dwell positions, shifting a maximum of ± 7 mm along each axis.

The Python script loads a patient treatment plan, then shifts all dwell positions by a specific value, which ranges from -7 mm to 7 mm in 1 mm increments along one axis with a new treatment plan created for every increment. Thus each initial patient treatment plan produces 14 altered treatment plans along each axis. This is then repeated for all three Ant-Post, Sup-Inf and Right-Left directions, producing a total of 42 altered treatment plans for each patient. Figure 4.3 demonstrates the dwell positions plotted for an intracavitary treatment plan. The tandem and lunar ovoid set can be identified since a Venezia applicator has been used for this treatment. The figures demonstrate a 7 mm shift of the original plan in each direction, revealing the Python displacement script's function.

Figure 4.3 demonstrates the definition of directions used when discussing the results. A positive shift relates to a posterior displacement along the Anterior-Posterior axes, a superior shift along the Superior-Inferior axes and a shift left when discussing the Right-Left direction. With a negative value signifying the opposite direction (anterior, inferior, right).

The original treatment plan and structure set as well as the 42 altered treatment plans are imported into RadCalc, the secondary check program (Lifeline Software, Austin, USA). This software is clinically used as an independent QA of treatment plans to verify the dose delivered. The program uses a TG-43 formalism to determine the dose to critical volumes and dose points. Space over which dose calculation will take place is set to 10 mm around all structures and a 1 mm³ voxel size is implemented for discretisation. All plans with the same structure set DICOM are bulk imported and are listed under a single patient ID. Individually, each treatment plan is opened and the dose to the bladder, rectum, and HR-CTV volumes are calculated. DVH parameters D_{2cc} is used as a measure of dose to OARs and the D_{90} is used to determine HR-CTV coverage both of which are commonly used as treatment guidelines [25]. D_{2cc} indicates the dose received by the most irradiated two cubic centimetres of each OAR and the D_{90} parameter signifies the dose 90% of the volume received.

The method of altering all dwell positions within a treatment plan without re-optimisation, followed by calculating how treatment endpoints are effected, is applied to both intracavitary (n=21) and interstitial (n=8) cases. Intracavitary treatments entail an applicator implanted within the vagina with the ovoids sitting firmly against the external os of the cervix and the tandem extending through the cervix. Interstitial plans use additional needles to treat a further spread of the disease. The difference in the treatment types can be seen in figure 4.4, where it is clear that the larger HR-CTV in 4.4ii requires peripheral catheters for adequate dose coverage.



(i) Intracavitary treatment with Fletcher applicator. (ii) Interstitial treatment with Venezia applicator and seven needles inserted.

Figure 4.4: The two treatment types used within the study demonstrated with the HR-CTV being treated in red

Additionally, applicator rotation for intracavitary cases has been considered to quantify the impact of failure during surgical insertion. Once the implant is placed against the external os of the cervix, surgical gauze is packed around the applicator to hold it in place. Inadequate or imbalanced packing can cause applicator rotation, which cannot be accounted for after imaging has taken place and thus a rotation of the applicator about the intrauterine tube (tandem) is being considered for intracavitary cases. Interstitial cases have been excluded since the needles which are inserted through the ovoids and tissue should provide a firm anchor, making rotation unlikely. The tandem has been taken as a possible axis of rotation for the applicator set as the cervix should limit rotation along other axes. A Python script has been developed to simulate applicator rotation by rotating all dwell positions about the tandem, $\pm 20^\circ$ in 5° increments. The script constructs a line between the first and last dwell position in the tandem and uses this as an axis of rotation, the effect of which can be seen in figure 4.5. 8 altered treatment plans are created for each of the 21 intracavitary patients. These plans were also recalculated in RadCalc without re-optimisation to determine the impact applicator rotation can have on treatment endpoints concerning dose to organs at risk and HR-CTV coverage.

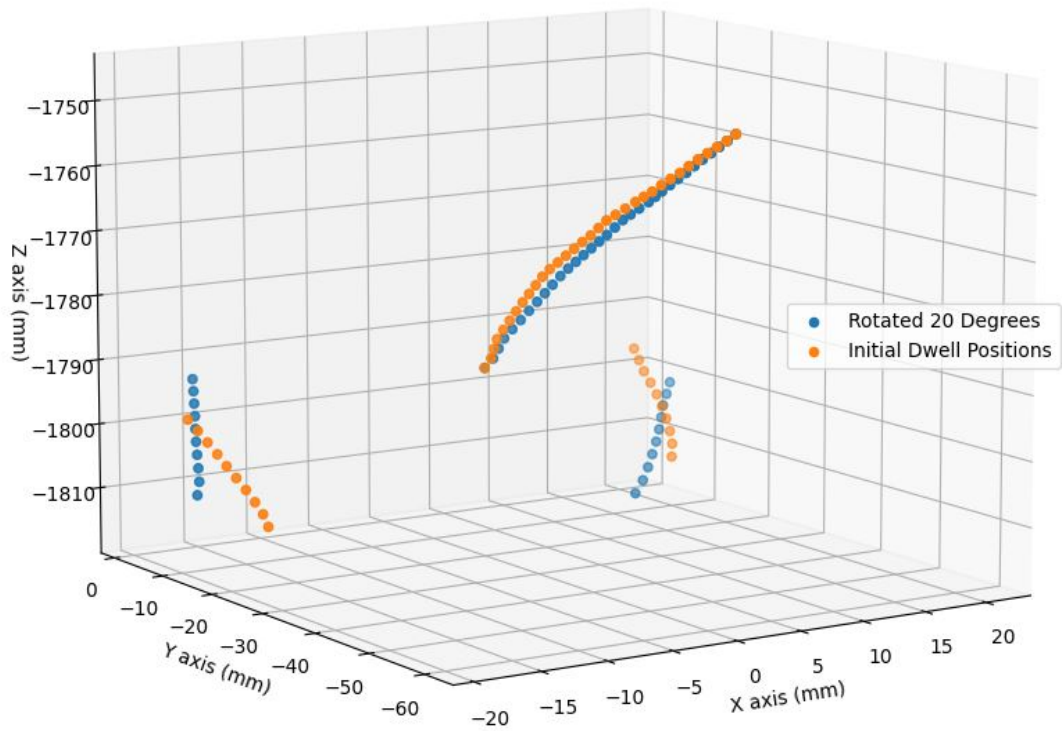


Figure 4.5: Fletcher applicator treatment plan rotated 20°

4.3 Results

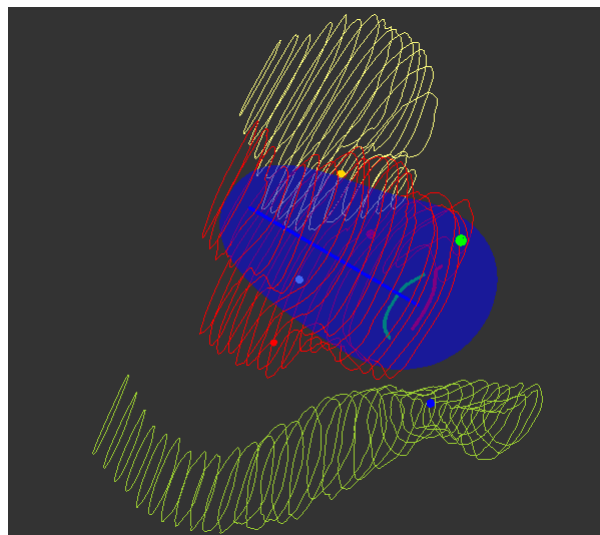


Figure 4.6: Isodose volume position in relation to the bladder, rectum and HR-CTV. The isodose volume is blue, HR-CTV red, bladder yellow and rectum a dark yellow.

The following results demonstrate the impact a displacement in applicator position has on the dose to the bladder and rectum as well as its effect on HR-CTV coverage. When interpreting results one must consider the dose distributions position in relation to the OAR and HR-CTV to identify if the

displacement corresponds with expected results. Figure 4.6 demonstrates the general geometry of an unaltered plan and the isodose volume with relation to the critical volumes in question, expecting an increase in dose as this shifts towards OAR and a decrease in coverage when moving out of the HR-CTV volume.

Figures 4.7 - 4.15 contain multiple boxplots which signify multiple patients at each attribute, whether it is a treatment type in figure 4.7 or a specific displacement in the subsequent figures. These boxplots demonstrate the distribution of each dataset and denote the median with a red line. The lower edge of the blue box illustrates the 25th percentile (Q1) and the upper edge the 75th percentile (Q3). Thus the length of the box signifies the interquartile range, encompassing the middle 50% of the dataset. The maximum and minimum lines are drawn up to 1.5 times the span of the interquartile range, data points which fall outside of which are considered to be outliers and are illustrated with a red “+” symbol.

A positive displacement translates to a Posterior shift when considering the Anterior-Posterior axes, Superior shift for the Superior-Inferior axes and displaces the dwell positions Left for the Right-Left directions. With a negative displacement corresponding to the opposite direction as expected, this is important when considering the expected impact of displacement as the relative change in dose is a function of the distance between dwell positions and the volume considered.

Results for displacement to intracavitary and interstitial plans are presented, as well as a test of the applicator rotation failure. A summary of the critical displacements is listed in table 4.1.

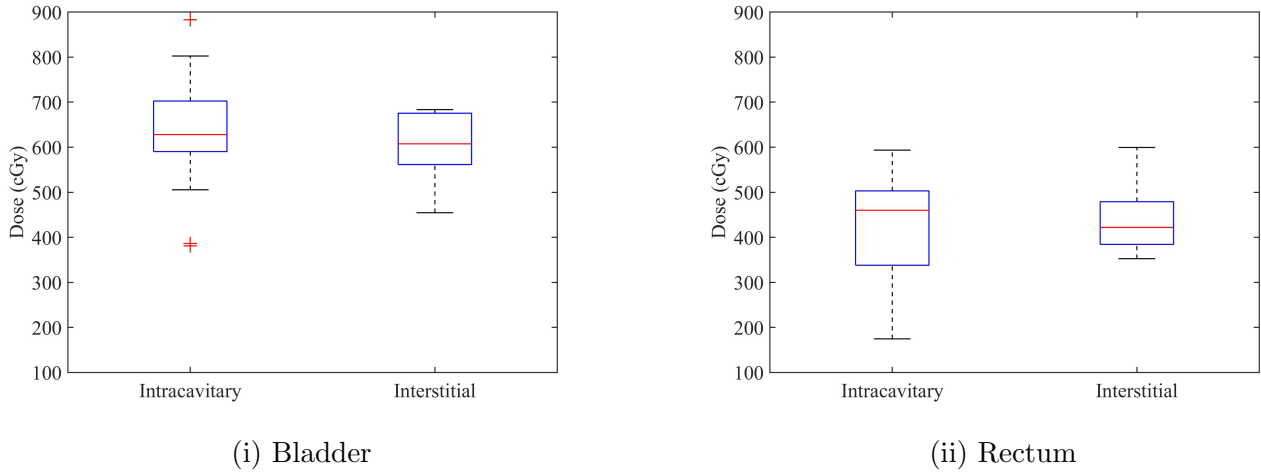


Figure 4.7: Prescribed D_{2cc} for the Organs At Risk

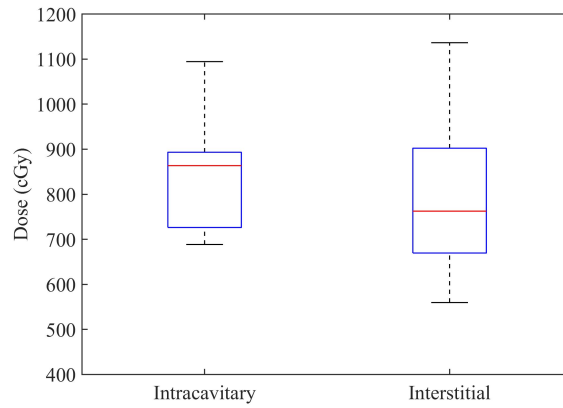


Figure 4.8: Prescribed D_{90} for the High Risk Clinical Treatment Volume

The figures 4.7 and 4.8 demonstrate the dose parameters of the original treatment plans. Generally, the bladder is allowed a higher dose as allowed by the current EMBRACE II guidelines, which is congruent within the dataset, in both interstitial and intracavitary cases. Variation in initial doses within the dataset can be explained by the differing needs of each patient when considering the extent of disease, differences in anatomy and the dose history of the patient. Most notably all cases examined are treatment plans from a single fraction which is part of a three to four fraction treatment schedule, in which dose escalation or de-escalation can occur during the following fractions. Within the governing recommendations, dose constraints are set for the whole treatment schedule, combining all EBRT and brachytherapy fractions.[25] Consequently, determining a threshold displacement based upon absolute dose is inappropriate since only a single fraction can be assessed per plan and

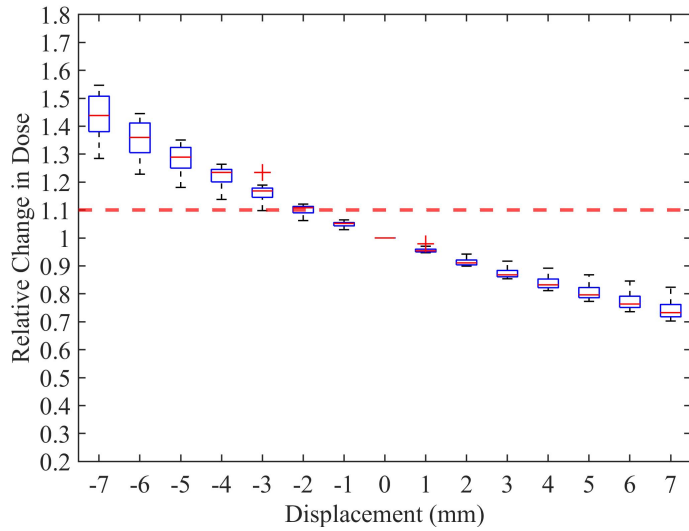
thus applicator displacement is evaluated with a relative measure for this study. [61] In line with the literature, a 10% change in prescribed dose to organs at risk or the HR-CTV has been enforced as a critical threshold.[62]

A relative increase in D_{2cc} for OAR can be detrimental to patient health, similarly, a 10% reduction in the D_{90} HR-CTV can diminish local control. The action level of a 10% relative change to more than 25% of the dataset has been set. Graphically, when the marked 10% threshold is within the blue box of the boxplot 25% of patients would receive more than a 10% relative change in dose for that displacement and the action level is met. This action level is considered the critical limit of applicator displacement and will define a safe HDR source tracking uncertainty for the End-to-end phantom.

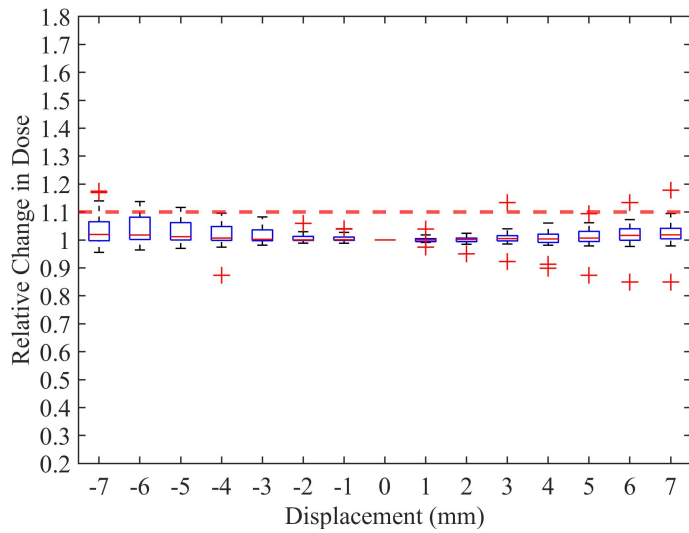
4.3.1 Intracavity Treatments

Applicator displacement has been evaluated for twenty-one intracavitary treatments for displacement in each direction and applicator rotation about the tandem (intrauterine tube).

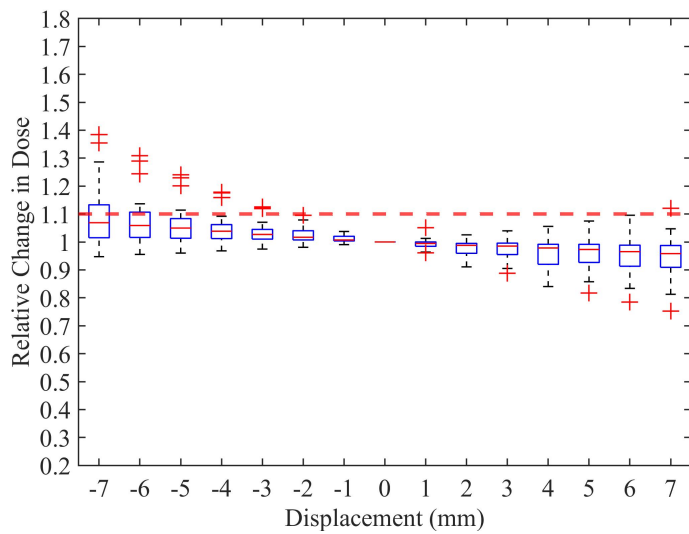
It is important to consider the direction of displacement with respect to the organ or volume in question, as stated in the method a positive shift along the relevant axes relates to dwell position displacement in the posterior, superior or left direction. With a negative displacement value signifying a shift in the opposite direction (anterior, inferior, right). Figure 4.9i reveals a 2 mm displacement meets the threshold, this is expected as dwell positions are being shifted anteriorly, towards the bladder. A shift of the dwell positions towards an organ at risk will be the most sensitive. This is apparent when compared to figures 4.9ii and 4.9iii, where the relative increase in dose is minimal for the bladder, and the error threshold is only met with a 6 mm shift in the inferior direction.



(i) Anterior-Posterior shift

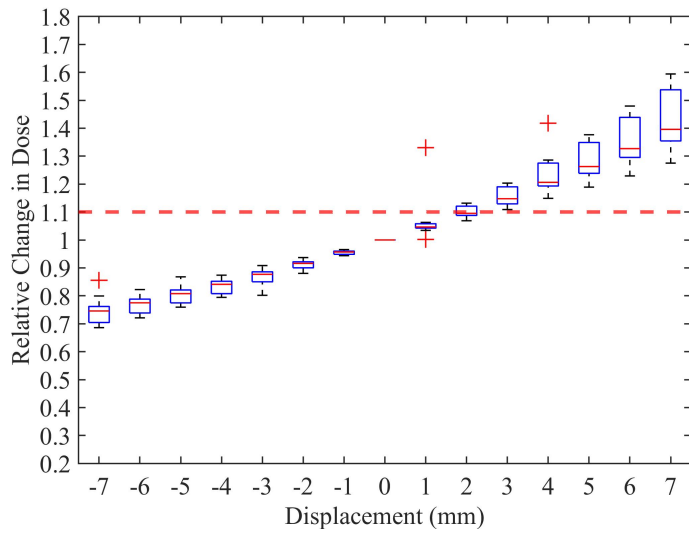


(ii) Right-Left shift

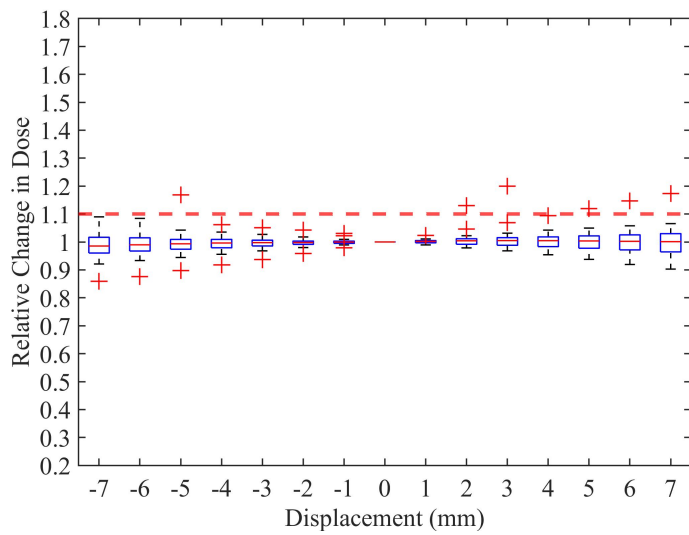


(iii) Superior-Inferior shift

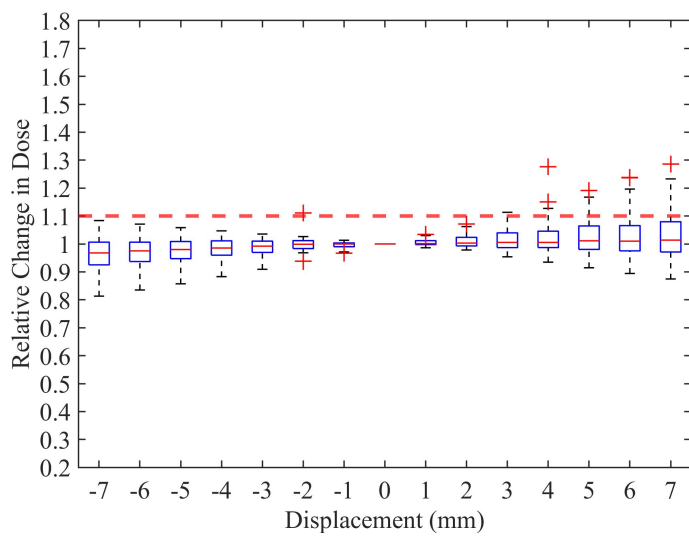
Figure 4.9: A relative change in dose to the bladder has been calculated for each displaced treatment plan. The red dashed line represents a critical change in dose.



(i) Anterior-Posterior shift



(ii) Right-Left shift



(iii) Superior-Inferior shift

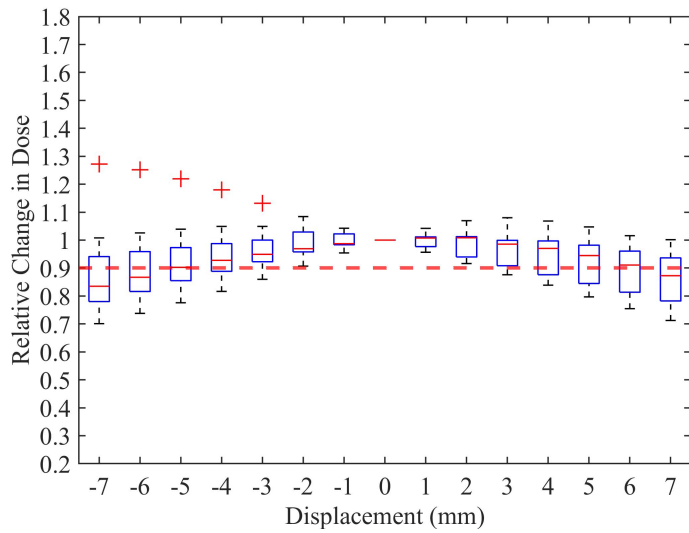
Figure 4.10: A relative change in dose to the rectum has been calculated for each displaced treatment plan. The red dashed line represents a critical increase in dose.

In conjunction with what is found for the bladder, the rectum also experiences the expected trend as posterior shift elicits a 2 mm limitation in applicator displacement and a decrease in dose with an anterior shift, as illustrated in figure 4.10i. A displacement within 7 mm in every other direction has not produced a 10% increase in relative dose to 25% or more of the cases. A clear HDR source tracking error threshold of 2 mm has been established in the Anterior-Posterior direction. There exists a clear sensitivity along this axis which can provide source tracking systems with guidance to prioritise this direction since it is substantially more sensitive. Additionally, a consequential sensitivity of ± 2 mm along the anterior-posterior axis can inform clinical protocol when considering possible treatment uncertainties such as applicator instability or reconstruction uncertainties.

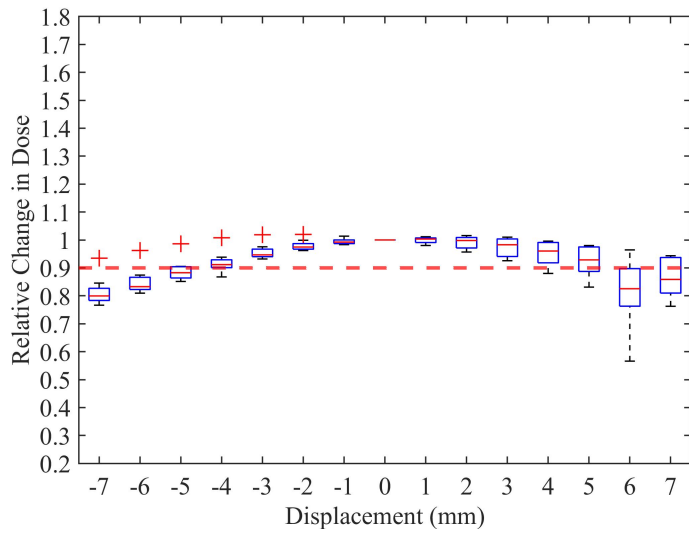
A shift in dwell position has a measurable effect in HR-CTV coverage as demonstrated in figure 4.11. Unlike the impact to OAR, HR-CTV coverage is affected by movement in almost every direction, which is expected when considering a shift in the blue isodose volume in figure 4.6 and how that will affect the coverage of the HR-CTV volume in red. A shift of 4 mm in the left, anterior, posterior and inferior directions causes a significant detriment to local control as well as a 5 mm shift to the right. The effect a displacement in dwell position has on decreasing local control is far less directional dependent since the HR-CTV volume symmetrically surrounds the catheters when considering the transverse plane which the Anterior-Posterior and Right-Left Axis exist on demonstrated in figure 4.4i. This causes the symmetric trend in dose either side of zero displacement displayed in figures 4.11i and 4.11ii. The reduction in dose as dwell positions are shifted inferiorly and escalation in dose superiorly in figure 4.11iii is expected considering the general shape of the HR-CTV volume and the position of the tandem and ovoid channels positioned within the inferior end of the volume. An inferior shift would cause the dwell positions to move towards exiting the volume and conversely a superior shift will drive the dwell positions closer to the middle of the volume. A growing interquartile range is apparent in figure 4.11iii in the superior direction due to a variation in plan and volume from patient to patient. A HR-CTV volume that is shorter in the Superior-Inferior direction will experience a higher sensitivity to a displacement in the superior direction as the tandem will be

removed from the volume and thus removing the dose distribution it provides.

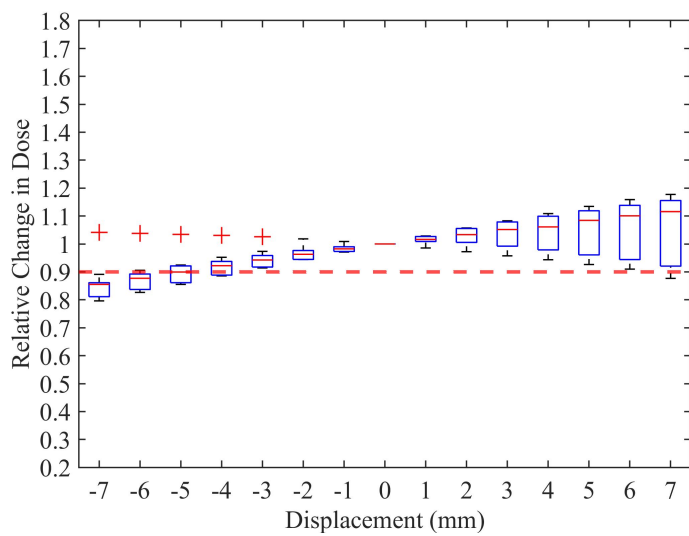
Applicator rotation has been evaluated as possible clinical uncertainty, within a limit that could go undetected during treatment. A rotation about the tandem is considered with the dwell positions within the ovoids shifting accordingly as displayed in figure 4.5. The effects are minimal due to the degree of rotation studied not being large enough to displace ovoid dwell positions close enough to organs at risk. With the bladder reaching its dose threshold at -20° and the rectum overcoming the set tolerance at 20° . Due to the rotational symmetry of the HR-CTV volume in the plane perpendicular to the tandem applicator rotation has no meaningful effect on HR-CTV coverage within the $\pm 20^\circ$ tested. This was an additional test to evaluate a possible clinical error of applicator rotation. Unlike the treatment plans which have been altered via translation, this does not provide a recommendation for HDR source tracking.



(i) Anterior-Posterior shift

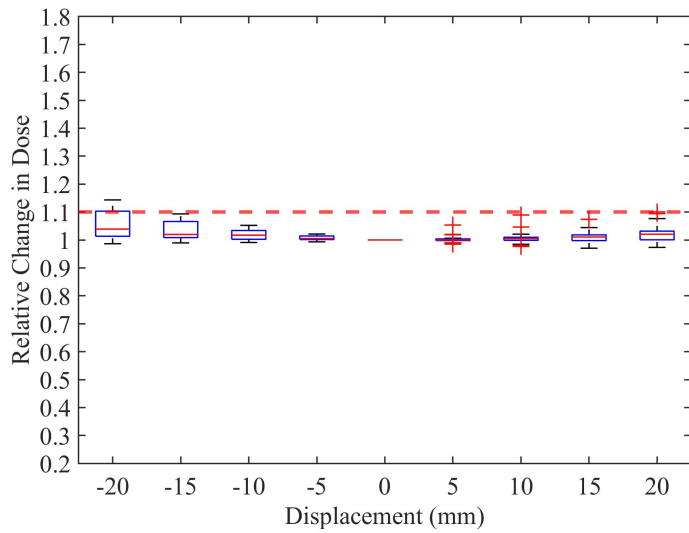


(ii) Right-Left shift

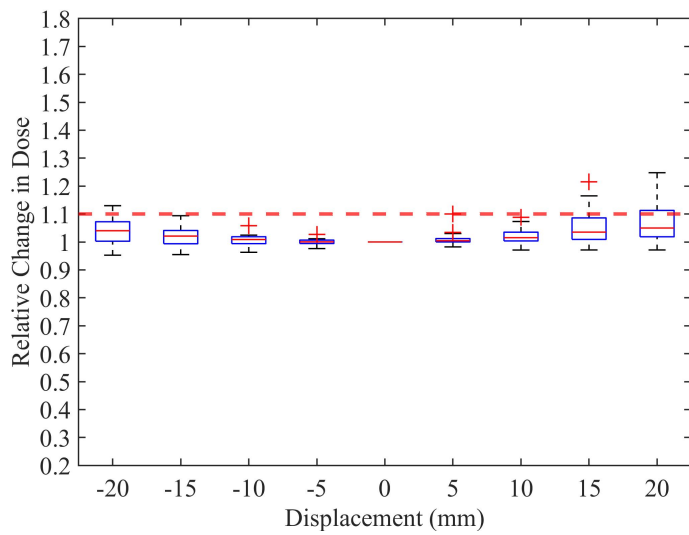


(iii) Superior-Inferior shift

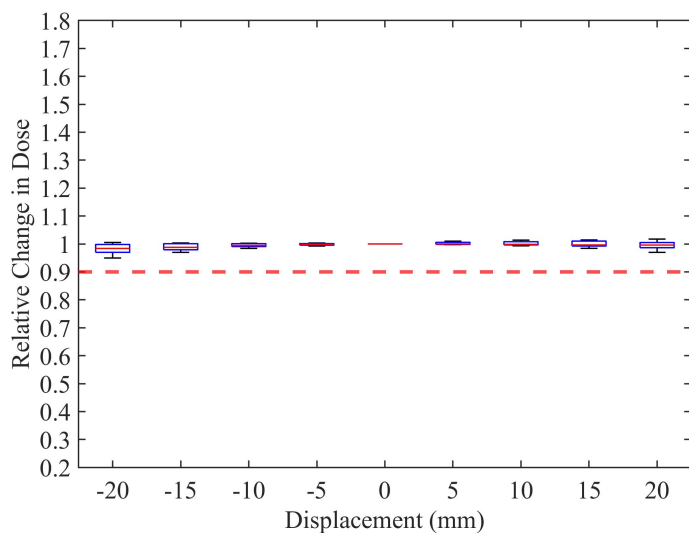
Figure 4.11: A relative change in HR-CTV coverage has been calculated for each displaced treatment plan. The red dashed line represents a critical reduction in dose.



(i) Applicator rotation impacting bladder dose.



(ii) Applicator rotation impacting rectal dose.



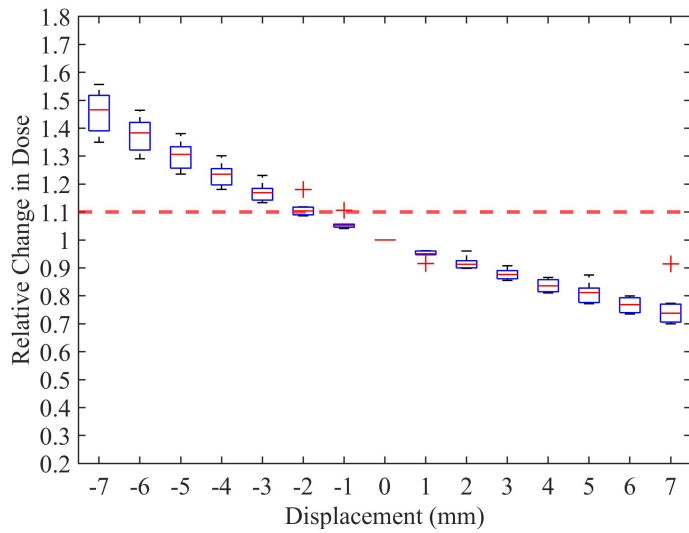
(iii) The effect of applicator rotation on HR-CTV coverage

Figure 4.12: A rotation of the applicator about the axis of the tandem and the relative change in dose. A 10% change in dose is denoted by the red dashed line.

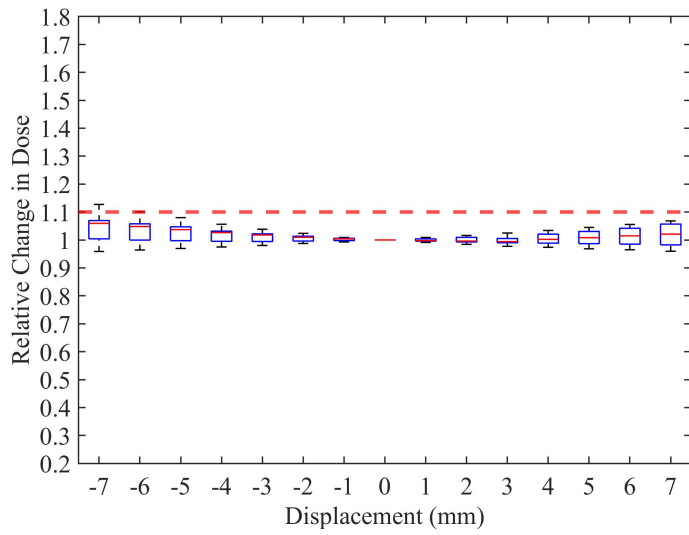
4.3.2 Interstitial Treatments

The displacement of interstitial treatment plans have produced results similar to the intracavitary cases, however, as expected are more sensitive in some cases as dwell positions may exist closer to OARs. Interstitial plans are identical to the intracavitary plans for the rectal and bladder critical limits of 2 mm and -2 mm respectively when considering the Anterior-Posterior direction as well as a null result along the Right-Left axis. The interstitial plans are more sensitive to displacement in the Superior-Inferior directions for both OARs, with the bladder's displacement limit being a 4 mm inferior shift and rectum a 5 mm superior shift.

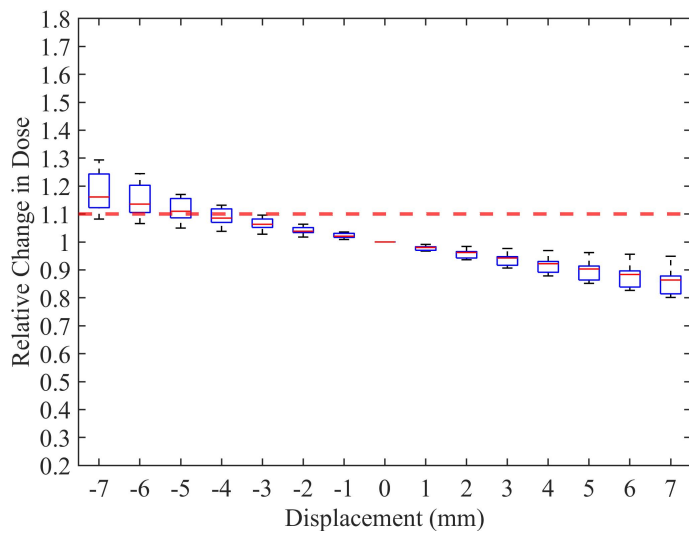
The HR-CTV again demonstrated a critical displacement in each direction, yielding a respective -5 mm and 3 mm shift in the Anterior-Posterior direction, a -4 mm and 5 mm displacement in the Right-Left direction and a -4 mm and 7 mm shift in the Superior-Inferior direction. Overall, the HR-CTV demonstrated similar traits to what has been found for the displacement of intracavitary plans. A direct comparison of interstitial and intracavitary treatment plans are demonstrated in table 4.1.



(i) Anterior-Posterior shift

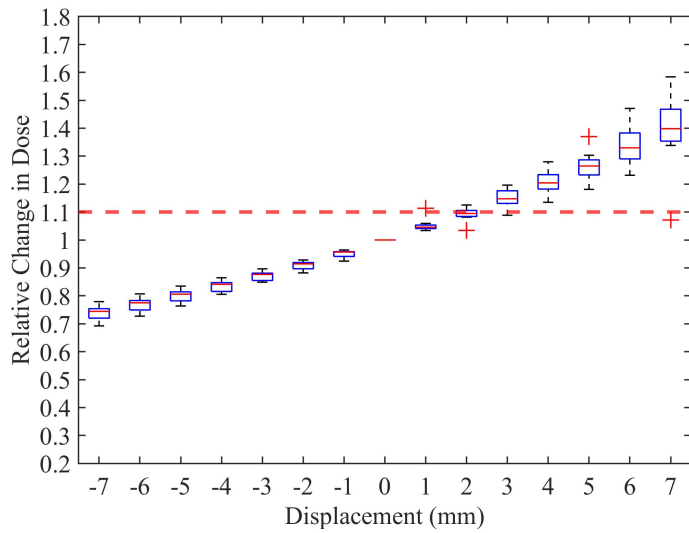


(ii) Right-Left shift

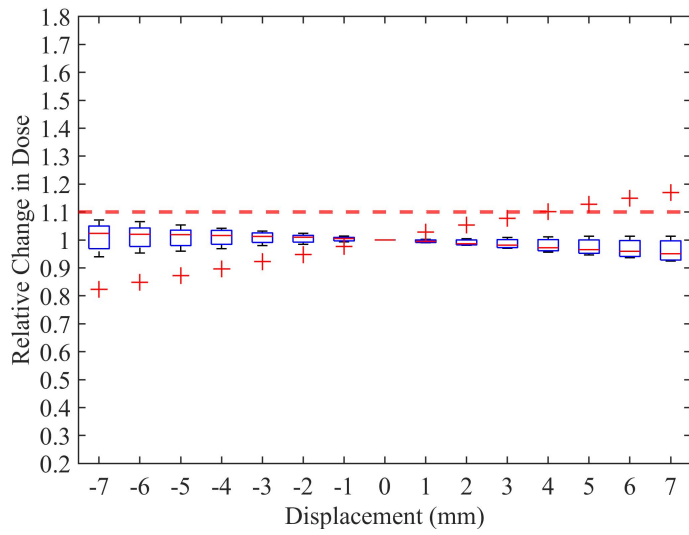


(iii) Superior-Inferior shift

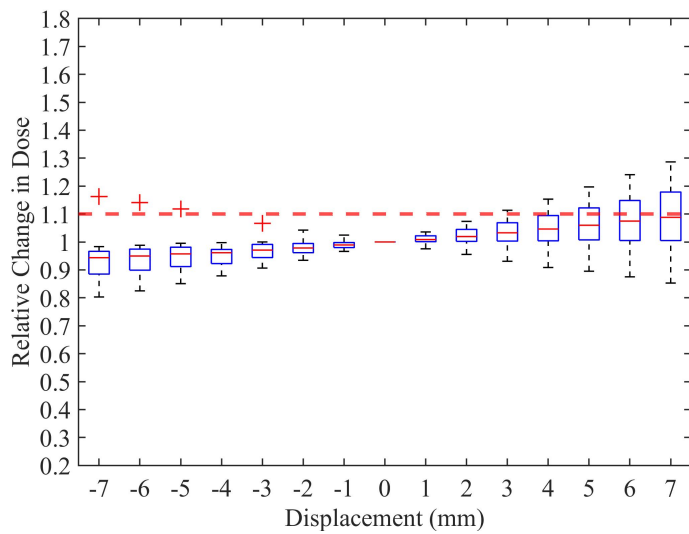
Figure 4.13: A relative change in dose to the bladder has been calculated for each displaced treatment plan. The red dashed line represents a critical change in dose.



(i) Anterior-Posterior shift

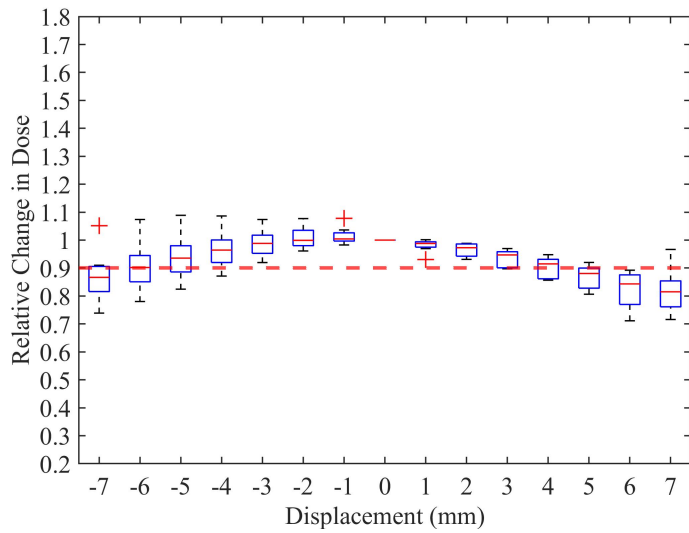


(ii) Right-Left shift

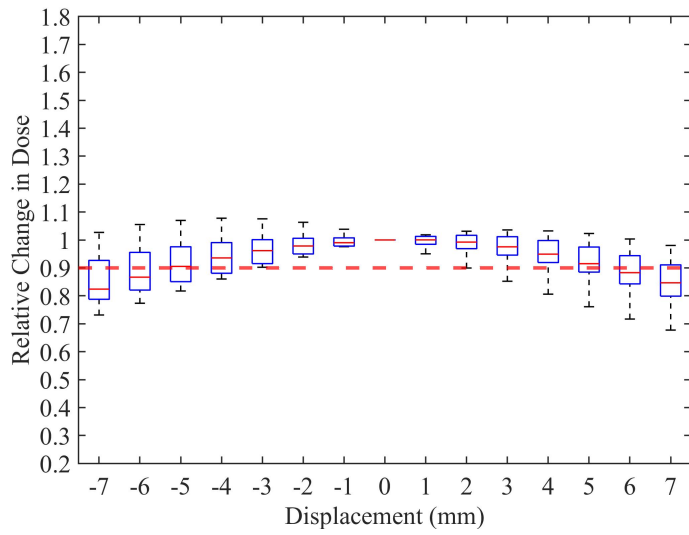


(iii) Superior-Inferior shift

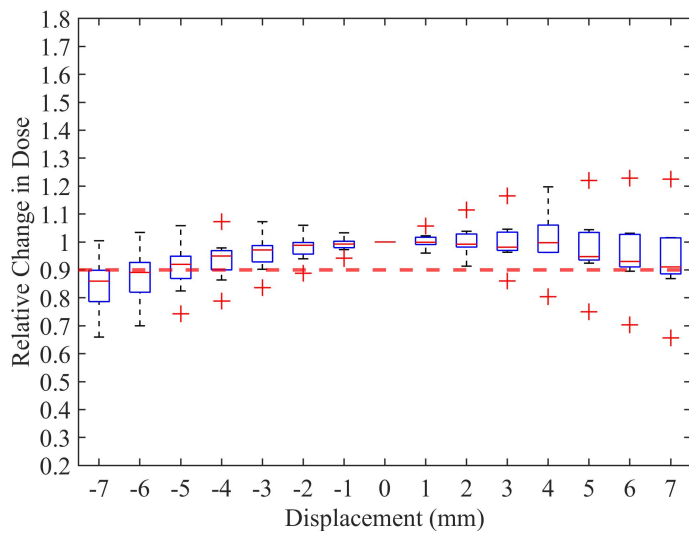
Figure 4.14: A relative change in dose to the rectum has been calculated for each displaced treatment plan. The red dashed line represents a critical change in dose.



(i) Anterior-Posterior shift



(ii) Right-Left shift



(iii) Superior-Inferior shift

Figure 4.15: A relative change in dose to the HR-CTV has been calculated for each displaced treatment plan. The red dashed line represents a critical change in dose.

Critical Volume	Direction	Intracavitary Plan Displacement(mm)	Interstitial Plan Displacement(mm)
Bladder	Anterior-Posterior	-2	-2
	Right-Left	Null	Null
	Superior-Inferior	-6	-4
Rectum	Anterior-Posterior	2	2
	Right-Left	Null	Null
	Superior-Inferior	Null	5
High-Risk CTV	Anterior-Posterior	-4,4	-5,3
	Right-Left	-5,5	-4,5
	Superior-Inferior	-4,7	-4,7

Table 4.1: Summary of critical applicator displacements. A positive displacement value is considered to be the posterior, superior or left direction of axis in question, with a negative displacement value signifying the opposite direction.

4.3.3 Outliers

There exists a patient to patient variation in treatment plans due to the individual's anatomy and treatment needs. This can cause the treatment plan to be either more or less sensitive to applicator displacement. If the individual's treatment plan contains dwell positions that are within 7 mm of a critical volume edge the displaced plan will enter or exit the volume leading to a large change in dose. During optimisation of the treatment plan dwell positions are weighted to accomplish an optimal plan for the programmed treatment endpoints. When plans are heavily optimised for the individual they can become sensitive to uncertainty since they can have individual dwell positions which contribute a large fraction of the dose. Once this heavily weighted dwell position is displaced it can cause a large change in the dose to critical volumes.[60] This variation in dwell weighting combined with anatomical diversity produces a variation within the dataset.

4.4 Conclusion

A displacement in dwell position due to the physical displacement of the applicator or catheter localisation uncertainties can cause a change to the delivered dose distribution. The objective of this study has been to determine the impact of this effect for two distinct purposes, to reveal the clinical importance of protocols that can limit these uncertainties and to advise the requirements of an HDR end-to-end source tracking system. In doing so the study has produced clear results which imply for both interstitial and intracavitary plans a 2 mm localisation is required in the Anterior-Posterior direction. Clinically, protocols should favour stability in this direction during surgical insertion, imaging and treatment planning. Source tracking systems require a 2 mm resolution along this axis, or at minimum is oriented to provide the most accurate information in this direction during QA.

These results coincide with the literature which finds a 10-12% increase in dose to the bladder and rectum for a 2 mm shift as found by Tanderup et al.[61] A study which also finds a 12% change in dose for OAR when considering a ± 3 mm shift, in all other directions. Alternatively, Tanderup et al found applicator and needle displacement in the inferior direction has demonstrated a tolerance of 4 mm for the bladder in interstitial cases and 6 mm in intracavitary cases. The increased sensitivity when compared to the findings listed in table 4.1, could be attributed to the study only evaluating a 3 mm and 5 mm shift and assuming a linear relationship between OAR dose and applicator translation.

Additionally, Schindel et al., finds a ± 4.5 mm shift in the Superior-Inferior direction to cause a change in OAR dose greater than 10%, these results are however an average impact over 20 patients. As demonstrated in figure 4.7 there can exist a large variation in treatment plans from patient to patient. Determining the impact of displacement based on mean value can allow outliers and a minority of heavily optimised treatment plans to influence the results.[62]The analysis used within the study conducted considers the impact to be critical when 25% of the patient cohort experiences a critical change and is expected to produce conservative results. Local control is effect by a shift in any direction for both interstitial and intracavitary cases, this most sensitive of which being a

posterior displacement limit of 3 mm for interstitial plans.

Applicator rotation was investigated as a possible clinical failure to determine the impact the rotation of an applicator set can have on the dose delivered. Minimal change in dose has been found within the $\pm 20^\circ$ investigated, with HR-CTV coverage un-affected and a 20-degree rotation required to elicit a 10% increase to bladder and rectal dose. The study has successfully demonstrated the requirements for HDR tracking within gynaecological brachytherapy by retrospectively evaluating the dosimetric effect a change in dwell position can have on patient outcomes. This can be used to inform the creating of HDR tracking devices to have an uncertainty within 2 mm in the Anterior-Posterior direction and within 4-5 mm in other directions. This is in line with the TG-56 recommendation of ± 2 mm recommendation of source localisation in relation to the applicator system[63]. Although uncertainty in HDR tracking position would act on each dwell position individually and is not necessarily representative of an entire plan displaced in a single direction, the study provides insight into the degree of sensitivity required and the directions which are most important for HDR tracking.

The primary limitation of the study presents as a simplification of possible applicator displacement, only evaluating the movement of applicator displacement along each axis demonstrates sensitivity to reconstruction uncertainty but does not account for all locations the applicator might take. The study does not account for changes in shape or size of the OAR due to rectal or bladder filling. The evaluation of applicator rotation serves as an example of a specific clinical scenario assessed for quality assurance. Utilising a python script to change dwell positions in a specific fashion that simulates a treatment scenario can serve as an archetype to test the influence of a multitude of different situations which are more complicated than displacing the entire treatment plan along one axis. An example of this could be assessing the bending of interstitial catheters due to oedema by adjusting dwell positions to sit along a bent path. Ultimately, the study has successfully demonstrated the impact of applicator displacement for the purpose of both determining the required accuracy of HDR tracking and providing clinical guidance on the treatment's sensitivity to reconstruction uncertainties and physical displacement.

Chapter 5

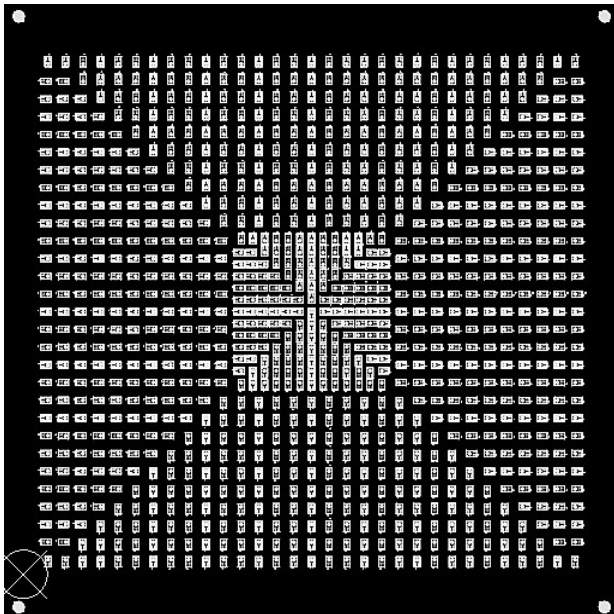
Characterisation of the MP987 for High Dose-rate Source Tracking

HDR source tracking is an integral aspect of the end-to-end phantom which is enabled by the MP987. This chapter serves to develop and evaluate a methodology for HDR source tracking with the MP987. Establishing methods of data processing, a source tracking algorithm and analysis techniques. The MP987, combined with the proposed methodology is characterised based on the temporal and spatial accuracy as well as its performance at varying depths. Ultimately, a preliminary source tracking experiment is performed to establish a complete validation of the MP987 for HDR source tracking.

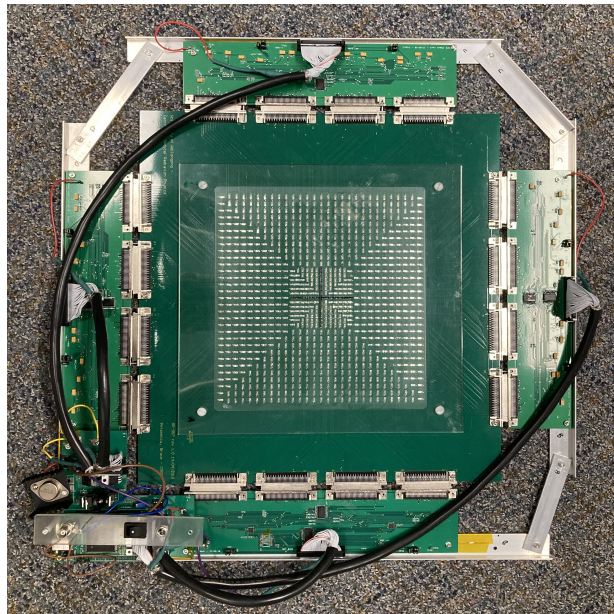
5.1 The MP987

The Centre of Medical and Radiation Physics (CMRP), Wollongong University has created multiple novel silicon diode arrays known as the Magic Plate which exist in multiple configurations such as the MP121 and MP512. The applications and properties of which are discussed in detail in Chapter 2, Section 2.8. The MP987 is a silicon diode array with 987 diodes arranged with two different pitch sizes, 7.5 mm and 5 mm. Figure 5.1i demonstrates the location of the finer pitch in the centre of the plate, and spans over a $13 \times 13 \text{ cm}^2$ area. Surrounding this middle region there are 29×31

pixels with a pitch of 7.5 mm giving an area of $21 \times 22.5 \text{ cm}^2$. A larger field of view is provided by the MP987 compared to the $10 \times 10 \text{ cm}^2$ of the MP121. This will enable the MP987 to track HDR brachytherapy at clinically relevant distances, making it central to the end-to-end phantom.[93]



(i) The silicon diode board, with individual segments visible.



(ii) The complete MP987 system with electronics and protective Perspex covering the diode array.

Figure 5.1: The Magic Plate 987 system

5.1.1 The Data Acquisition System

The Centre of Medical and Radiation Physics (CMRP), Wollongong University have developed a data acquisition system (DAQ) with similar components to those used for previous Magic Plate diode arrays, such as the MP512 and MP121.[81][77]. The readout system made for multi-channel detector devices, consists of the commercial AFE0064(AFE) by Texas Instruments, an analogue-to-digital converter and a Field Programmable Gate Array(FPGA). The AFE is an integrator, accumulates charge from an input current.[94] The amount of charge which can accumulate is adjustable, with 7 distinct levels between 0.1 pC and 9.6 pC, set as the range. [95] Range ultimately determines the detector's sensitivity, as a lower range will mean less charge is accumulated per count and sensitivity of the detector will increase. The AFE is suited to use for detector arrays as each AFE can accommodate 64 channels simultaneously, thus 16 AFE chips are used for the MP987 to provide

an adequate number of 1024 channels for the 987 detector elements. The AFE chips are distributed around the detector with 4 chips used for each of the four segments the array is divided into, illustrated in figure 5.1. AFEs output to an analogue-to-digital converter both of which are managed by the FPGA, which also enables output to a computer via USB.[81] An in-house graphical user interface has been created by CMRP to visualise detector output, manage acquisition parameters and decode raw data. The decoded files present as multiple lines of 1024 channel outputs, a line for each frame acquired. Each line is then mapped to the 2D diode location illustrated in figure 5.2i.

5.2 Frame Processing

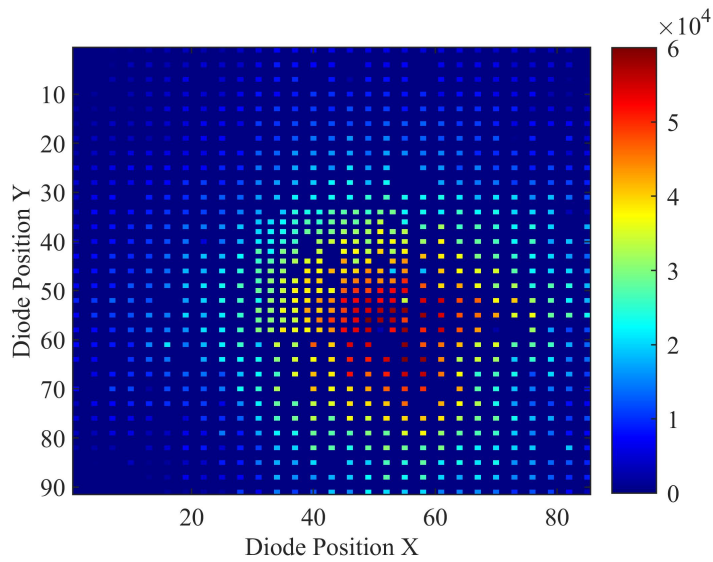
A requirement of accurate HDR tracking with the Magic Plate 987 is the selection of the appropriate acquisition settings and post-acquisition frame processing for the end-to-end phantom. Suppressing noise is extremely important when attempting to accurately track an HDR source over a range of depths. Ideally, the 2-dimensional distribution or frame will be free from fluctuations in signal and will have a gaussian shaped profile at the source location. Dead pixels, a difference in response from diodes and AFEs will affect the 2D distribution and ultimately source tracking accuracy. Fluctuation within each frame can originate from electronic noise due to radiofrequency interference from equipment in the brachytherapy treatment room, mains powerlines and the AFE DAQ electronics boards.[93] Due to Compton Scatter events and an inverse squared reduction in signal with distance, the signal-to-noise ratio will deteriorate when measuring at an increasing distance from the MP987. To achieve accurate source tracking at distances that are clinically relevant and enable a flexible end-to-end phantom geometry, well-defined acquisition parameters and post-processing methods are necessary.

An acquisition software has been previously developed for the MP987's use in linear accelerator profile measurements. The software displays live readout, enables the user to set acquisition parameters and decodes files. For all measurements, an integration time of 9000 μs and an AFE sensitivity range of 2 is selected. The integration time used is close to the maximum (9920 μs) the system is

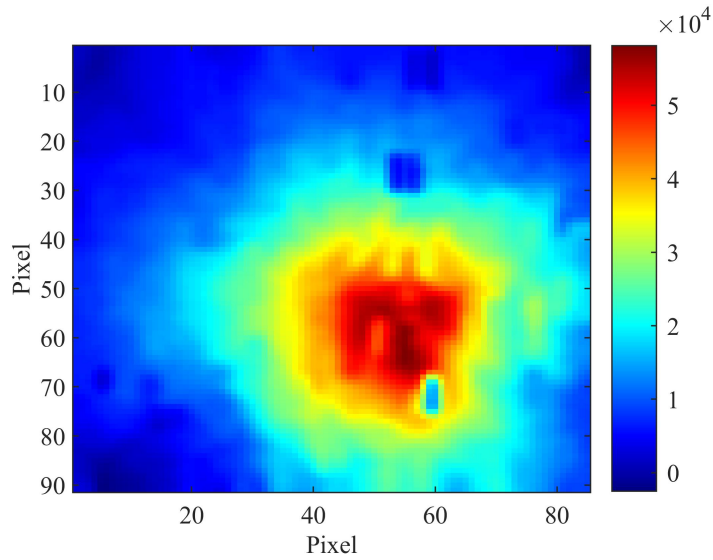
capable of. A larger integration time allows an increased signal-to-noise ratio.[93] This is an adequate compromise as a temporal resolution finer than 0.01 seconds is not required. Accordingly, further averaging of every 10 frames occurs to allow for more accurate source localisation, thus a frame is produced every 0.01 seconds. The effect of frame averaging can be seen in figure 5.10, where a distinct improvement in localisation is achieved, however, the impact this will have on resolving dwell time is discussed in section 5.4. An AFE range of 2 allowed a balance that avoids detector saturation and resolves the source over a 4-10 cm distance from the magic plate.

Equalisation was conducted by CMRP in previous studies to ensure an even response for each diode and AFE within the detector. This was achieved by delivering 200MU with a flattened 6MV beam, with a 30x30 cm² field at 100 cm SSD. The detector was at a depth of 10 cm of Solid Water and a further 10 cm of Solid Water is placed below as backscatter material. The outputs from all channels were normalised to a channel that had the least variation in response throughout the measurement, producing an equalisation factor for each diode. These factors are applied at the start of frame processing to allow an even relative response.

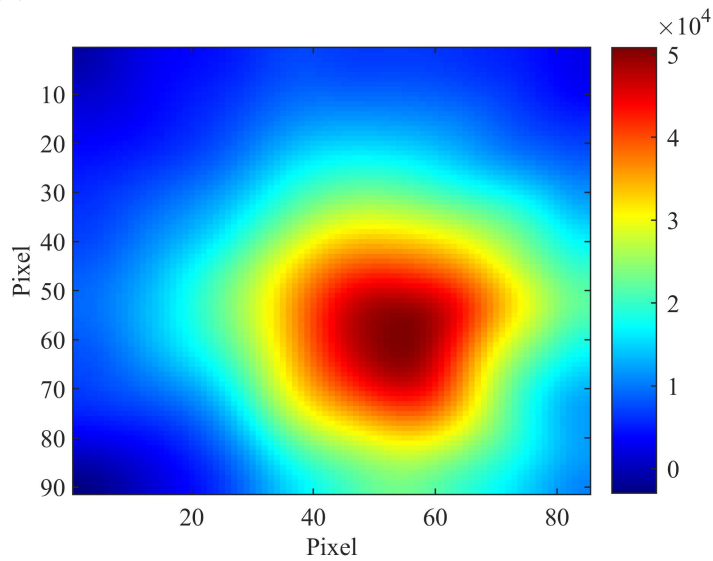
Acquisitions are started with at minimum 5 seconds worth of data collected before the source is present. The average response from each diode over the first 5 seconds of the measurement is taken away as a baseline of electronic noise from all subsequent frames.



(i) Responses mapped to diode location with 2.5 mm pitch, preceding interpolation and filtering.



(ii) The use of two 1D interpolations applied along each axis.



(iii) Processed frame with 2D radial basis function interpolation.

Figure 5.2: Measurements taken at a perpendicular distance of 5.5 cm between the source and magic plate through Solid Water. The frame demonstrates processing which occurs prior to source tracking.

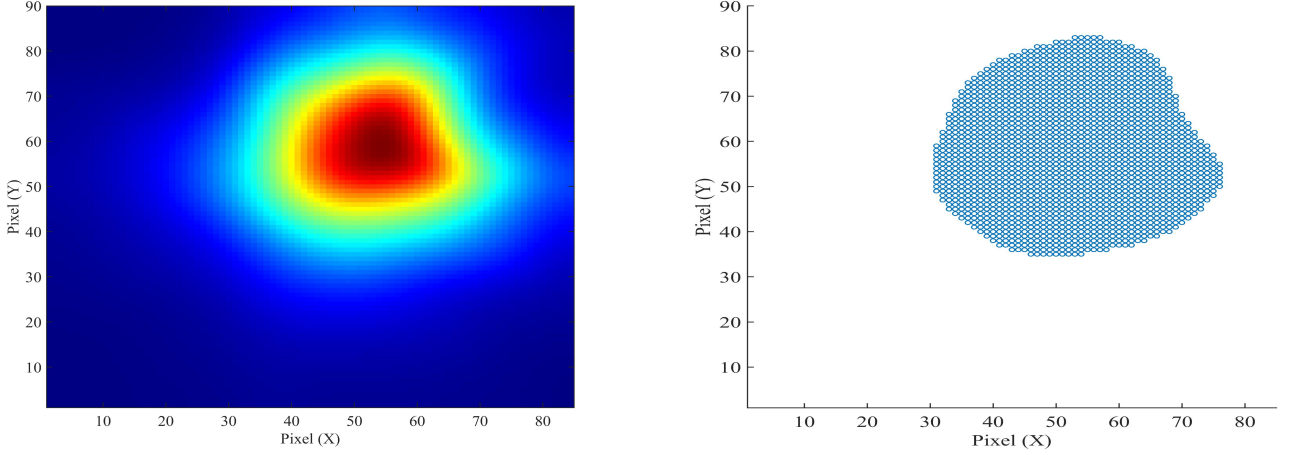
The diode responses are then mapped to a 2D array, demonstrated in figure 5.2i to represent the position of the diodes on the plate. The array is an 85 x 91 grid, with an even 2.5 mm pitch. This allows both the 7.5 mm and 5 mm pitch regions to take a position within the array while the diodes maintain their original locations. Interpolation is then required to give an even distribution of data, without which the diode dense region in the middle of the plate would skew source tracking results. Two methods of interpolation were considered, figure 5.2ii represents a 1-dimensional spline interpolation, conducted along each column then each row for the 2-dimensional data. Although a 1-dimensional interpolation successfully provided an even spread between the regions of two different pitch, dead pixels and noisy regions still had a large impact on the distribution's shape. If data is sparse along a column or row the interpolation will expectedly be poor. Since the source tracking method relies on a centre of mass calculation, a skew in the response due to dead pixels or electronic noise will produce inaccurate localisation. Figure 5.2iii demonstrates the use of a 2D radial basis function (RBF) interpolation of the diode response map in figure 5.2i. The use of a 2-dimensional interpolation method enables response to be interpolated from surrounding pixels and not exclusively diodes in the same row or column. 2-dimensional interpolation combined with a gaussian filter to overcome dead pixels and noisy regions of the magic plate. Ultimately a 2D interpolation is completed using a Python script and all frames are imported into MatLab where the source tracking method is implemented.

5.3 Source Tracking Methodology

A series of calculations are done to each frame to determine the source location (x,y,z) at a point in time. To eliminate false positives a condition is required to ensure source tracking only occurs when the source is present. The AFE operating at a specific range has a maximum number of counts before saturation. For a range of 2, the maximum response is $2^{16} - 1$ and for source tracking to occur a response 10% of this value needs to be detected.

$$x = \frac{\sum_{i=1}^n s(X_i, Y_i) \cdot X_i}{\sum_{i=1}^n s(X_i, Y_i)} \cdot \delta \quad (5.1)$$

$$y = \frac{\sum_{i=1}^n s(X_i, Y_i) \cdot Y_i}{\sum_{i=1}^n s(X_i, Y_i)} \cdot \delta \quad (5.2)$$



(i) A frame which has undergone the processing procedure and meets the cut-off to undergo the source tracking
(ii) Pixel locations used in the x-y source tracking calculation

Figure 5.3: Single frame utilised for source tracking algorithm.

To determine the source's position in the x-y plane a calculation that is analogous to determining the centre of mass is performed. The position of each pixel is weighted with its response as demonstrated in equations 5.1 and 5.2. Firstly, a threshold is implemented where only pixels which are above 30% of the maximum response in the frame are used for the calculation. The n number of positions each with the pixel location X and Y are plotted in figure 5.3ii, with the corresponding response at each position being $s(X_i, Y_i)$. The position is weighted by an associated response, summed and normalised by the total response. The calculation tends towards a final location that places the source closer to those pixels which have a larger response and thus determines the location in the x-y plane. A factor δ is applied to transfer the units from pixel location to the (x,y) position. Taking the bottom left pixel to be (0,0) the value of δ is equal to the pitch (0.25 cm).

Source localisation in the Z direction is accomplished through the TG-43 formalism discussed in

section 2.2.1. A point source approximation is used given the relatively large distance between the MP and source. The TG-43 updated formalism states that most TPS systems used this approximation, but recommends a 2D approach for distances less than 1 cm.[36].

In every frame, pixels greater than 90% of the maximum pixel are used to calculate the distance between the source and MP987. The response of each pixel is converted to a dose rate and using the equation 2.1 the distance is calculated. Firstly, a measurement is taken with the source at a single dwell position a known distance from the Magic Plate. The dose rate is then calculated using the 1D TG-43 formalism and divided by response. This provides a calibration factor between dose and response which is used for all following measurements.

The response is converted into dose rate via the calculation factor. Using equation 2.1, S_k when the measurement is taken, radial dose and inverse-square functions are input. The dose-rate equation is then solved radial distance between source and diode. The anisotropy function is neglected as it is assumed that the diodes greater than 90% of the maximum response will be directly below the source and thus will have a θ of approximately 90 degrees. As demonstrated in figure 2.7, any deviation away from 90 degrees will not have a large impact. With 90 ± 20 degrees causing a 1% change in dose.[3]

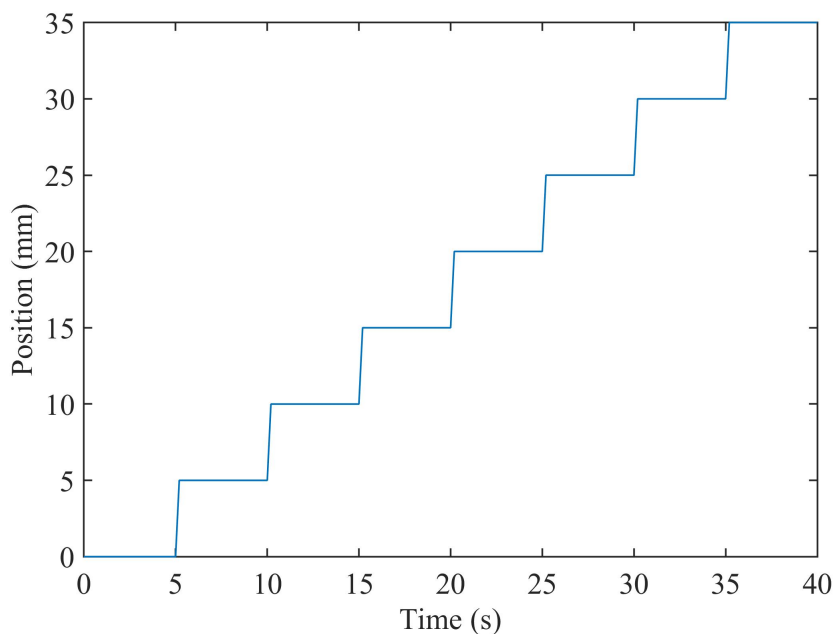


Figure 5.4: A treatment plan with 5 mm step size and 5 second dwell time.

Figure 5.4 demonstrates the ideal time and location of a treatment plan which has a 5 mm step size and 5 second dwell times for a single catheter. Realistically, a source tracking system will be able to determine the timing and location of a source within a certain resolution, providing a distribution of dwell times and positions. Figure 5.5 is a measurement of the same plan, with the catheter running along the Y direction of the MP987. Compared to figure 5.4 the effect of the system's finite localisation accuracy illustrated through a spatial variation at each dwell position. Additionally, the time resolution only enables a single acquisition point for source transit between dwell positions.

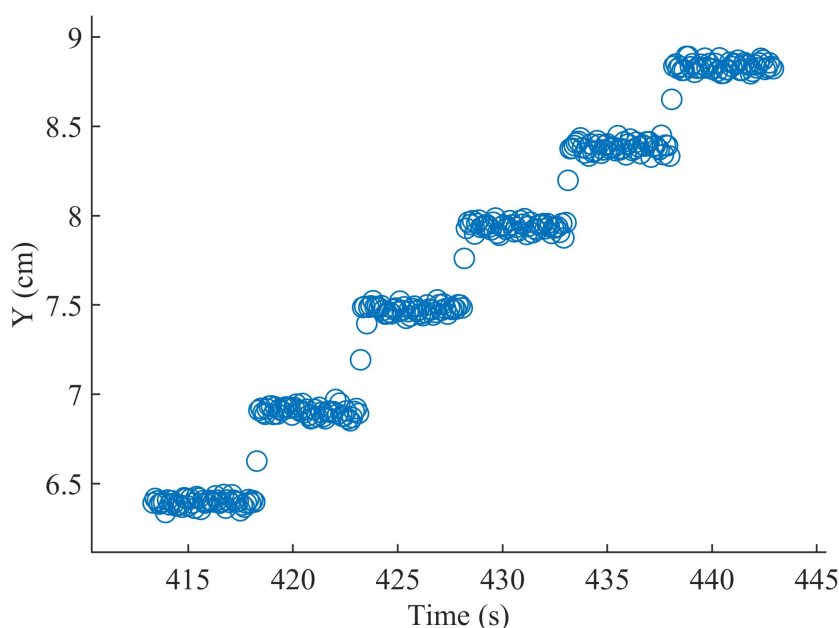


Figure 5.5: Measured output of a 5 mm step size, 5 second dwell time treatment plan

Dwell times and positions are calculated based on a histogram produced along the axis of which the source is travelling. This has been selected as it will provide the greatest separation between dwell points. Ideally, the histogram will present as demonstrated in figure 5.6, where all measured dwell positions are differentiable, and a very small bin width can be used. Source transit has been neglected and a point generated every 0.1s at each dwell position for the histogram. If the measurement of a perfect system was being displayed there would be an even amount of positions measured between each dwell position, to denote the source transit demonstrated in figure 5.4. For the source localisation method proposed, a good separation of dwell times is required. Although the source transit does

contribute some counts to bins between dwell positions, it is negligible due to the implemented 0.1s acquisition rate.

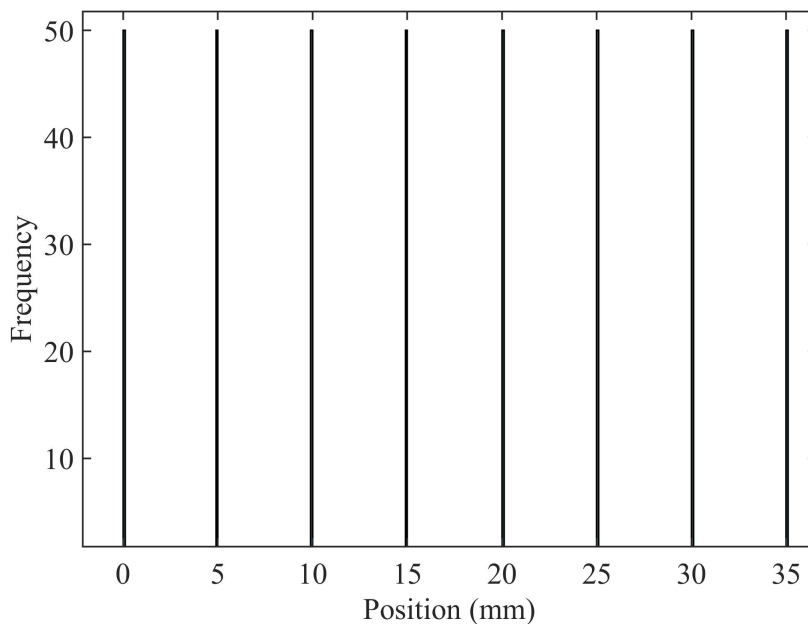


Figure 5.6: A treatment plan with 5 mm step size and 5 second dwell time

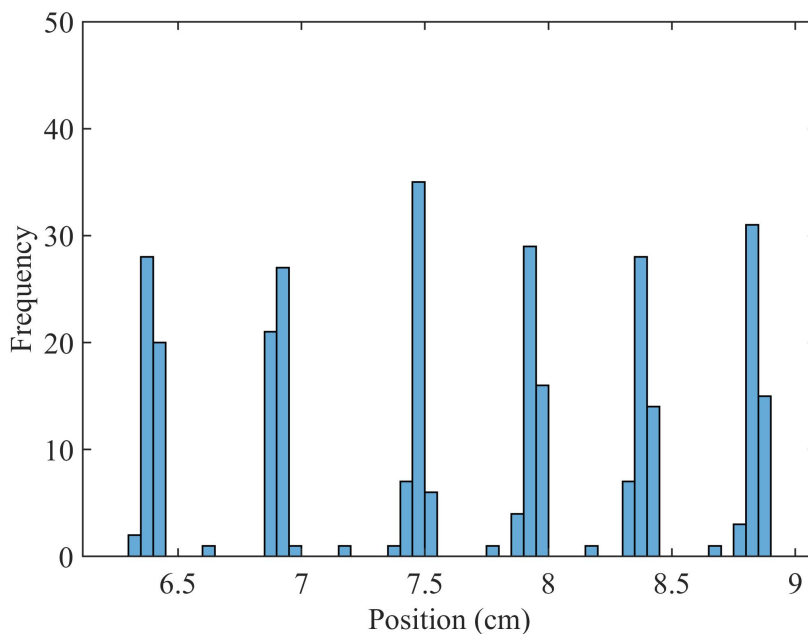


Figure 5.7: The measured histogram used for of 5 mm step size, 5 second dwell time plan

To calculate a dwell position an average is taken of the measured points. A histogram is used with a bin width of 0.5 mm to separate an output into individual dwell positions. The output in Figure 5.5 is represented by the histogram in figure 5.7, where the six dwell positions are denoted by the six

groups of neighbouring bins. The grey line within the histogram illustrates an implemented threshold of 1. Bins with a frequency below this threshold are used to differentiate dwell positions. Outputs of data which is less spatially accurate will have a greater number of counts between dwell positions and a larger threshold and will need to be implemented to gain a separation of dwell positions.

Once measured points have been grouped into dwell positions, their corresponding location along each other axis is averaged.

Dwell time is equal to the sum of the frequencies of neighbouring bins multiplied by the sampling rate of 0.1 s^{-1} . An example of this can be seen in figure 5.4, where a 5s dwell time produces a frequency of 50 for each position. A sample mean is calculated with equation 5.3 to determine dwell position along a single axis. Each group of neighbouring histogram bins represents a dwell position where f_i is the frequency and x_i is the bin location.

$$P_{av} = \frac{\sum_{i=1}^n f_i \cdot x_i}{\sum_{i=1}^n f_i} \quad (5.3)$$

5.4 Temporal Resolution

The MP987 system and source tracking process requires an evaluation of its temporal characteristics since a source tracking system's function is to provide source localisation and timing information.

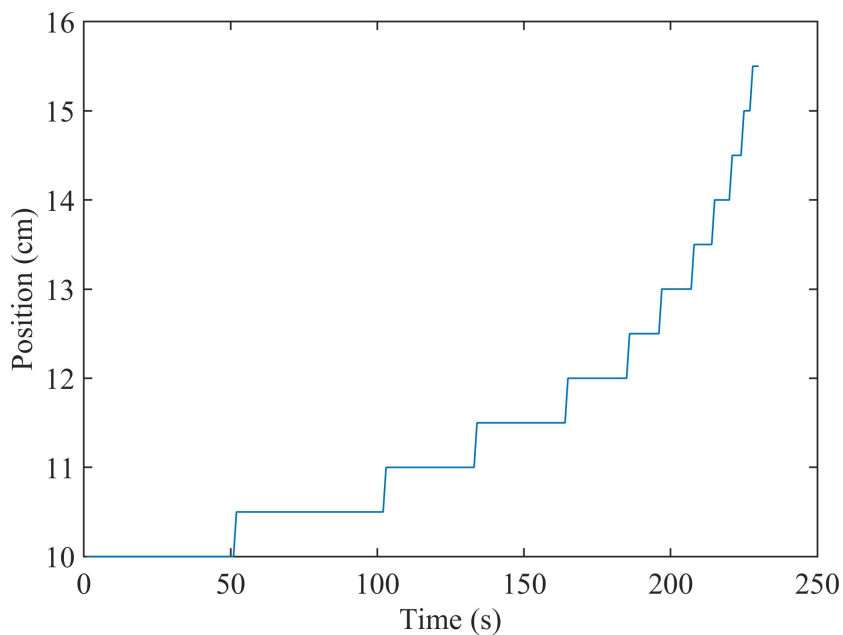
The aims within this section are to:

- Determine the system's optimal processing parameters
- Define the system's limitations when determining dwell time

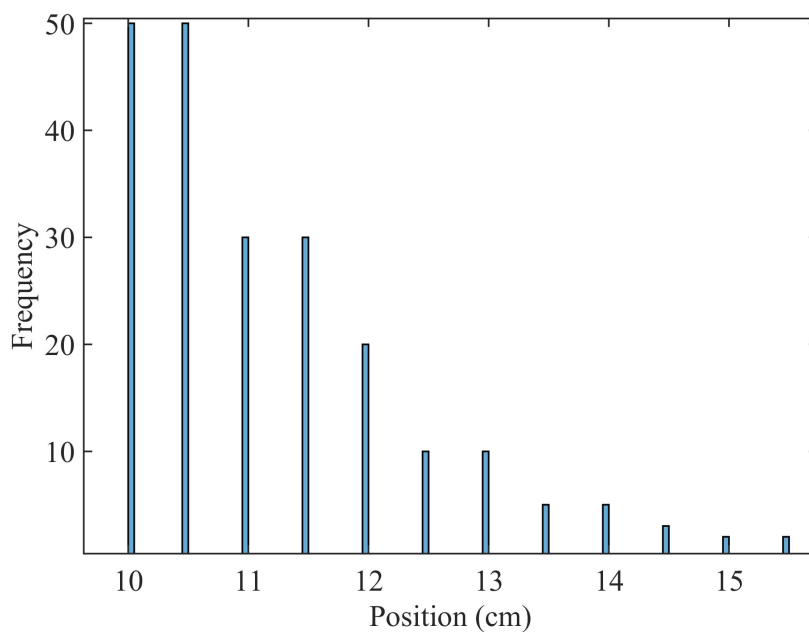
5.4.1 Method

To test the temporal resolution of the system, and determine the optimal amount of frame averaging during processing, measurements are taken of a two catheter plan. Each catheter has the same series of dwell times and a single step size of 5 mm.

Two catheters are placed at a distance of 6.5 cm from the MP987 separated by Solid Water. The two catheters are placed parallel both 5 cm from the middle of the MP as shown in figure 5.15. A treatment plan which steps the source 5 mm between each dwell position is used, with a series of different dwell times demonstrated by the histogram 5.8ii. To represent the treatment plan points were generated every 0.1 seconds. The dwell times in order are 5 s, 5 s, 3 s, 3 s, 2 s, 1 s, 1s, 0.5 s, 0.5 s, 0.3 s, 0.2 s, 0.2 s.



(i) Treatment plan for the temporal resolution test, with a 5 mm step size and varying dwell times



(ii) A histogram of the treatment plan, where points are generated every 0.1 s

Figure 5.8: Treatment plan for temporal resolution test

Each catheter has been analysed individually using the procedure developed above, where measured points are grouped into dwell positions. A threshold of 1 is used for the measurement process using a 10 frame average. Without frame averaging, the single frame measurement requires a threshold of 5 to differentiate dwell positions. This implements the finest temporal resolution of 0.2 s and 0.05 s for the averaged and single frame measurements respectively.

5.4.2 Results

The temporal resolution test was conducted with and without frame averaging to determine the optimal processing parameters. Outputs from the two catheters are displayed in figures 5.10 and 5.9. The histograms of these results in figures 5.11 and 5.12 provide insight into the tracking system's interpretation of the measurement. The dwell time for each position is calculated from their respective histogram. Where residuals represent the difference between the programmed dwell time and what is measured at each dwell position, displayed in figures 5.13 and 5.14.

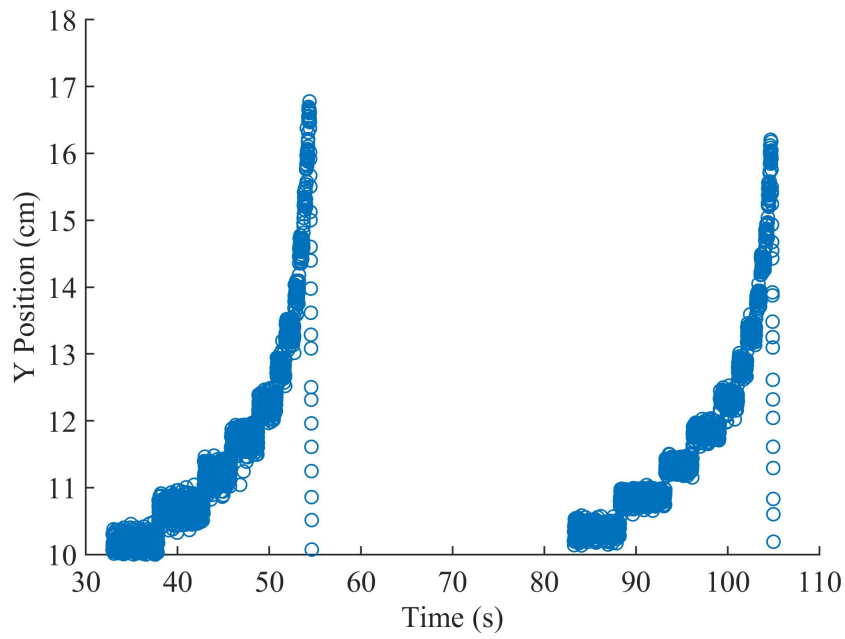


Figure 5.9: Temporal resolution test without frame averaging.

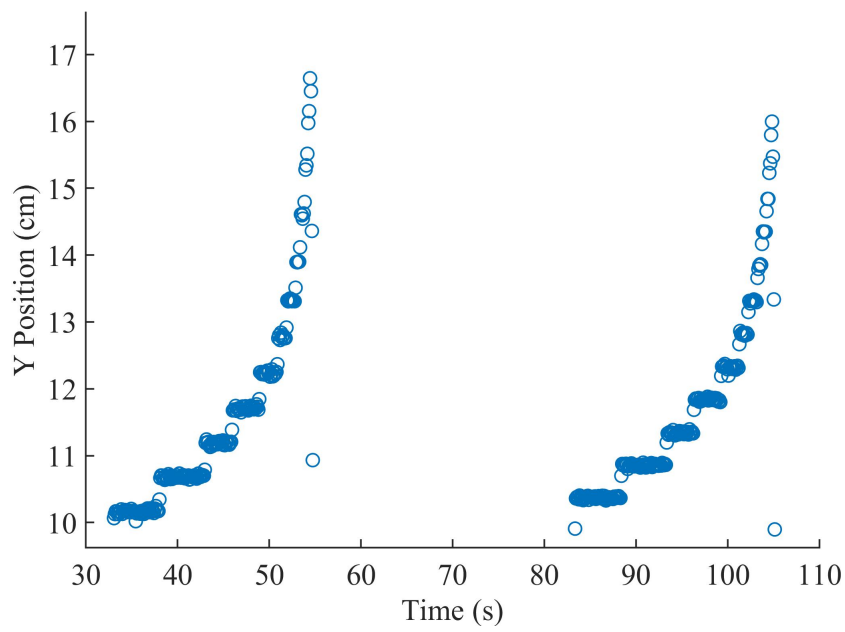
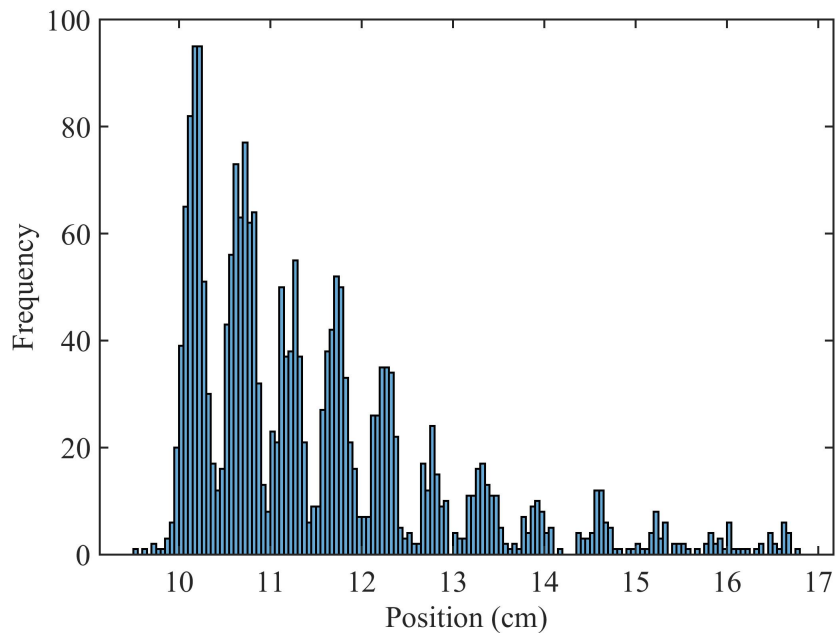
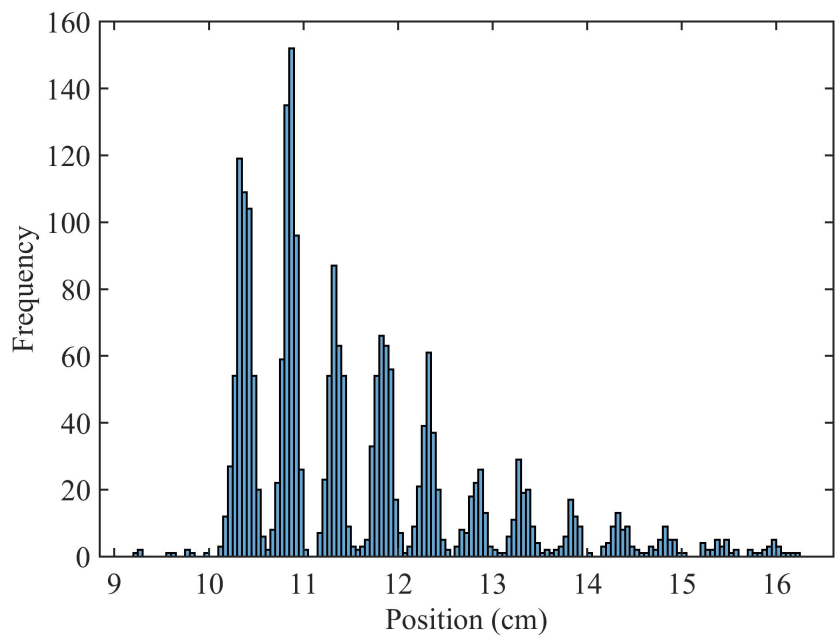


Figure 5.10: Temporal resolution test averaging 10 frames.

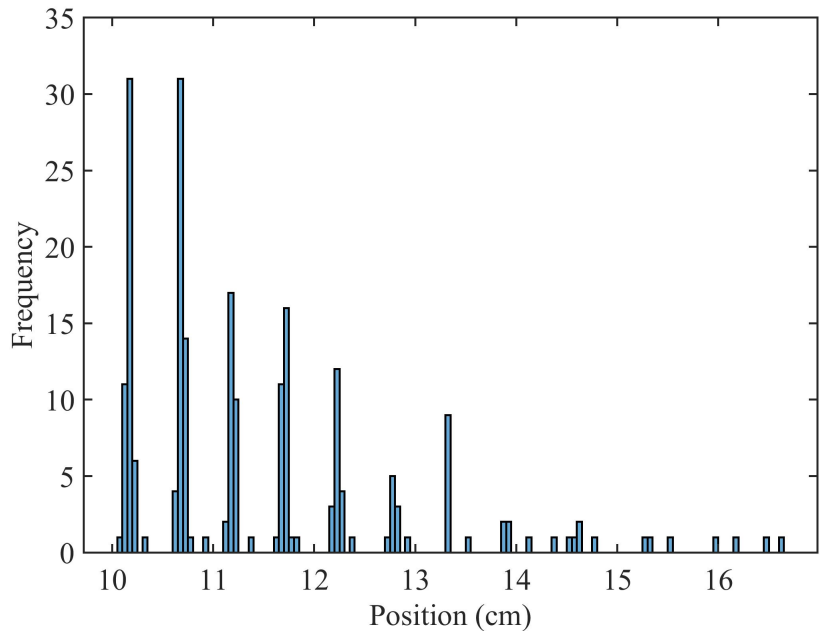


(i) Catheter one

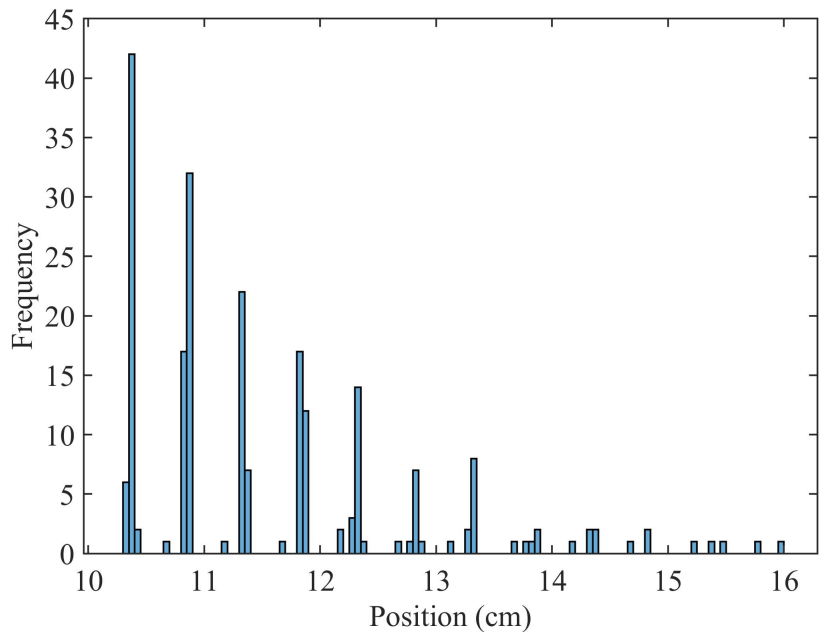


(ii) Catheter two

Figure 5.11: Catheters processed without frame averaging

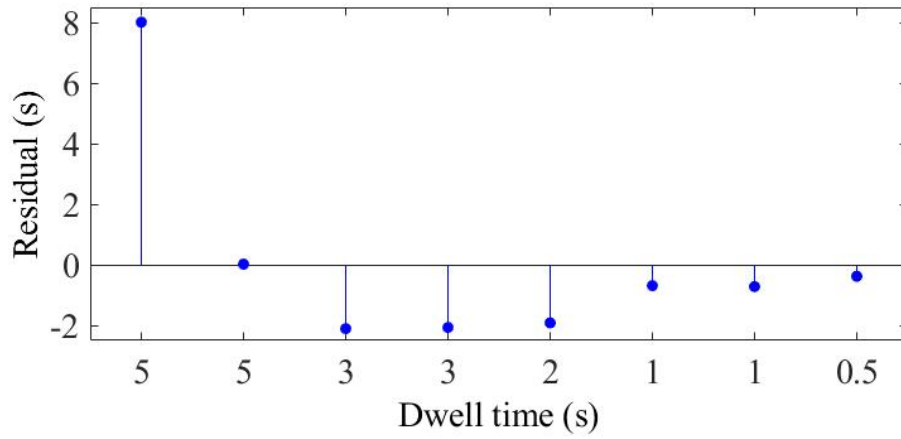


(i) Catheter one

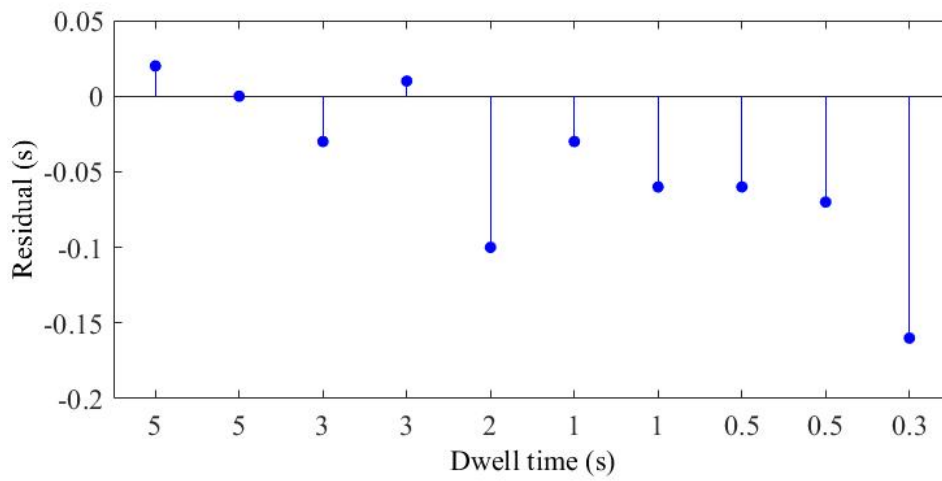


(ii) Catheter two

Figure 5.12: Catheters processed averaging 10 frames

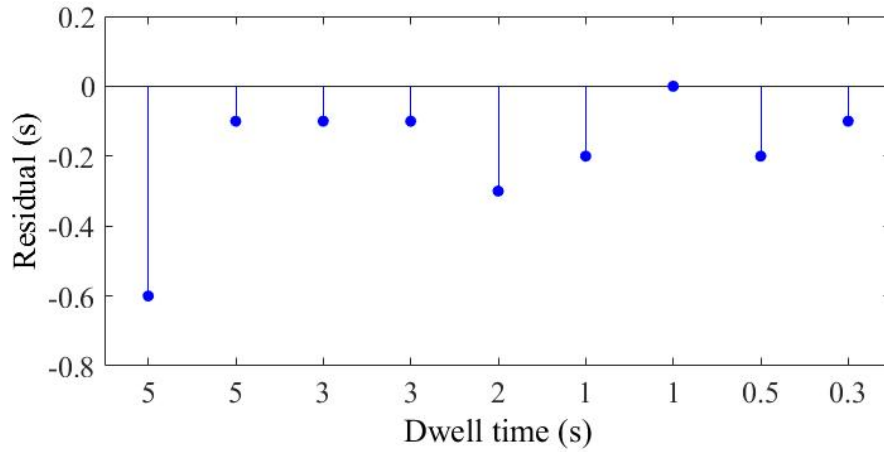


(i) Catheter 1

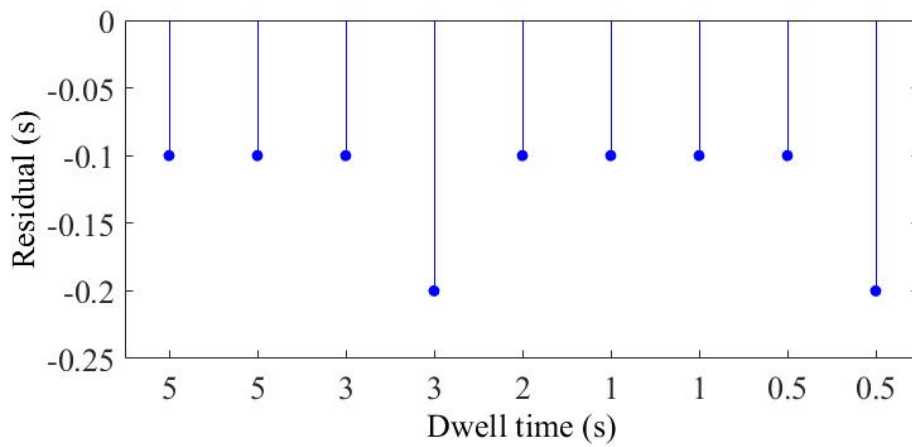


(ii) Catheter 2

Figure 5.13: Residuals when using single frames.



(i) Catheter 1



(ii) Catheter 2

Figure 5.14: Residuals for each dwell time when averaging 10 frames.

5.4.3 Discussion

The temporal resolution dictates a minimum dwell time for which a dwell position can be recognised and the accuracy in determining dwell times. It is expected that dwell times measured by the MP987 are fractionally less than that of the treatment planning system as the afterloader corrects for transit time. This is apparent throughout most measurements as the residuals are commonly negative.

In figure 5.10 and 5.9, the effect of frame averaging on the spatial resolution is apparent, where the inter-dwell spaces cannot be resolved without frame averaging. Figure 5.10 however does exhibit spaces between each dwell position, which has come at the expense of a reduction calculation frequency. When averaging 10 frames a point is calculated every 0.1s, reducing the 0.01 s^{-1} acquisition

rate output by the AFE-DAQ system. Acquisition at this high rate can provide superior temporal accuracy, demonstrated by the residuals calculated in figure 5.13ii for the second catheter. In this case, the source tracking has determined 5 s, 3 s within 0.05 s and all other dwell position up to 0.3 s within 0.15 s. Averaging 10 frames, the minimum dwell time measured is 0.3 s, within 0.1 s for catheter 2. Catheter one with frame averaging produced an error less than 0.4 s for all dwell positions, besides the first 5s dwell position. Although the measurements which are free from frame averaging produce superior temporal precision for catheter two, figure 5.13i demonstrates a dominant inaccuracy for catheter one. Dwell times are calculated to be over 100% different to what is expected, with an inability to resolve a dwell position for times below 0.5s. Comparing figure 5.11i for catheter one with figure 5.11ii for catheter two demonstrates a higher noise level for catheter two. Figures 5.12i and 5.12ii demonstrate a 10F average minimising this noise. Frame averaging provides a robust outcome given the proposed methodology is sensitive to a lack of spatial separation of measured points between dwell positions. Noise within the data can be attributed to radio frequencies inducing electrical noise at 50 Hz, the MP987 increasing in temperature and an inaccurate equalisation leading to overresponse in sections. With frame averaging a dwell position with a time of 0.5 s will be detected with an expected accuracy of 0.2 s.

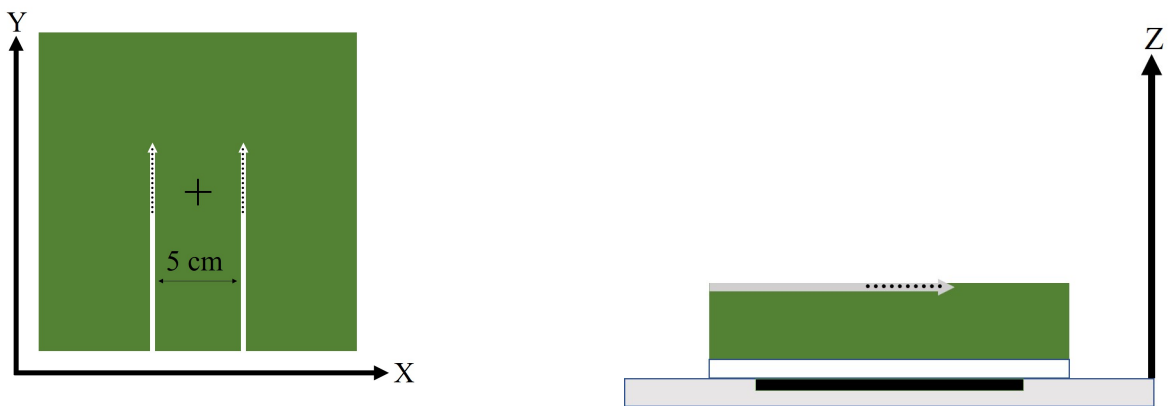
5.5 Source Localisation

The aims within this section are to:

- Calculate the fluctuation within a dwell position as a function of depth
- Determine the error in the calculated mean when determining dwell position as a function of dwell time

5.5.1 Method

The precision for localisation is determined by quantifying fluctuation within dwell positions to one standard deviation. This has been calculated with equation 5.4 and defines the expected variation in each measured point. The variation is a function of depth and could also depend on the region of the MP987. σ has been calculated for measurements taken of a treatment plan at multiple depths. The setup used is illustrated in figure 5.15. A 1 cm Perspex plate with channels to house the catheters is used to prevent them from moving. The plan consists of a 5 mm step size and a 3s dwell time for each catheter. The 12 dwell positions in the treatment plan are centred over the middle of the MP. Measurements are taken in 1 cm increments from a depth of 4.5 cm to 10.5 cm. An average σ is calculated for the two catheters at each depth.



(i) Two parallel catheters are fixed on top of the solid water 5 cm apart.

(ii) The MP987's silicon diode array is signified in black, above which there is 5 mm of perspex. The Solid Water is placed on top of this protective surface for all measurements.

Figure 5.15: Set up for source tracking at different depths

A dwell position is calculated by determining an average position from the generated histogram. The error for this average is calculated to one standard deviation using equation 5.5. While the fluctuation has been characterised using σ , the uncertainty in this average needs to be quantified as a function of time to outline the methodology's limitations given the chosen bin size and frame averaging. Since treatment plans include a range of dwell times, so the setup used for this test is identical to the temporal resolution test in section 5.4, with dwell times ranging from 5 to 0.3s.

$$\sigma = \sqrt{x^2 - \bar{x}^2} \quad (5.4)$$

$$\Delta P_{av} = \sqrt{\frac{1}{n} \sum_{i=1}^n (x_i - P_{av})^2} \quad (5.5)$$

5.5.2 Results

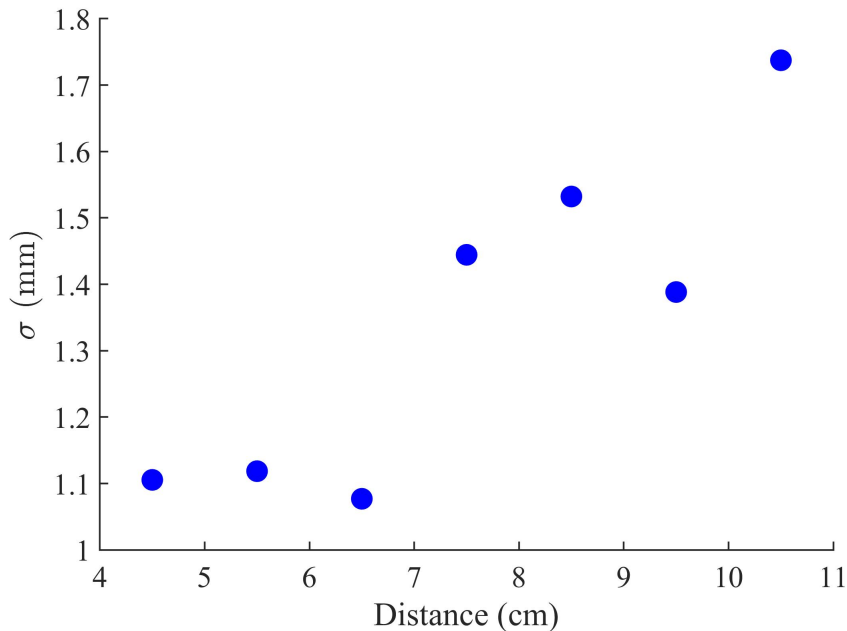


Figure 5.16: A measure of variance in dwell position for different distances between source and MP

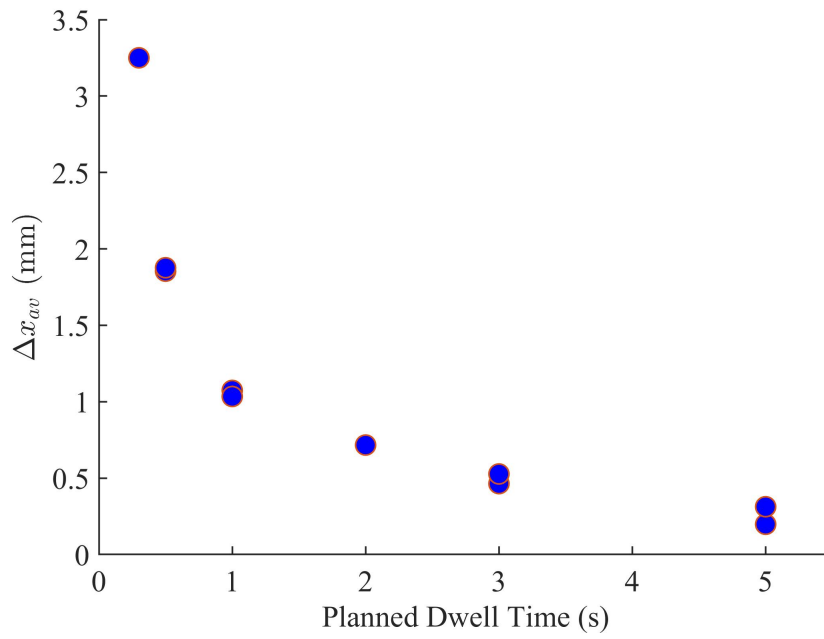


Figure 5.17: A change in mean error with dwell time along the Y axis

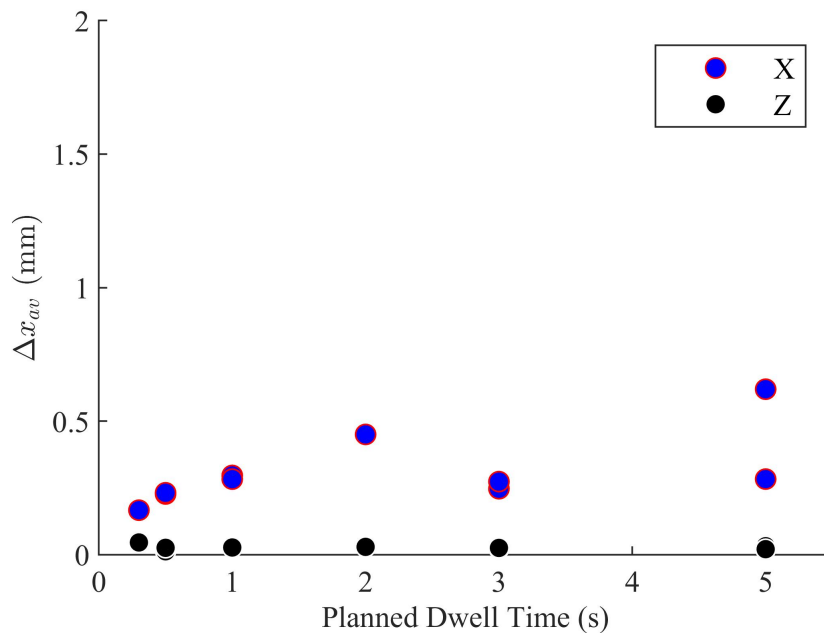


Figure 5.18: A change in mean error with dwell time along the X and Z axes

5.5.3 Discussion

The fluctuation has been quantified for a series of different depths between 4.5-10.5 cm. The standard deviation of two catheters has been averaged to provide an uncertainty at each depth. An increase in uncertainty with depth is as expected given a decrease in signal and increase in Compton scatter. From 4.5 to 6.5 cm the fluctuation is constant within (1 ± 0.01) mm. Within this range, the primary signal strength is dominant and an error of approximately 1.1 mm is apparent. Outside of this range, there is a general increase in σ between 7.5 and 10.5 cm as expected. A reduction in signal and increase of noise due to scattering causes growth in fluctuation. A decrease in σ is seen for a depth of 9.5 cm, this can be attributed to the shift in catheter position when setting up the measurement as noise level can differ for different regions of the MP. Ultimately, the measurement of dwell positions at depths between 4.5 cm and 10.5 cm has a standard deviation of 1.1 to 1.7 mm respectively.

Since treatment plans include an array for different dwell times, accuracy needs to be evaluated as a function of dwell time given the histogram methodology outlined in this chapter. To determine how dwell time affects accuracy, standard deviation has been calculated for the treatment plan in section 5.4. Figure 5.17 reveals an increase in standard deviation for smaller dwell times. A reduction in accuracy is expected for smaller dwell times as fewer measurements are taken in this location. Given the source is moving in the Y direction, this reduction in data has a large impact on precision due to the rate of change in the Y position compared to the constant X and Z position. Additionally, the source's transit toward and away from the dwell position may contribute to the spread in the calculated position. Which will have a larger effect with small sample sizes. Figure 5.18 demonstrates the standard deviation for the Z and X directions, where the expected reduction in accuracy is not clear. The standard deviation is less than 0.6 mm and does not decrease with dwell time. A low sampling rate has little effect on the localisation within these axes as the source's position along the axis is constant. Figure 5.18 demonstrates a variation in standard deviation which can be due to factors that affect the response of the MP987 such as electronic noise, inadequate equalisation

or heating of the MP. An example of this is the two successive measurements of a 5s dwell time seen in figure 5.18 differing in standard deviation by 0.3 mm. A time-dependent error needs to be considered with the current methodology since the average location used to define dwell position and a larger sample of measurements decreases the error in the calculation. Additionally, a fluctuation in dwell position is always present and is dictated by the value of the variance (σ). Localisation error is expected to be less than 2 mm for depths between 4.5 cm and 10.5 cm and dwell times greater than 0.5s. For dwell times of 5s and greater an accuracy of 0.25 mm is expected.

5.6 Source Tracking at Different Depths

The aims within this section are to:

- To determine the accuracy the MP987 can provide in the Z direction
- Evaluate the impact depth has on source tracking in the X and Y directions

5.6.1 Method

The Z position is determined using a TG-43 based formalism and response to dose calibration factor, described in section 5.3. The MP987's ability to determine source position in the Z direction was tested via measurement of two catheters through varying depths of Solid Water, with the set up shown in figure 5.15. A single calibration point for conversion from signal to dose-rate at a distance of 5.5 cm has been used across all measurements. A dwell time of 5 s and a step size of 5 mm was used for 12 dwell positions, these are all measured at depths from 4.5 - 10.5 cm in 1 cm increments. The catheters are placed within perspex channels to prevent them from moving. The distance between the two channels used was measured with a ruler to be (5 ± 0.2) cm. To determine spatial linearity with depth, the distance between the two catheters will be measured as a function of depth. As per figure 5.15i, the source's x position should be constant for each catheter. The average x position

was calculated for each catheter. The difference in average x position between the two catheters was determine for different depths.

5.6.2 Results

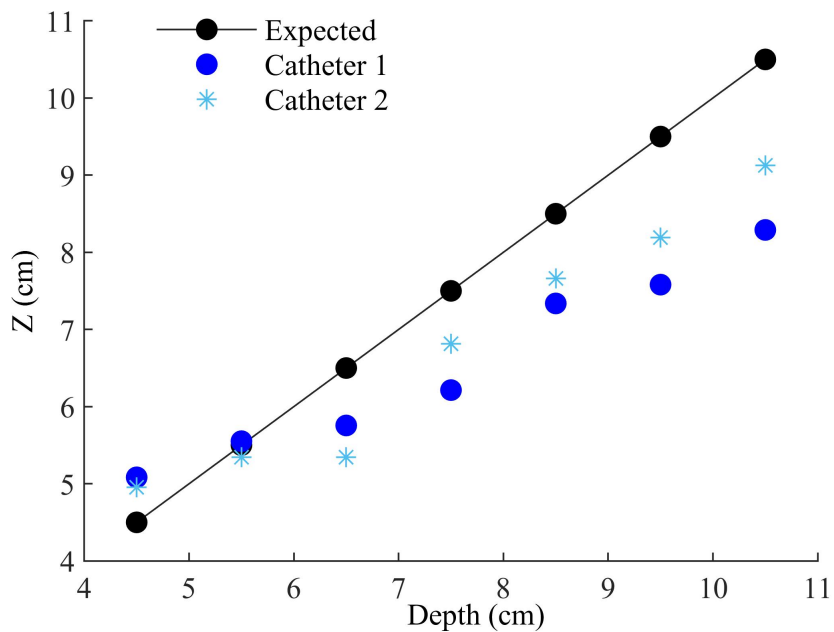


Figure 5.19: Measured Z position at different depths

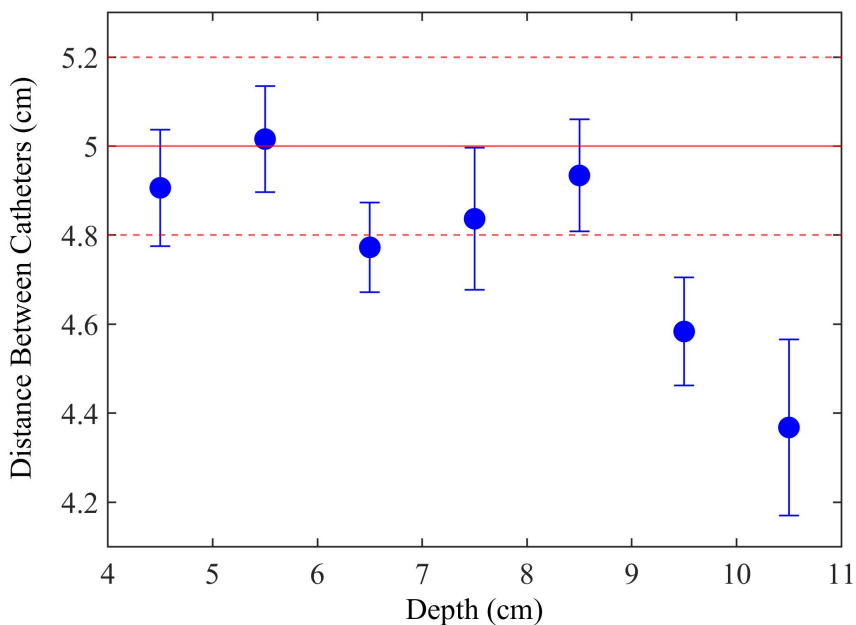


Figure 5.20: Spatial linearity at different depths

5.6.3 Discussion

Calculating source position in the Z direction has been tested to determine the efficacy of the proposed TG-43 based methodology. Figure 5.19 demonstrates the expected depths compared to what is measured. The calibration factor used was at a distance of 5.5 cm. Depth measured for 5.5 cm is within the calculated error for both catheters. Both catheters measured at 4.5 cm have produced a measurement close to 5 cm, this can be attributed to detector saturation. Measuring at a higher AFE range will decrease sensitivity and allow adequate data within this region. At depths further than the 5.5 cm calibration point, the calculated distance is less than expected. At a depth of 8.5 cm, the difference between, the expected and measured Z is (1.16 ± 0.01) cm and (0.84 ± 0.01) cm for catheters 1 and 2 respectively. This discrepancy continues to increase to 10.5 cm, reaching (2.21 ± 0.01) cm and (1.48 ± 0.01) cm for catheters 1 and 2 respectively. Given the shape of the two separate gradients for measurements between 4.5 cm to 7.5 cm and 8.5 cm to 10.5 cm there could be an error in the implementation of the TG-43 formalism. Investigation into scripts developed for the calculation is required. Additional uncertainties stem from a lack of full scattering conditions specified by TG-43, despite the inverse square reduction in dose being dominant. An assumed water equivalence of the Perspex catheter channels and MP cover will also add to uncertainty. Since the MP987 is a novel silicon diode array it has not undergone radiation hardening, a possible dose-rate dependence would also have a large effect on localisation in the Z direction.

Additionally, multiple time-variant factors affect the response of the MP987. An accurate equalisation needs to be performed to ensure an even response from each region of the MP987. Over time the equalisation required can change and so repeating this process will ensure an equal response from each diode and AFE. A build-up of heat throughout the measurement can cause over and under response in sections of the Magic Plate. Although a fan was used throughout data acquisition, an increase in temperature on the power supply was present, leading to a small change in bias on the detectors. Electronic noise due to RF frequencies within the treatment room can induce fluctuations

in signal. The effect of electronic noise had been reduced by shielding the electronics with aluminium, however, it is still present during acquisition. Since the depth is completely dependant on diode response, these factors which alter the output signal have a large effect on accuracy in the Z direction. Additionally, a difference between the two catheters demonstrates a variation in response for different regions of the MP987. Filtering and frame processing do well to supplement data allowing accurate source tracking in the X and Y directions, but do not remedy response irregularity.

Figure 5.20 demonstrates the distance between two catheters given different depths. The spatial consistency in the X-Y plane for different depths is imperative for source tracking as treatment plans can include catheters at multiple depths. The distance between the two channels in which the catheters are housed is measured with a ruler to be (5 ± 0.2) cm. For depths from 4.5 cm to 8.5 cm, the measured distance between catheters is within error. For distances of 9.5 cm and 10.5 cm, distance between the catheters has decreased. At a distance of 10 cm, the off-axis profile demonstrates a width of 12 cm for a response of 70% of the maximum [93]. A spread in the distribution off the detector skews the measurement, shifting the centre of mass centrally. End-to-end phantom measurement should be taken in the middle of the detector and less than 8.5 cm away.

5.7 Preliminary Source Tracking

The concepts and methods established within this chapter will be utilised to enable preliminary source tracking in preparation for a complete end-to-end test. The aims within this section are to:

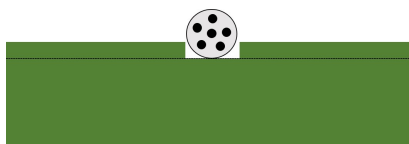
- Evaluate source tracking in 3-dimensions with the use of a replica multichannel applicator

5.7.1 Method

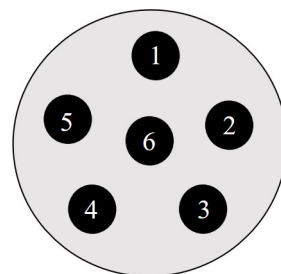
A 6 channel cylindrical vaginal applicator which is 25 mm in diameter, was 3D printed with polylactic acid (PLA) and a 100% infill. PLA has been shown to provide a good agreement to water, limiting additional attenuation.[96].

As displayed in figure 5.21 the applicator was placed on top of a 30 cm x 30 cm x 6 cm block of Solid Water, with 1 cm of solid water on each side. The setup was taped together to prevent components from moving and positioned on top of the MP and aligned with its centre. The top end of the applicator is positioned 5 cm above the centre in the Y direction and the midline of the applicator was aligned with the middle of the Magic Plate. Catheters are inserted into each channel and afterloader connected in the arrangement demonstrated in figure 5.21ii. The same sequence of dwell positions and times are planned for all catheters. A step size of 5 mm was used over the 80 mm treatment length. With the source stepping towards the top end of the applicator, the first 30 mm has a dwell time of 5s and the remaining 50 mm has a dwell time of 2 s.

An absolute analysis of position compared to a CT based treatment plan was completed in end-to-end testing. Within this preliminary study, results are analysed with respect to the discrepancy in dwell times, the ability to determine the distance between dwell positions and the relative difference in-depth for each catheter.



(i) 3D printed Multichannel Vaginal Applicator placed on 6 cm of Solid Water



(ii) Displays configuration of afterloader to applicator connection, with each number corresponding to a channel.

Figure 5.21: MVC setup for preliminary source tracking



Figure 5.22: Applicator orientation

5.7.2 Results

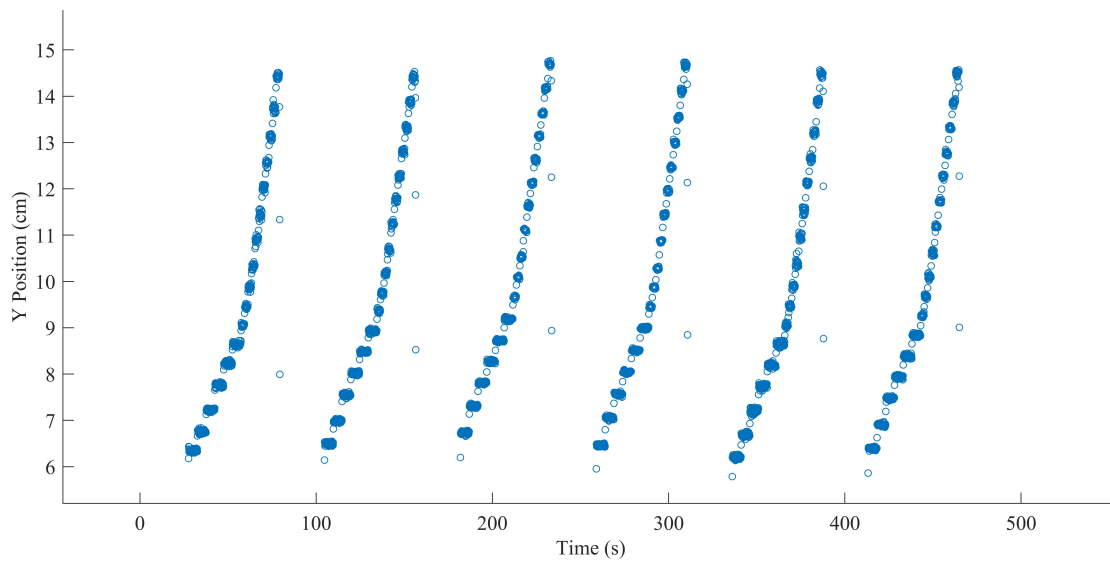


Figure 5.23: Source tracking along the Y axis

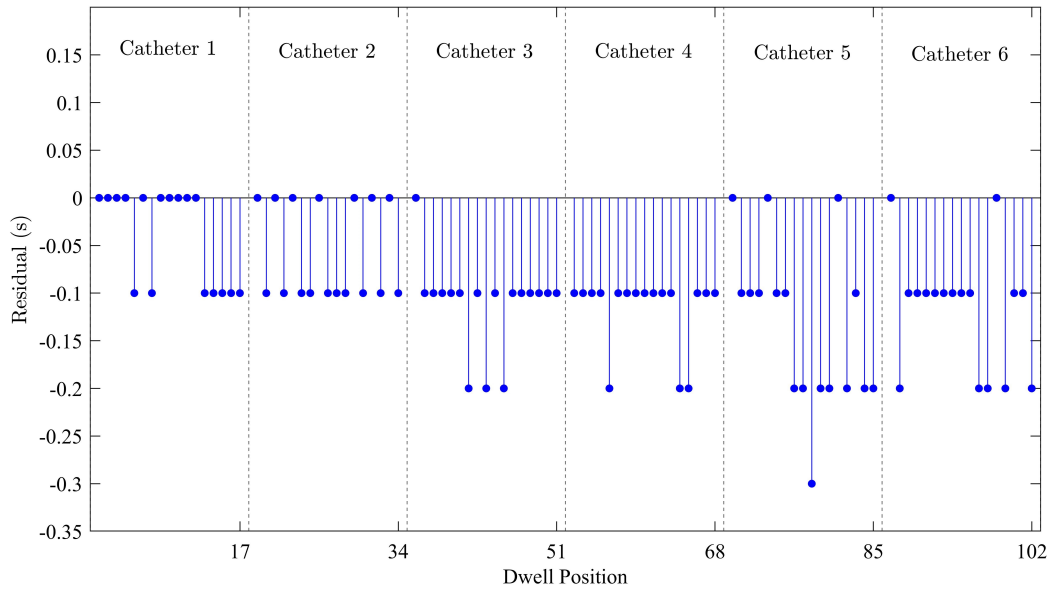


Figure 5.24: Difference in dwell times from treatment plan

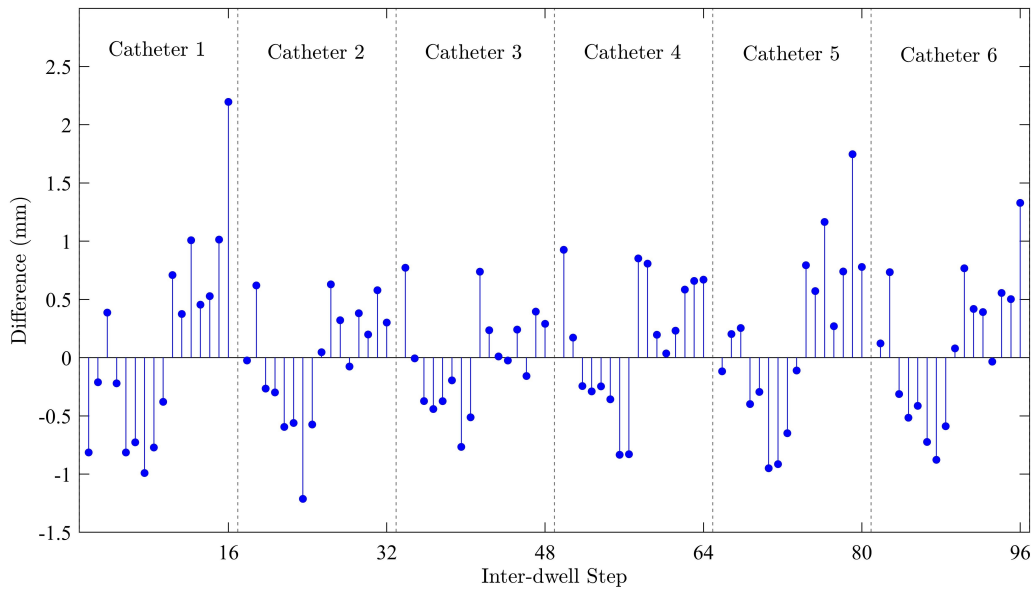


Figure 5.25: Difference in step size

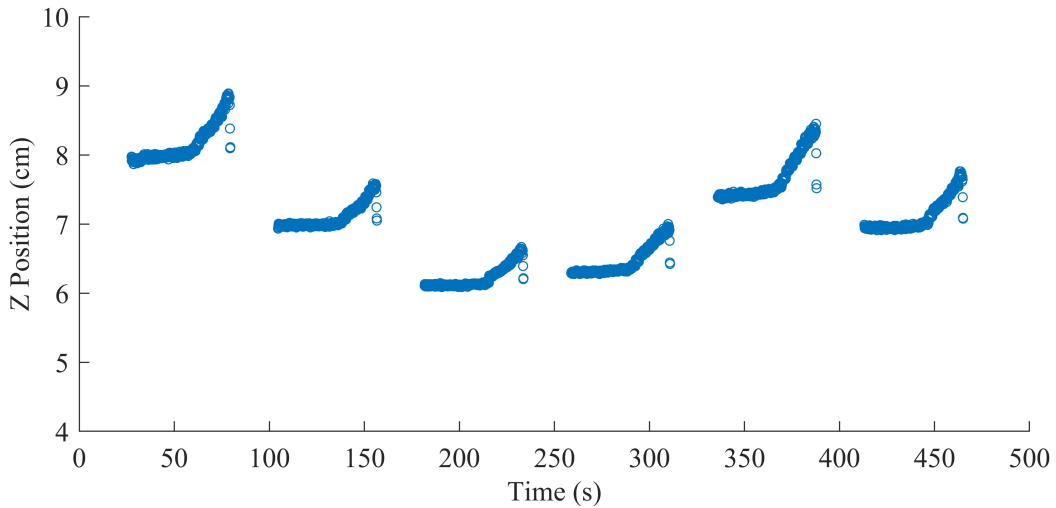


Figure 5.26: Source tracking along the Z axis

5.7.3 Discussion

Results from the preliminary source tracking study demonstrate the accuracy expected for pre-treatment quality assurance. Figure 5.23 displays the data output along the length of the catheter. Each dwell position is resolved for all catheters. A source position has also been measured during transit in most cases, as well as two points between catheters illustrating the source's retraction. A clear change in gradient can be seen for all catheters after the first six dwell positions, signifying the change from a 5s to a 2s dwell time. Unlike the clinically used multichannel applicators where each active channel is connected to the afterloader, interstitial catheters are inserted into the 3D printed applicator. These catheters are subject to movement in and out of the applicator leading to a marginal offset of each catheter in the Y direction. Figure 5.24 demonstrates the difference between the measured dwell times and the 5s and 2s dwell times planned. With 17 dwell positions in each catheter, 81% of all dwell positions have been determined within 0.1s and only 1 dwell position with a residual of 0.3s. An average magnitude of the difference is calculated to be (0.1 ± 0.01) s, which is the expected minimum temporal resolution. Additionally, measured dwell times are all below what has been planned since the afterloader corrects for transit dose, and reduces the actual dwell times accordingly. Figure 5.25 displays the difference between programmed step size and what is measured. These measurements compound the uncertainty from two calculated dwell positions. The absolute

value of the difference between the planned and measured step size is averaged to give (0.58 ± 0.04) mm.

The uncertainties calculated for the average magnitude of the residuals are type A, statistical uncertainties, quantifying the precision of the result based on the standard error of the data collected. Type B, systematic uncertainties include the limitation of the HDR afterloader specified to a dwell position accuracy of ± 1 mm, and a dwell time accuracy of ± 0.1 s for example.[97]

Figures 5.21ii demonstrates the sequence of channels the source travels through, from 1 to 6. Noting the different distances each channel is from the MP and the order in which this occurs a qualitative comparison to the output in figure 5.26 can be made. Within catheter 1 the source has its largest Z value, followed by the next two catheters which are below one another. Catheter 3 and 4 have similar depths followed by catheter 5 and 6 which are in their expected configuration. All catheters are 0.5 mm closer to the MP than expected, performing better than the underestimation demonstrated in figure 5.19. It is expected that the Z position stays constant for each catheter. However, in figure 5.26 there is an increase in Z with time after the first 30 mm of the treatment plan. The catheters are within a rigid body and so the increase in Z position is attributed to an under response of the MP987. This effect is occurring for all catheters over the same region of the Magic Plate. A relative decrease in response could occur in a specific region due to the reasons addressed in 5.6.3. Additionally, there exist multiple dead pixels near this region and an interpolation that is not representative of the real response could cause a deviation in the Z direction. Although an inverse square fall off in signal is the dominant interaction, the TG-43 based calculation requires full scattering conditions which are not met, this will be as a source of error which changes as the source steps towards the tip. An increase of 1 cm can be seen in most cases. The measurement was repeated with the same feature present in both acquisitions. A live readout system with source tracking will enable the user to monitor data as it is acquired and determine if suitable results have been taken. Moving the applicator to a different region of the MP987 could produce better results in the Z direction.

5.8 Conclusion

Characterisation of the MP987 has required the development and evaluation of a source tracking methodology and frame processing. The source tracking system has been examined with respect to accuracy when determining dwell time and location. Data that has been output from the MP987 requires processing to enable HDR source tracking. Equalisation, baseline removal and frame averaging take place to minimise variation in response across the MP. Interpolation is required to provide an even pitch and supplement data from dead pixels. Once the frame is processed a source tracking algorithm is implemented to produce dwell times and positions. A centre of mass approach is successfully utilised for the X and Y positions, with a TG-43 based calculation used for the Z direction. Once positions have been calculated every 0.1 s, dwell positions are identified via binning the measurements in a histogram and calculating an average.

Although measurements with a high acquisition frequency can produce a finer temporal resolution, the methodology relies on accurate localisation to accomplish this, making frame averaging a robust solution. It has been established that the MP987 HDR source tracking system can predictably resolve dwell times 0.5s and above, with an accuracy of ± 0.2 s.

Source localisation has been evaluated as a fluctuation of measured positions within each dwell location. This fluctuation has been determined as a function of depth. The measurement of dwell position between 4.5 cm and 10.5 cm has a standard deviation of 1.1 mm to 1.7 mm respectively. Fluctuation in the measured position is below 1.2 mm for 4.5 cm to 6.5 cm and increases beyond this. 9.5 cm produces an unexpected reduction in σ , below the 7.5 cm measurement. This might be attributed to a different region of the MP being used. This experiment will benefit from repetition and ensuring an even response across the MP.

Since an average location is calculated to determine the final dwell position, a time-dependent error in localisation has been determined. An increase in error along the direction of travel is apparent, with a dwell time of 0.5 s producing an uncertainty under 2 mm. The error is below 0.6

mm irrespective of dwell time for the dimensions in which the source's position is relatively constant. Accuracy in the Z direction is determined through a comparison of what is measured and the true depth for a single calibration point. Measurement at 4.5 cm is overestimated, this may be attributed to detector saturation. The end-to-end phantom should be constructed to avoid the source being 4.5 cm or closer to the MP987. At depths further from the 5.5 cm, the calculated distance is less than expected. At a depth of 8.5 cm, the difference between, the expected and measured Z is (1.16 ± 0.1) cm, this discrepancy continues to increase with depth reaching (2.21 ± 0.1) cm at 10.5 cm. Two separate gradients are present for measurements between 4.5 cm to 7.5 cm and 8.5 cm to 10.5 cm. This signifies a possible error in the implementation of the TG-43 formalism, an examination of the calculation will be beneficial. Generally, the response across the MP987 can differ, which has a large impact on localisation in the Z direction. The sensitivity of each AFE regulated segment can change over time. Performing another equalisation will ensure an even response from each segment of the magic plate. Irradiation with a Co-60 source will remove possible dose rate dependence and stabilise response. Both thorough RF shielding of the electronics instead of the aluminium sheets used and adequate cooling will ensure a stable, reproducible response. Improvements that regulate response across the MP will enable accurate localisation in the Z direction.

When tracking in three-dimensional space a consistent representation of the X and Y positions is required at different depths. For depths of 9.5 cm and 10.5 cm, an expected narrowing of the distance between catheters is measured. This occurs due to the projection of the distribution widening when further away. Since both catheters are off-centre, some of the distribution is no longer in the field of view. This results in the centre of mass calculation shifting catheters closer together.

All established methodology has been applied within a preliminary tracking experiment to evaluate its performance using a replica multichannel applicator. An average magnitude of the residual dwell times gives a value of (0.10 ± 0.1) s for the entire plan. This is within the projected 0.2s accuracy. The difference between the planned and delivered step size was also calculated to evaluate localisation accuracy. The absolute value of which is averaged to give (0.58 ± 0.04) mm. This in line with

the accuracy established within the chapter. The Z position relative to other catheters within the applicator is consistent when considering the order of delivery. An increase in Z position is displayed for all catheters in the final 50 mm of the treatment plan. Since this occurs for all catheters when the source is above the same region of the MP, the deviation in the Z position can be attributed to a variation in response across the plate. This could be attributed to multiple dead pixels which exist in that region. If the source is directly above a cluster of dead pixels, interpolation can struggle to supplement this data accurately. The experiment will benefit from repeating measurement above a different region of the MP. Additionally, the multitude of factors previously discussed will contribute to variation in the distribution of counts and cause uncertainty in the Z localisation. Validation of the MP987 for HDR source tracking has been achieved through the preliminary experiment. A complete characterisation has been performed for HDR source tracking with the MP987. A methodology has been developed for end-to-end analysis and the expected temporal and spatial limitations outlined.

Chapter 6

Validation of the End-to-end Verification Phantom

The End-to-end phantom enables testing of a treatment procedure to determine faults that present as a difference between the treatment plan and what is delivered. An end-to-end test can assess the implementation of a new device, software or protocol and its cohesion into the current workflow. This is accomplished through testing data transfer, function and its ultimate impact on the treatment.

The End-to-end phantom requires a component that houses a gynaecological applicator and method for HDR source tracking. The MP987 has been characterised for HDR tracking, providing positional and timing information.

The purpose of this chapter is the validation of the End-to-end phantom to establish and define its use and limitations for vaginal and cervical cases. This will be accomplished via different setups for each treatment type, while undergoing the same sequence of tests. The phantom will undergo construction, imaging, treatment planning and monitoring of the treatment's delivery through source tracking. The system's ability to detect common clinical errors will also be evaluated for both treatment types.

6.1 Validation of the End-to-end Phantom for a Vaginal Brachytherapy Treatment

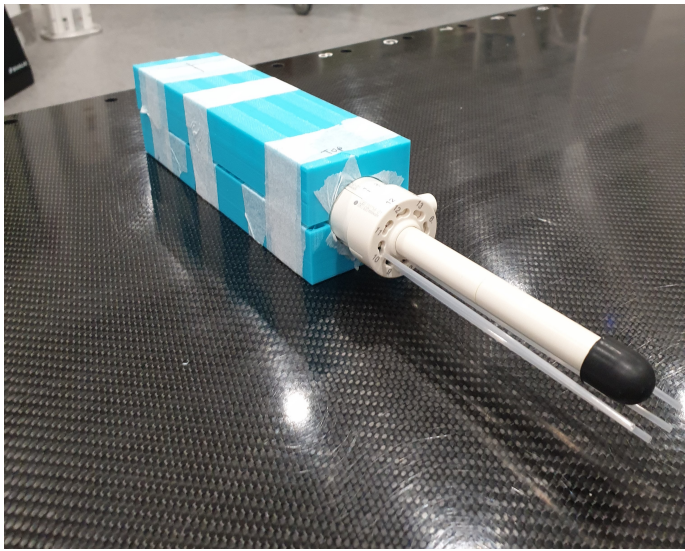
Validation of the end-to-end phantom's use for vaginal brachytherapy is performed through imaging, planning and delivering a clinical treatment plan.

The aims within this section are to:

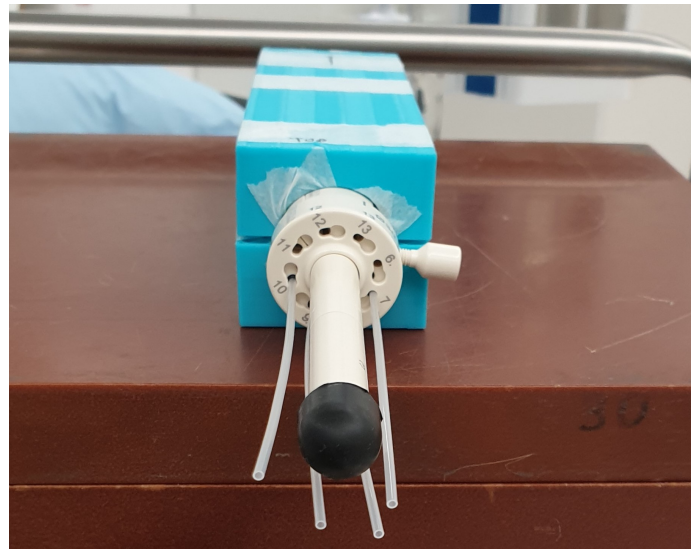
- Evaluate the system's ability to undergo a vaginal brachytherapy workflow and monitor delivery of the treatment, determining dwell times and positions
- Determine if the following common clinical errors can be detected: catheter swap, incorrect indexer length, a miscalibration in activity

6.1.1 Method

Applicator preparation, imaging, treatment planning and treatment delivery are the key aspects within the clinical workflow, and as such, are conducted for the end-to-end test. For treatment of the posterior vaginal wall a 30 mm, multichannel vaginal applicator (MVC) is loaded with 4 catheters, as displayed in figure 6.1. The phantom consists of a prepared applicator on a (30 x 30 x 3) cm³ slab of Solid Water. A 3D printed applicator holder has been made to provide the applicator with stability within the setup. The holder has an infill of 10% and no surrounding backscatter material is used for the measurement. Full scattering conditions are not necessary since the end-to-end phantom's function is source tracking based and does not calculate dosimetry.



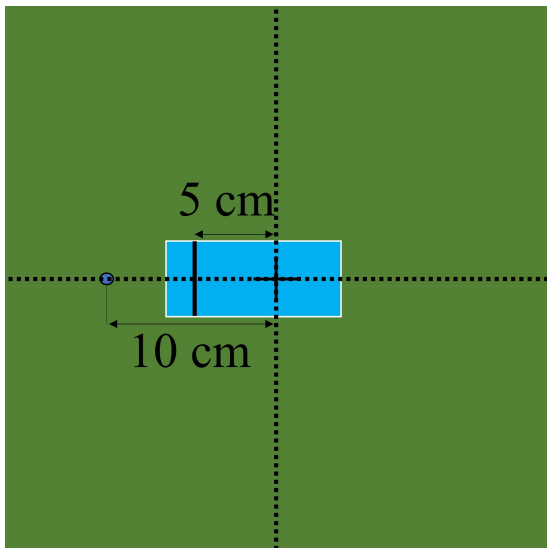
(i) 3D printed applicator holder to allow a stable, reproducible experimental setup.



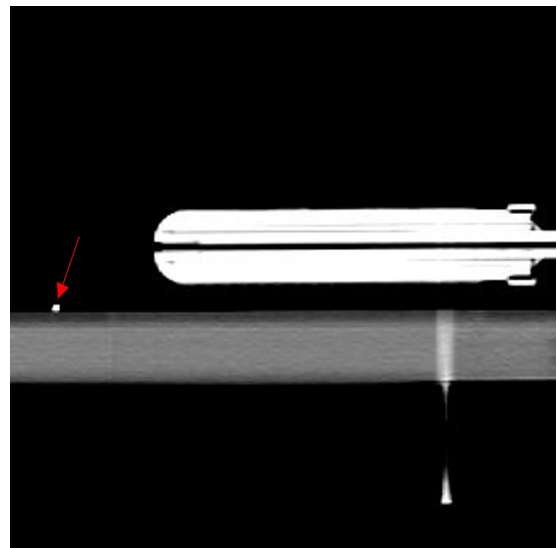
(ii) Multichannel vaginal applicator posteriorly loaded with four catheters.

Figure 6.1: Prepared applicator for end-to-end test.

The applicator is positioned as demonstrated in figure 6.2i, with its superior tip lined up to be 5 cm left of the Solid Water's centre. The applicator's position is marked with a pencil to minimise the effect of applicator displacement between imaging and planning. A ball bearing is placed 10 cm left of the middle of the plate. The ball bearing serves as a reference point to co-register the coordinate systems of the TPS and MP987.



(i) Position of applicator and reference point



(ii) Red arrow shows reference point for co-registration with TPS. Applicator visualised to the right, a large central channel can be seen but will not be used for this treatment.

Figure 6.2: MVC end-to-end phantom

A CT is taken under treatment parameters, with a 2 mm slice thickness. A reconstructed image of the CT is shown in figure 6.2ii, where the applicator and reference point is visible. The CT is imported into the Oncentra Brachytherapy treatment planning system (Elekta, Stockholm, Sweden). Within the TPS, an MVC applicator model is selected from a library. The virtual model of the applicator is aligned with the CT data to allow a reconstruction of the channel positions. The model is aligned using three anchor points, followed by slight rotations to ensure the channels are aligned within orthogonal views. A PTV is then drawn posteriorly as shown in figure 6.3, to simulate the appropriate vaginal wall therapy. The volume is 80 mm along the Superior-Inferior axis. 800 cGy is prescribed to the volume and optimisation is performed to give dwell positions and times.

The ball bearing shown in figure 6.2ii is saved as a point of interest to obtain its coordinates in the TPS reference frame. A co-registration will be done between the MP reference frame and the TPS as the reference point's coordinates are known in both spaces.

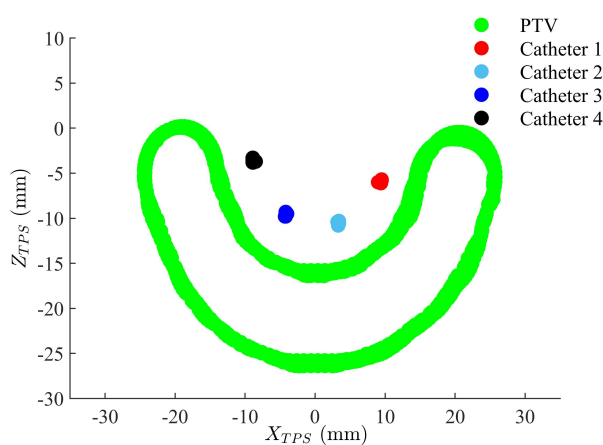


Figure 6.3: PTV drawn for vaginal wall treatment and reconstructed channels shown in the TPS co-ordinate system.

The middle of the phantom and the MP987 are aligned. The applicator's catheters are connected to the appropriate transfer tube and the treatment is delivered. The MP acquires data before and during delivery of the treatment to allow for a baseline to be measured.

Simulating clinical errors requires a slight variation at the treatment planning or delivery stage of the method. These variations are stated below for the appropriate error.

- Catheter Swap: Before delivering the treatment, the transfer tubes are swapped between catheters 1 and 4. The TPS and afterloader do not have a method of detecting this failure and will result in the incorrect dose delivery.
- Indexer Length Error: Indexer length informs the afterloader of the channel length. Within this error, the indexer length is reduced. Catheter 1 is reduced by 2 mm, catheter 2 by 5 mm and catheter 3 by 10 mm. No indexer length change is implemented for catheter 4. The reduction in indexer length shifts dwells positions along their catheter.
- Activity Miscalibration: During treatment planning, a 5% increase in prescribed dose is implemented, leading to a new treatment plan with a prescription of 840cGy. This simulates an incorrect activity being entered into the TPS or treatment communication console (TCC) when the source is changed.

6.1.2 Results

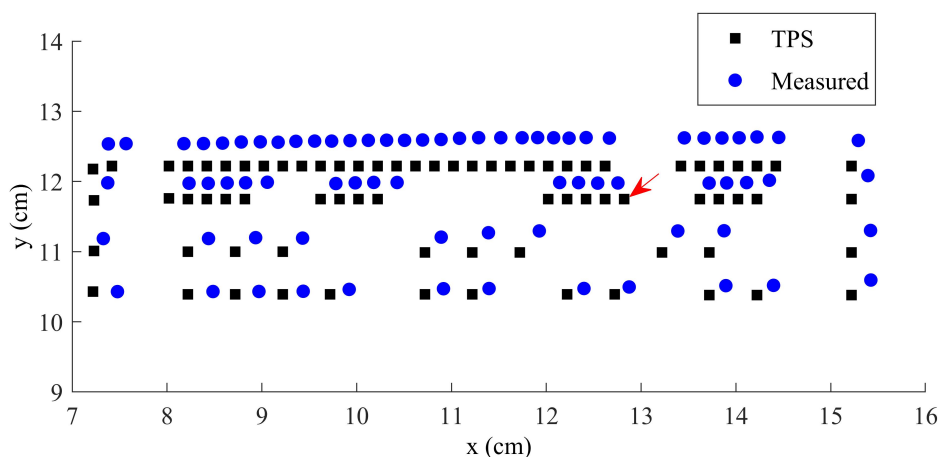


Figure 6.4: Measurement of vaginal treatment plan. Undetected dwell position highlighted by the red arrow.

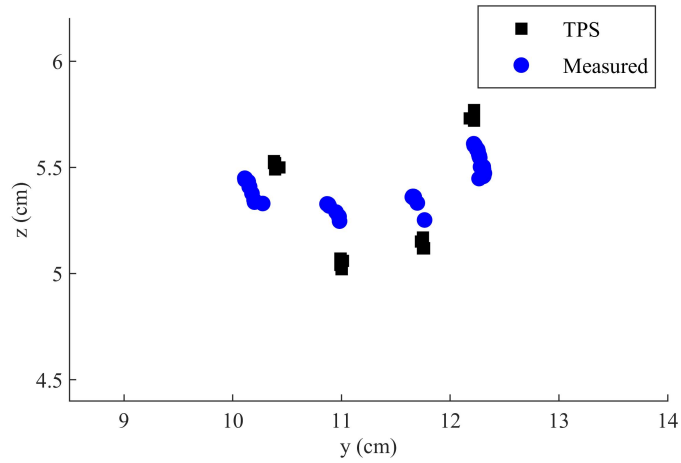


Figure 6.5: A view of the measurement and treatment plan in the Z direction.

The absolute value of the difference between the treatment plan and measurement is averaged for each dimension.

	X (mm)	Y (mm)	Z (mm)	Time (s)
Mean Difference	0.16	0.24	0.20	0.10
Error	0.01	0.01	0.01	0.01

Table 6.1: Mean difference between treatment plan and source tracking

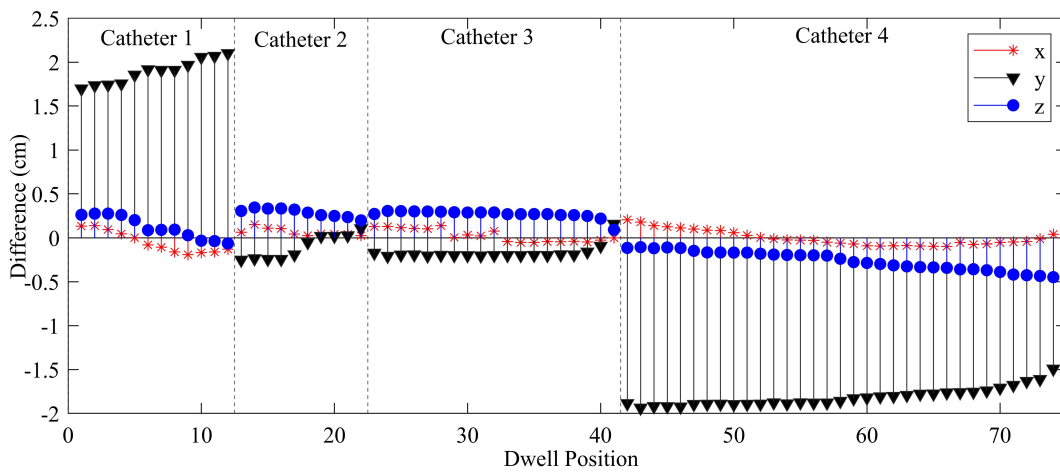


Figure 6.6: Residuals for catheter swap error

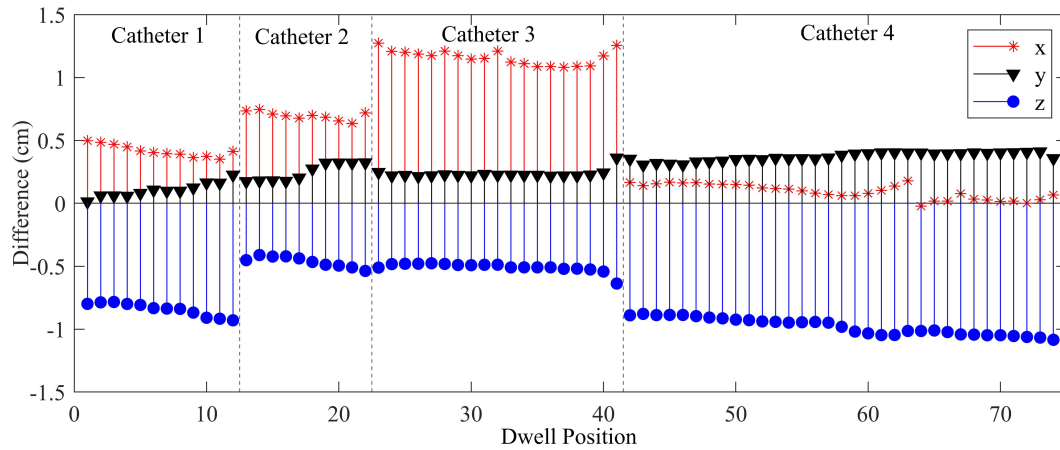


Figure 6.7: Residuals for incorrect indexer lengths

Catheter	X (mm)	Y (mm)	Z (mm)
1	2.13 ± 0.12	0.17 ± 0.04	7.36 ± 1.11
2	5.15 ± 0.37	0.00 ± 0.00	2.11 ± 0.12
3	9.98 ± 0.66	-0.06 ± 0.00	2.94 ± 0.09
4	0.03 ± 0.00	-0.05 ± 0.00	7.62 ± 0.14

Table 6.2: The difference between normal and indexer length error measurements

For the activity error and increase in the average difference in magnitude of dwell time is (0.69 ± 0.08) s, compared to the measured (0.10 ± 0.01) s for the normal plan.

6.1.3 Discussion

The end-to-end phantom successfully monitored a vaginal treatment, with imaging, planning and delivery. Co-registration was performed, however, a setup error in the MVC's alignment when moving from imaging to treatment was apparent. A 1 cm shift was required by the entire dataset along the X-axis. A script is run to find the most common difference between the plan and measurements in the X-Y plane for all points. The same translation is applied to all measured points. Figure 6.4 demonstrates a comparison between the measured data and the TPS. Although this remedied the setup error, removal of an external reference point prevents the source tracking from being a completely independent check. For example, an index error that has shifted all catheters by the same value will not be detected.

One dwell position has gone undetected, declared by the red arrow. The position went undetected as its dwell time was 0.2s, which is too short for the current system to detect. The minimum detected dwell time is established in 5.4.3 is (0.3 ± 0.1) s. Figure 6.5 demonstrates a view of the Z position measured compared to the TPS. A flatter distribution of dwell positions can be seen compared to the treatment plan which exists at various depths. The low gradient seen in section 5.6.3, figure 5.19, where there is a flatness in output for depths 4.5 cm to 7.5 cm. The issues within localisation in the Z direction have been outlined in 5.6.3. Despite this, table 6.1 demonstrates localisation in all directions are well above the expected accuracy. A mean difference in dwell time is (0.10 ± 0.1) s for the treatment plan, which is very accurate considering the afterloader's reduction in dwell time for transit dose. The end-to-end phantom has successfully undergone a clinical workflow that provides validation for its application in vaginal brachytherapy.

A repeated evaluation of the system's capabilities within this setting will be accomplished while testing its ability to detect common clinical errors. A catheter swap error occurs when the incorrect transfer tube is connected to a catheter and thus all dwell positions and times are swapped. Since catheters 1 and 4 have a similar z value, the major difference in position between the two catheters exists in the Y direction. Figure 6.6 demonstrates the discrepancy between dwell positions in the treatment plan and what has been measured. The catheter swap error is displayed in figure 6.6, where a positive displacement in the y-direction for catheter one is seen. Correspondingly, a negative displacement in the y-direction is demonstrated for catheter 4. This clearly, indicates a swap in catheter position of catheter 1 and 4. The mean residual for dwell times should be unaffected for this treatment plan and as such produces a result of (0.08 ± 0.01) s.

The detection of an indexer length error has been tested. Each applicator channel has a specified indexer length, entering the incorrect indexer length shifted the dwell positions along the path of the channel. Figure 6.7 compares measurement of the indexer length error to the original treatment plan. Since the rounded tip of the MVC is facing the negative x-direction, reducing the endpoint of each channel should see an increase in residuals corresponds with the indexer length error. The

implement 2 mm, 5 mm, 10 mm and 0 mm reduction in indexer length for channels 1 to 4 respectively is displayed in figure 6.7. An indexer error for each catheter can be detected. Table 6.2, is the difference between the measured normal plan and indexer length error for each catheter. A comparison between measurements demonstrates each catheter shift relative to a baseline measurement. Each implemented shift has been determined within the calculated error. For localisation in the Z direction, a large discrepancy is apparent for both comparisons against the TPS and the error-free measurement. This variation in Z position is not a result of the indexer length error as catheter 4 did not undergo a change in length. Inconsistencies in the Z localisation can vary with time, an under-response of the MP has caused a deviation of less than 1 cm. The dwell times for this plan have remained the same and has produced a mean magnitude of discrepancy of (0.09 ± 0.01) s.

To simulate the incorrect activity being entered into either the TPS or TCC during calibration, dwell times are increased through an increase in prescription. The mean difference in dwell time has been calculated to be (0.69 ± 0.08) s, signifying an activity error has this is larger than the maximum discrepancy of (0.10 ± 0.1) s previously measured.

Comparing the treatment plan made to simulate the activity error with the error-free treatment plan gives the expected mean discrepancy. The expected change in dwell time is 0.61s which is within error for what is calculated.

The end-to-end phantom has successfully undergone a clinical workflow and monitored treatment delivery within the expected accuracy. Catheter swap, indexer length and activity miscalibration errors were successfully detected. The end-to-end phantom is proficient in its application for vaginal brachytherapy with well-defined limitations.

6.2 Validation of the End-to-end Phantom for a Cervical Brachytherapy Treatment

The end-to-end phantom is evaluated for multiple treatment types to determine its performance in different clinical applications. To validate the end-to-end phantom's function for cervical brachytherapy treatment a Fletcher applicator was used, enabling imaging, planning and monitoring the treatment's delivery.

Similar to the previous section, the aims are to:

- Evaluate the system's ability to undergo a cervical brachytherapy workflow and monitor the delivery of the treatment by determining dwell times and positions
- Determine if a miscalibration in activity can be detected

6.2.1 Method

Validation of the End-to-end Phantom for cervical brachytherapy presents unique challenges given the difference in channel shape and length as demonstrated in figure 6.8. Once the phantom was constructed, an end-to-end test was performed via imaging, treatment planning and monitoring of treatment delivery.

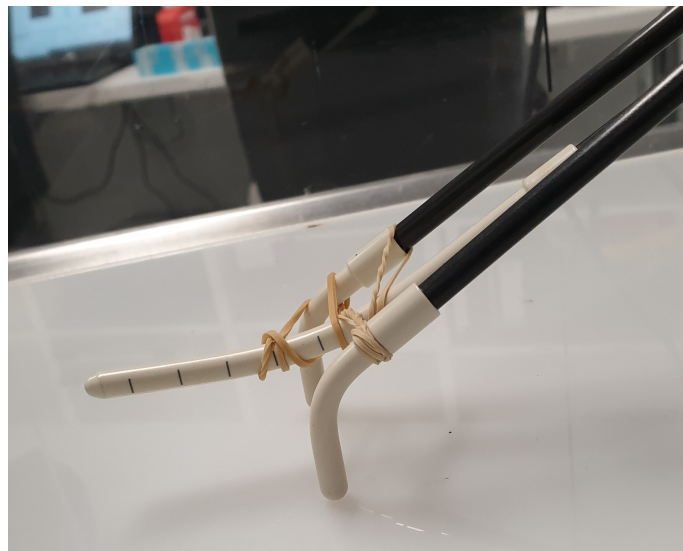


Figure 6.8: Ovoid and tandem channels.

A Fletcher applicator was assembled and firmly held in place within a water tank. Once the phantom was constructed, an end-to-end test was performed. The tandem and two ovoid channels are assembled and rigidly fastened together with additional rubber bands. Thermoplastic was heated in a basin and wrapped around the applicator and ring clamp as demonstrated in figure 6.9. Once the plastic cools, it hardens, forming an applicator specific holder.

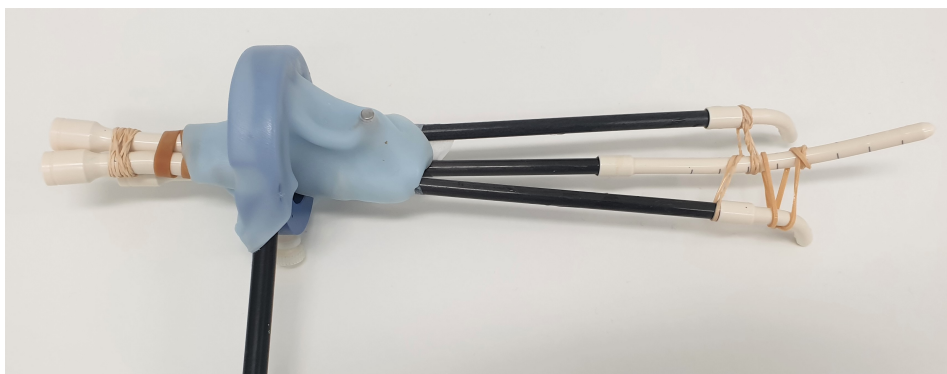


Figure 6.9: Fletcher applicator constructed and attached to ring-clamp with thermoplastic.

The coupled applicator and clamp was fixed to an adjustable bracket within the water tank to give the required phantom displayed in figure 6.10. A ball bearing was stuck to the middle of the 415 mm wide water tank, and at a height of 145 mm from the base. The phantom was CT scanned with treatment parameters, including a 2 mm slice thickness.

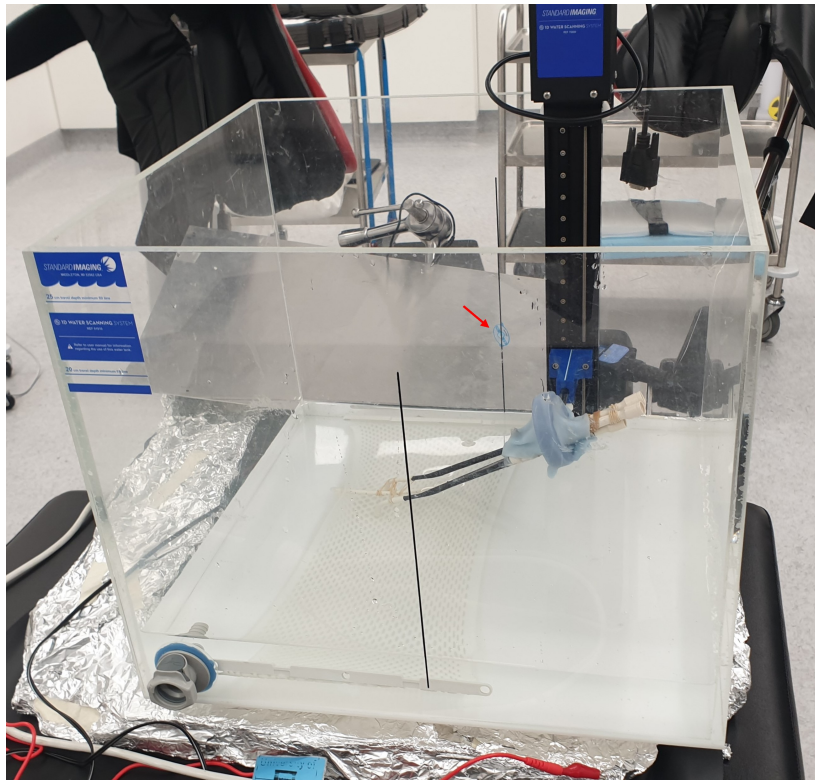


Figure 6.10: The End-to-end phantom, with fletcher applicator positioned in the water tank. The red arrow demonstrates a ball bearing, which is used for co-registration.

When treatment planning the channels are reconstructed by noting their position in each transverse slice. Fine adjustments are then made through altering the channel position in a sagittal view. Point A and B prescription was used for the treatment plan. As described in the section 2.2, point A describes a point of interest that is 2 cm superior and 2 cm lateral from the external os of the cervix. In this case, the cervical os was taken to be the stopper of the applicator. Point B exists at the same position superiorly but is 3 cm lateral from point A. These points of interest are generated on the right and left side as displayed in figure 6.11.[30]

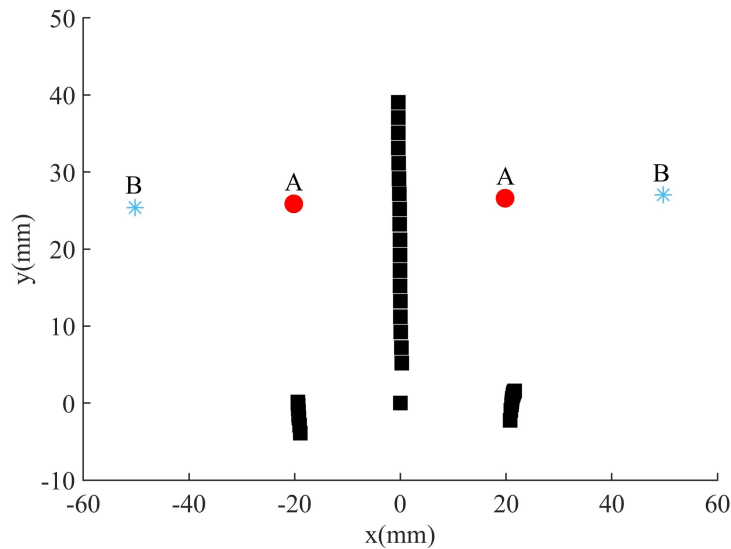


Figure 6.11: Cervical point-based treatment plan

An 800 cGy, point A prescription was implemented. Ultimately this generates a treatment plan which has a 2 mm step size, with dwell times ranging from 6.9s to 17.3s. The active length of each ovoid was 1.8 cm and 3.4 cm used within the tandem. The ball bearing was saved within the TPS as a reference point. 40 mm of Solid Water was placed on the MP before the water tank to provided space between the tank and electronics around the M987. A corner of the tank was lined up to be co-incident with a corner of the Solid Water to simplify the calculation of the reference point position. Once positioned correctly the water tank was filled with water, up to 5 cm above the applicator. Although full scattering conditions were neglected in the previous experiment, given the use of a water tank within this setup, full scattering conditions were tested. The treatment plan was delivered and monitored. A treatment plan was created to simulate an activity calibration error by increasing the prescribed dose by 5%. This simulates an incorrect activity being entered into the TPS or treatment communication console (TCC) when the source is changed.

6.2.2 Results

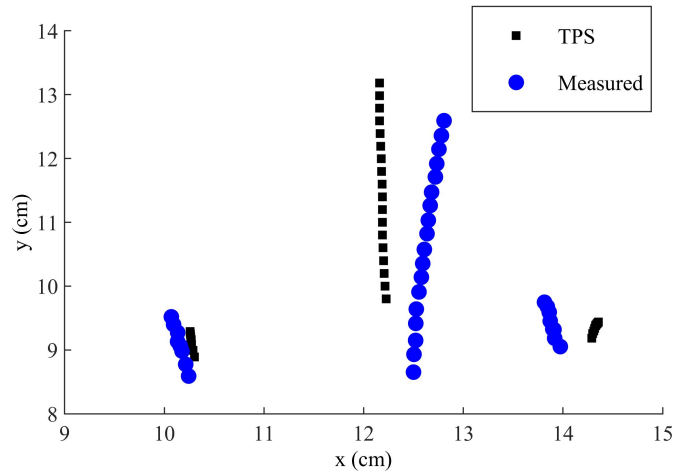


Figure 6.12: Measurement of cervical treatment plan in XY plane

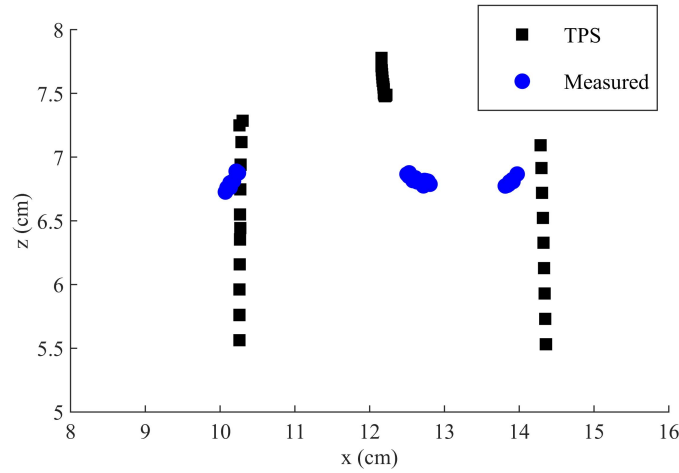


Figure 6.13: Measurement of cervical treatment plan in ZX plane

	X (mm)	Y (mm)	Z (mm)	Time (s)
Mean Difference	3.49	4.74	6.14	0.19
Error	0.57	0.77	1	0.03

Table 6.3: Mean difference between TPS and measured dwell positions

For the activity error and increase in the average difference in magnitude of dwell time was (0.53 ± 0.08) s, compared to the measured (0.19 ± 0.03) s for the error-free plan.

	X (mm)	Y (mm)	Z (mm)
Mean Difference	3.73	3.91	6.24
Error	0.61	0.63	1.01

Table 6.4: Mean difference between TPS and measured position for activity miscalibration.

6.2.3 Discussion

Validation of the End-to-end Phantom for a cervical brachytherapy treatment has been performed. A co-registration between the TPS and magic plate is imperative in accurately monitoring and evaluating source tracking. Figure 6.10 demonstrates the reference point used. Co-registration was attempted with the measurement of the reference point location taken in space and a point of interest assigned during treatment planning. Despite the known position of the reference point in each frame, the calculated co-registration did not place the two data sets accurately. Shifting the origin within the MP software to a well-defined point in the water tank will allow better co-registration. Further investigation is required and necessary to allow an independent definition of dwell positions. To compare the TPS to the measured dwell positions, an average of the programmed dwell position was shifted to the location of the measured dataset's average position. All TPS dwell positions are translated by the same value.

Figure 6.12 demonstrates both the measured dwell positions and TPS. The ovoid channels show a much larger spread than expected in the y-direction. Dwell position measurement within these channels were poor given the channel shape in figure 6.8. The source steps towards the MP in 2 mm increments, making its change in position in the Y direction less than 1 mm for each step. Since the source tracking methodology relies on determining a difference in position with time, accuracy is low for the ovoid channels. Ideally, the source tracking methodology would utilise the source's change in direction along the Z-axis to localise individual dwell positions. Figure 6.13 demonstrates the expected variation in source position in this direction when viewing the TPS programmed dwell positions. However, when compared to the measured data, the Z position was approximately constant throughout the treatment. A lack of change in calculated dwell position when the source changes depth was present in figure 5.19 and figure 6.5. The reasons for this effect have been established and have a large effect on the cervical treatment given the source's path. Tables 6.3 and 6.4, indicate the mean difference between the treatment plan and measured dwell position. The mean difference

in all directions was larger than expected with the largest discrepancy existing in the Z direction. A comparison has been calculated for both the error-free treatment plan and the activity error since they have the same programmed dwell positions. Localisation error in the X and Y directions can be attributed to poor separation between dwell positions as well as an inaccurate co-registration.

The mean difference in dwell time was (0.19 ± 0.03) s which is within the calculated error for the expected 0.2s accuracy. The activity discrepancy error was detected, producing a significantly larger mean difference of (0.53 ± 0.08) s.

The End-to-end phantom's ability within the application of cervical brachytherapy has been evaluated and clearly defined limits established. The phantom can successfully undergo a complete cervical brachytherapy treatment workflow. Improvements in source localisation in the Z direction and co-registration methodology will allow significant improvements in monitoring treatment delivery.

6.3 Conclusion

This chapter has determined the End-to-end phantom's viability for evaluating clinical treatments and define the system's limitations. A complete clinical workflow has taken place for vaginal and cervical treatments to validate the End-to-end phantom.

The vaginal brachytherapy workflow has been successfully evaluated through imaging, treatment planning and source tracking. Attempted co-registration produced a misalignment of 1 cm in the Y-direction, a virtual correction is implemented where all data points are shifted by the same value. It is important to minimise the phantom's reliance on virtually shifting the dataset, as this will enable the source tracking to be an independent check.

Co-registration was also a point of concern in the cervical case where a virtual shift needed to be applied. Due to the MP origin existing at the bottom left pixel, calculating the exact distance away from this as a reference point can be difficult. This can be improved within the software, through calibration of the origin to a visible location. Similar to the co-registration performed by Smith and colleagues, when source tracking with a flat panel detector, a phantom that has the MP987 and fiducials built into it can provide accurate co-registration.[98]

The vaginal end-to-end study produced both localisation and temporal accuracy which is within the expected accuracies of ± 0.25 mm and ± 0.2 s, established in the previous chapter. The mean discrepancy measured to be within (0.24 ± 0.01) mm, for all dimensions and a mean difference in dwell time of (0.10 ± 0.01) s. The catheter swap, indexer length error and activity miscalibration error have all been detected.

The cervical treatment was successfully conducted, producing well-defined limitations. Uncertainty in co-registration and the inaccuracies experienced in the Z direction were the main sources of discrepancy between the expected and delivered results. Due to the source stepping in the Z direction within the ovoid channels, localisation relied on accuracy in the Z direction. Previous results explored the issues with source tracking along the Z direction. Some of these include inaccurate

equalisation, insufficient RF shielding of the electronics and a possible issue with the implementation of the TG-43 formalism. Using the phantom for applicators which allow the source to travel in the X-Y plane is recommended, such as tandem-ring or Venezia applicators. Dwell time accuracy is within the expected 0.2s with all dwell positions identified and have an associated dwell time. The activity miscalibration error which has led to a 5% increase in delivered dose has been detected. Within the limitations which have been established, a complete end-to-end procedure has been conducted for cervical brachytherapy using the End-to-end phantom.

Validation of the End-to-end phantom has been accomplished for both vaginal and cervical treatments. Each phantom has successfully undergone the complete clinical workflow and limitations within each setup have been established. This end-to-end test has the ability in both cases to identify and distinguish common clinical errors providing source position and timing information. An end-to-end quality assurance method provides a complete view of the workflow. Evaluating data transfer methods, the function of new devices and ultimately assessing the treatment a patient will receive. Source localisation and timing properties can distinguish possible treatment failures and uncertainties. The End-to-end phantom's ability to provide these features of quality assurance have been verified for gynaecological brachytherapy.

Chapter 7

Conclusion

Validation of the End-to-end phantom required the development of an HDR source tracking methodology, of which the optimal processing and acquisition parameters have been determined. The End-to-end phantom was for verification of both vaginal and cervical workflows, undergoing imaging, planning and monitoring of the treatment. End-to-end testing enables full evaluation treatment practices which are vital in maintaining treatment quality and additionally useful when implementing new protocols or devices. The test presents any incongruencies between the treatment plan and what is delivered by testing the function of each component within the treatment procedure and their cohesion.

Complete verification of the End-to-End phantom for gynaecology has been performed and current limitations have been defined. The use of a retrospective treatment planning study provided insight into the importance of protocols that suppress applicator displacement. The study also provided a clinical benchmark concerning source localisation accuracy for cervical brachytherapy. If a patient has had a substantial bladder or rectal dose in previous fractions or from EBRT, the impact of applicator displacement should be considered. Constraints for applicator reconstruction and patient transport can be adjusted. When paired with source tracking, the quantified displacement limit can provide clinical justification for a required localisation source accuracy. [92] As discussed within the outliers section, the study demonstrated a variation in response to applicator displacement due to

differences in anatomy or planned dose to OARs. This will make it difficult to set a single “source tracking error threshold” for all patients.

Ultimately, the study demonstrates a 2 mm limitation in source localisation accuracy to protect from a clinical error. Shifts in the Right-Left directions exclusively have an impact on HR-CTV coverage. A 4 mm limit in all directions will ensure local control does not reduce critically. The study successfully determines a critical applicator displacement value.

Validation of the End-to-end phantom for cervical brachytherapy treatment demonstrated a mean difference of (3.49 ± 0.57) mm, (4.74 ± 0.77) mm, (6.14 ± 1) mm in the X, Y and Z directions respectively. Considering the tandem’s position through the cervix and into the uterus, the Z-direction axis can be considered analogous to the anterior-posterior axis. The mean difference in the TPS and measured dwell positions in the Z direction are above the 2 mm established limit. The improvements discussed for localisation in the Z direction are pivotal for end-to-end testing of the cervical brachytherapy treatment procedure. For the Right-Left and Superior-Inferior axes, the measured discrepancy in the X and Y direction is within the calculated error of the critical applicator displacement in that axis. However, given the characterisation experiments, with improvements to the co-registration and Z localisation method, localisation accuracy could be within 2 mm in each direction. Despite the localisation accuracy in the Z direction being less than clinically necessary, the End-to-end phantom still produced accurate timing information, with a mean difference of (0.19 ± 0.03) s.

Multiple end-to-end systems have been developed, most of which differ substantially due to the choice of dosimetry used. Film and ion chambers have been used for end-to-end testing of gynaecological procedures.[85][86][99] Both methods are time-consuming and do not provide the same timing information as the End-to-end phantom. Comparable results have been accomplished with the use of an imaging panel, with a standard deviation in a position of 0.2 mm in the X and Y directions and 1.6 mm in the Z direction. The MP produced an accuracy of 0.25 mm for similar dwell times and a larger variation in Z. The EPID produces an accuracy of 0.2 s with the MP987 capable of a 0.1s

accuracy. Localisation in the Z direction with the use of an imaging panel was far more accurate and enabled a measurement distance of 22 cm. The imaging panel however requires extensive calibration. Additionally, a robotic arm has been used to position the EPID panel, which will require a large financial investment and has not been tested for cervical treatments.[78] Overall, the MP987 based End-to-end phantom has produced a simple solution for end-to-end verification of gynaecological treatments.

A source tracking methodology has been outlined and tested during the characterisation of the MP987 for HDR source tracking. The optimal processing parameters and required operations have been outlined. This has been used to enable source tracking for the End-to-end phantom. Utilising these parameters to produce an online processing application will enable quick pre-treatment verification and eventually in vivo source tracking. The larger MP987 has allowed development ahead of the MP121, enabling source tracking at larger distances.[77] This allowed the creation of the End-to-end phantom which can test multiple applicator types.

End-to-end testing of a vaginal treatment workflow has been accomplished with submillimetre accuracy and mean difference of (0.10 ± 0.01) s in dwell time. Both vaginal and cervical treatment validations resulted in the detection of the implemented errors. Improvements in co-registration techniques, equalisation and shielding of the detector will enable a uniform response and provide an increase in accuracy in the Z direction. Additionally, the phantom could benefit from the exploration of a new methodology to determine the Z position.

The uncertainties calculated within this chapter are measures of statistical precision of the system, determined by the standard error. The error values listed are not the absolute error in position or time. Systematic uncertainty such as in the uncertainty in catheter position, catheter reconstruction uncertainty and HDR afterloader accuracy are not included within this calculation.[100] Results have been presented in this fashion since the precision of the system is of interest and not the overall uncertainty in the HDR brachytherapy workflow.

The End-to-end phantom has been developed and characterised for the verification of gynaeco-

logical brachytherapy treatments. The phantom enables quality assurance of the complete workflow, including imaging, treatment planning, data transfer and treatment delivery. Considering the multifaceted nature of image-based HDR brachytherapy, a meticulous evaluation of the complete procedure is required to ensure patient safety.

7.1 Future Work

- The impact of applicator displacement will be evaluated relative to the development of a “robustness factor” parameter. The robustness factor is calculated by determining the weight and distance of each dwell position to an OAR and summing the product of these two values. This will indicate how robust a treatment plan is to displacement. The displacement study data will show if there’s a correlation between the proposed factor and the plan’s sensitivity to displacement. Ideally, minimising this robustness factor will eventually be part of the treatment planning process.
- A refined End-to-end phantom and standardised protocol will enable centres to carry out independent evaluations for system audits and commissioning of new devices. A water tank phantom with attached applicator holders which is rigidly fixed to the MP987 will provide a permanent and easily verified co-registration. Moving the electronics to a housing beneath the MP will also make the entire phantom more compact.
- The MP987 can be used for in vivo source tracking during treatments. Embedding the MP within the treatment couch will allow alignment between the patient anatomy and detector using a C-Arm X-Ray machine. A live view of the source path relative to the anatomy provides HDR treatment monitoring.

Bibliography

- [1] Christine Haie-Meder, Richard Pötter, Erik Van Limbergen, Edith Briot, Marisol De Brabandere, Johannes Dimopoulos, Isabelle Dumas, Taran Paulsen Hellebust, Christian Kirisits, Stefan Lang, et al. Recommendations from gynaecological (gyn) gec-estro working group(i): concepts and terms in 3d image based 3d treatment planning in cervix cancer brachytherapy with emphasis on mri assessment of gtv and ctv. *Radiotherapy and oncology*, 74(3):235–245, 2005.
- [2] Ravinder Nath, Lowell L Anderson, Gary Luxton, Keith A Weaver, Jeffrey F Williamson, and Ali S Meigooni. Dosimetry of interstitial brachytherapy sources: recommendations of the aapm radiation therapy committee task group no. 43. *Medical physics*, 22(2):209–234, 1995.
- [3] REP Taylor and DWO Rogers. An egsrc monte carlo-calculated database of tg-43 parameters. *Medical physics*, 35(9):4228–4241, 2008.
- [4] Hsiang-Chi Kuo, Keyur J Mehta, Ravindra Yaparpalvi, Linda Hong, Dinesh Mynampati, Wolfgang A Tomé, and Shalom Kalnicki. Feasibility study and optimum loading pattern of a multi-ring inflatable intravaginal applicator. *Journal of contemporary brachytherapy*, 5(2):93, 2013.
- [5] Ervin B Podgoršak et al. *Radiation physics for medical physicists*, volume 1. Springer, 2006.
- [6] Elekta Team. Brachytherapy gynecology. *Elekta AB*, 2019.
<https://www.elekta.com/brachytherapy/gynecology/>.

- [7] Gynaecological-cancer.canceraustralia.gov.au. Gynaecological cancer statistics gynaecological cancers. [https://gynaecological cancer.canceraustralia.gov.au/statistics](https://gynaecological-cancer.canceraustralia.gov.au/statistics).
- [8] M. Kamrava and R. Banerjee. "brachytherapy in the treatment of cervical cancer: a review". page 555.
- [9] Jyoti Mayadev, Sonja Dieterich, Rick Harse, Susan Lentz, Mathew Mathai, Sunita Boddu, Marianne Kern, Jean Courquin, and Robin L Stern. A failure modes and effects analysis study for gynecologic high-dose-rate brachytherapy. *Brachytherapy*, 14(6):866–875, 2015.
- [10] A Espinoza, Marco Petasecca, Iolanda Fuduli, Andrew Howie, J Bucci, Stephanie Corde, Michael Jackson, Michael LF Lerch, and Anatoly B Rosenfeld. The evaluation of a 2d diode array in magic phantom for use in high dose rate brachytherapy pretreatment quality assurance. *Medical physics*, 42(2):663–673, 2015.
- [11] Neerja Bhatla, Jonathan S Berek, Mauricio Cuello Fredes, Lynette A Denny, Seija Grenman, Kanishka Karunaratne, Sean T Kehoe, Ikuo Konishi, Alexander B Olawaiye, Jaime Prat, et al. Revised figo staging for carcinoma of the cervix uteri. *International Journal of Gynecology & Obstetrics*, 145(1):129–135, 2019.
- [12] Pedro T Ramirez, Michael Frumovitz, and Nadeem R Abu-Rustum. *Principles of Gynecologic Oncology Surgery E-Book*. Elsevier Health Sciences, 2018.
- [13] Roland T Skeel and Samir N Khleif. *Handbook of Cancer Chemotherapy*. Lippincott Williams & Wilkins, 2011.
- [14] Myrna Candelaria, Alicia Garcia-Arias, Lucely Cetina, and Alfonso Dueñas-Gonzalez. Radiosensitizers in cervical cancer. cisplatin and beyond. *Radiation Oncology*, 1(1):15, 2006.
- [15] Trevor J McMillan, Simon Tobi, Santiago Mateos, and Catherine Lemon. The use of dna

- double-strand break quantification in radiotherapy. *International Journal of Radiation Oncology* Biology* Physics*, 49(2):373–377, 2001.
- [16] CS Sureka and Christina Armpilia. *Radiation Biology For Medical Physicists*. CRC Press, 2017.
- [17] Elzbieta van der Steen-Banasik. Primary brachytherapy as a radical treatment for endometrial carcinoma. *Journal of Contemporary Brachytherapy*, 6(1):106, 2014.
- [18] Alexander Sedlis, Brian N Bundy, Marvin Z Rotman, Samuel S Lentz, Laila I Muderspach, and Richard J Zaino. A randomized trial of pelvic radiation therapy versus no further therapy in selected patients with stage ib carcinoma of the cervix after radical hysterectomy and pelvic lymphadenectomy: A gynecologic oncology group study. *Gynecologic oncology*, 73(2):177–183, 1999.
- [19] D. Gelblum E. Yorke and E. Ford. ”patient safety in external beam radiation therapy”,. 196(4):768–772.
- [20] Devarati Mitra, Remi Nout, Paul J. Catalano, Carien Creutzberg, Nicole Cimbak, Larissa Lee, and Akila N. Viswanathan. Rectal bleeding after radiation therapy for endometrial cancer. *Radiotherapy and Oncology*, 115(2):240–245, 2015.
- [21] Philip Mayles, Alan E Nahum, and Jean-Claude Rosenwald. *Handbook of radiotherapy physics*. Taylor and Francis, 2007.
- [22] Peter Gorayski, Mark Pinkham, and Margot Lehman. Advances in radiotherapy technology for prostate cancer. *What every GP should know*, 44(9):663–667, 2015.
- [23] John Ng, Igor Shuryak, Yanguang Xu, K.S. Clifford Chao, David J. Brenner, and Ryan J. Burri. Predicting the risk of secondary lung malignancies associated with whole-breast radiation therapy. 2019.

- [24] Vivian P. Cosgrove, Ulrich Jahn, Mathias Pfaender, Susanne Bauer, Volker Budach, and Reinhard E. Wurm. Commissioning of a micro multi-leaf collimator and planning system for stereotactic radiosurgery. *Radiotherapy and Oncology*, 50(3):325–335, 1999.
- [25] Richard Pötter, Kari Tanderup, Christian Kirisits, Astrid de Leeuw, Kathrin Kirchheiner, Remi Nout, Li Tee Tan, Christine Haie-Meder, Umesh Mahantshetty, Barbara Segedin, et al. The embrace ii study: The outcome and prospect of two decades of evolution within the gec-estrogyn working group and the embrace studies. *Clinical and translational radiation oncology*, 9:48–60, 2018.
- [26] Mark J. Rivard, Jack L. M. Venselaar, and Luc Beaulieu. The evolution of brachytherapy treatment planning. *Medical Physics*, 36(6Part1):2136–2153, 2009.
- [27] E. Stefano G. Viani, G. Manta and L. de Fendi. "brachytherapy for cervix cancer: low-dose rate or high-dose rate brachytherapy a meta-analysis of clinical trials". 28(2):47.
- [28] Israel Deutsch William M. Burke June Y. Hou Cande V. Ananth Yongmei Huang Alfred I. Neugut Dawn L. Hershman and Jason D. Wright Sonali S. Patankar, Ana I. Tergas. High versus low-dose rate brachytherapy for cervical cancer. page 534?541.
- [29] Meng Welliver, William Yuh, Julia Fielding, Katarzyna Macura, Zhibin Huang, A. Ayan, Floor Backes, Guang Jia, Mariam Moshiri, Jun Zhang, and Nina Mayr. Imaging across the life span: Innovations in imaging and therapy for gynecologic cancer. *Radiographics : a review publication of the Radiological Society of North America, Inc*, 34:1062–1081, 07 2014.
- [30] Gustavo S Montana, Wesley C Fowler, Mahesh A Varia, Leslie A Walton, Yvonne Mack, and Lynn Shemanski. Carcinoma of the cervix, stage iii. results of radiation therapy. *Cancer*, 57(1):148–154, 1986.
- [31] Manish K. Goyal, D.V. Rai, Than S. Kehwar, Jayanand Manjhi, Bret H. Heintz, Kathleen L. Shide, and Jerry L. Barker. Anatomy-based definition of point a utilizing three-dimensional

- volumetric imaging approach for high-dose-rate (hdr) intracavitary brachytherapy dose prescription when treating cervical cancer using limited resources. *Journal of Applied Clinical Medical Physics*, 17(6):69–77, 2016.
- [32] Yasir Bahadur. Using the computed tomography in comparison to the orthogonal radiography based treatment planning in high dose rate (hdr) brachytherapy in cervical uteri cancer patients; a single institution feasibility study. *Journal of the Egyptian National Cancer Institute*, 20(1), 2008.
- [33] Alina Sturdza, Richard Pötter, Lars Ulrik Fokdal, Christine Haie-Meder, Li Tee Tan, Renaud Mazon, Primoz Petric, Barbara Šegedin, Ina Maria Jurgenliemk-Schulz, Christel Nomden, et al. Image guided brachytherapy in locally advanced cervical cancer: Improved pelvic control and survival in retroembrace, a multicenter cohort study. *Radiotherapy and Oncology*, 120(3):428–433, 2016.
- [34] Richard Pötter, Kari Tanderup, Maximilian Paul Schmid, Ina Jürgenliemk-Schulz, Christine Haie-Meder, Lars Ulrik Fokdal, Alina Emiliana Sturdza, Peter Hoskin, Umesh Mahantshetty, Barbara Segedin, et al. Mri-guided adaptive brachytherapy in locally advanced cervical cancer (embrace-i): a multicentre prospective cohort study. *The Lancet Oncology*, 22(4):538–547, 2021.
- [35] Christopher S. Melhus and Mark J. Rivard. Approaches to calculating aapm tg-43 brachytherapy dosimetry parameters for cs-137,i125,ir-192,pd-0103 and yb-169 sources. *Medical Physics*, 33(6Part1):1729–1737, 2006.
- [36] Mark J Rivard, Bert M Coursey, Larry A DeWerd, William F Hanson, M Saiful Huq, Geoffrey S Ibbott, Michael G Mitch, Ravinder Nath, and Jeffrey F Williamson. Update of aapm task group no. 43 report: A revised aapm protocol for brachytherapy dose calculations. *Medical physics*, 31(3):633–674, 2004.

- [37] Ron S Sloboda, Hali Morrison, Brie Cawston-Grant, and Geetha V Menon. A brief look at model-based dose calculation principles, practicalities, and promise. *Journal of contemporary brachytherapy*, 9(1):79, 2017.
- [38] Luc Beaulieu, Åsa Carlsson Tedgren, Jean-François Carrier, Stephen D Davis, Firas Mourtada, Mark J Rivard, Rowan M Thomson, Frank Verhaegen, Todd A Wareing, and Jeffrey F Williamson. Report of the task group 186 on model-based dose calculation methods in brachytherapy beyond the tg-43 formalism: current status and recommendations for clinical implementation. *Medical physics*, 39(10):6208–6236, 2012.
- [39] Dayee Jacob, Melissa Lamberto, Lana Lawrence, and Firas Mourtada. Clinical transition to mbdca from tg 43 formalism for hdr brachytherapy: A retrospective analysis of the treatment of cervix using tandem and ring applicator. *Brachytherapy*, 15:S165–S166, 05 2016.
- [40] Magdalena Bazalova, Jean-Francois Carrier, Luc Beaulieu, and Frank Verhaegen. Dual-energy ct-based material extraction for tissue segmentation in monte carlo dose calculations. *Physics in medicine and biology*, 53:2439–56, 06 2008.
- [41] Justin K Mikell, Ann H Klopp, Michael Price, and Firas Mourtada. Commissioning of a grid-based boltzmann solver for cervical cancer brachytherapy treatment planning with shielded colpostats. *Brachytherapy*, 12(6):645–653, 2013.
- [42] Mourougan Sinnatamby, Sathyanarayana Reddy K Vivekanandan Nagarajan, Gunaseelan Karunanidhi, and Vivekanandam Singhavajala. Dosimetric comparison of acuros bv with aapm tg43 dose calculation formalism in breast interstitial high-dose-rate brachytherapy with the use of metal catheters. *Journal of contemporary brachytherapy*, 7(4):273, 2015.
- [43] Ashley A Weiner and Julie K Schwarz. Intracavitary brachytherapy for gynecologic malignancies: Applications and innovations. *Missouri medicine*, 112(5):366, 2015.

- [44] Ashraf Hassouna, Yasir Abdulaziz Bahadur, and Camelia Constantinescu. Assessment of air pockets in high-dose-rate vaginal cuff brachytherapy using cylindrical applicators. *Journal of contemporary brachytherapy*, 6(3):271, 2014.
- [45] Bhudatt Paliwal and Dinesh Tewatia. Advances in radiation therapy dosimetry. *Journal of Medical Physics/Association of Medical Physicists of India*, 34(3):108, 2009.
- [46] Matthew J. Williams and Peter E. Metcalfe. Radiochromic film dosimetry and its applications in radiotherapy. *4th SSD Summer School: Concepts and Trends in Medical Radiation Dosimetry, Wollongong: AIP.*, pages pp. 75–99, 2019.
- [47] E.B. Podgorsak. *Radiation Oncology Physics: A Handbook for Teachers and Students*.
- [48] C-M Ma, CW Coffey, LA DeWerd, C Liu, R Nath, SM Seltzer, and JP Seuntjens. Aapm protocol for 40–300 kv x-ray beam dosimetry in radiotherapy and radiobiology. *Medical physics*, 28(6):868–893, 2001.
- [49] Sathiyam Saminathan, Henry Finlay Godson, Retna Ponmalar, Ravikumar Manickam, and James Mazarello. Dosimetric evaluation of newly developed well-type ionization chamber for use in the calibration of brachytherapy sources. *Journal of medical physics*, 41(4):234, 2016.
- [50] Sonja Dieterich, Eric Ford, Dan Pavord, and Jing Zeng. Chapter 24 - special procedures. pages 313–326, 2016.
- [51] Daniel Goodwin. Point dose measurements in vmat : an investigation of detector choice and plan complexity. 2017.
- [52] Rodica Alecu and Marius Alecu. In-vivo rectal dose measurements with diodes to avoid misadministrations during intracavitary high dose rate brachytherapy for carcinoma of the cervix. *Medical physics*, 26(5):768–770, 1999.
- [53] Introduction to the mosfet dosimeter, technical note: 4. *Bestmedicalcanada.com*, 2019.

- [54] Céline Bassinet, Christelle Huet, Marion Baumann, Cécile Etard, Jean-Luc Réhel, Gilbert Boisserie, Jacques Debroas, Bernard Aubert, and Isabelle Clairand. Characterization of mosfet detectors for in vivo dosimetry in interventional radiology and for dose reconstruction in case of overexposure. *Health physics*, 104(4):379–384, 2013.
- [55] Christian Kirisits, Mark J Rivard, Dimos Baltas, Facundo Ballester, Marisol De Brabandere, Rob van der Laarse, Yury Niatsetski, Panagiotis Papagiannis, Taran Paulsen Hellebust, Jose Perez-Calatayud, et al. Review of clinical brachytherapy uncertainties: analysis guidelines of gec-estro and the aapm. *Radiotherapy and oncology*, 110(1):199–212, 2014.
- [56] Taran Paulsen Hellebust, Christian Kirisits, Daniel Berger, José Pérez-Calatayud, Marisol De Brabandere, Astrid De Leeuw, Isabelle Dumas, Robert Hudej, Gerry Lowe, Rachel Wills, et al. Recommendations from gynaecological (gyn) gec-estro working group: considerations and pitfalls in commissioning and applicator reconstruction in 3d image-based treatment planning of cervix cancer brachytherapy. *Radiotherapy and Oncology*, 96(2):153–160, 2010.
- [57] Larry A DeWerd, Geoffrey S Ibbott, Ali S Meigooni, Michael G Mitch, Mark J Rivard, Kurt E Stump, Bruce R Thomadsen, and Jack LM Venselaar. A dosimetric uncertainty analysis for photon-emitting brachytherapy sources: Report of aapm task group no. 138 and gec-estro. *Medical physics*, 38(2):782–801, 2011.
- [58] Eric C Ford, Ray Gaudette, Lee Myers, Bruce Vanderver, Lilly Engineer, Richard Zellars, Danny Y Song, John Wong, and Theodore L DeWeese. Evaluation of safety in a radiation oncology setting using failure mode and effects analysis. *International Journal of Radiation Oncology* Biology* Physics*, 74(3):852–858, 2009.
- [59] Richard Pötter, Christine Haie-Meder, Erik Van Limbergen, Isabelle Barillot, Marisol De Brabandere, Johannes Dimopoulos, Isabelle Dumas, Beth Erickson, Stefan Lang, An Nulens, et al. Recommendations from gynaecological (gyn) gec-estro working group (ii): concepts and terms

in 3d image-based treatment planning in cervix cancer brachytherapy 3d dose volume parameters and aspects of 3d image-based anatomy, radiation physics, radiobiology. *Radiotherapy and Oncology*, 78(1):67–77, 2006.

- [60] Joel Poder and May Whitaker. Robustness of ipsa optimized high-dose-rate prostate brachytherapy treatment plans to catheter displacements. *Journal of contemporary brachytherapy*, 8(3):201, 2016.
- [61] Kari Tanderup, Taran Paulsen Hellebust, Stefan Lang, Jørgen Granfeldt, Richard Pötter, Jacob Christian Lindegaard, and Christian Kirisits. Consequences of random and systematic reconstruction uncertainties in 3d image based brachytherapy in cervical cancer. *Radiotherapy and Oncology*, 89(2):156–163, 2008.
- [62] Joshua Schindel, Winson Zhang, Sudershan K Bhatia, Wenqing Sun, and Yusung Kim. Dosimetric impacts of applicator displacements and applicator reconstruction-uncertainties on 3d image-guided brachytherapy for cervical cancer. *Journal of contemporary brachytherapy*, 5(4):250, 2013.
- [63] Ravinder Nath, Lowell L Anderson, Jerome A Meli, Arthur J Olch, Judith Anne Stitt, and Jeffrey F Williamson. Code of practice for brachytherapy physics: report of the aapm radiation therapy committee task group no. 56. *Medical physics*, 24(10):1557–1598, 1997.
- [64] Daniel A Low, William B Harms, Sasa Mutic, and James A Purdy. A technique for the quantitative evaluation of dose distributions. *Medical physics*, 25(5):656–661, 1998.
- [65] Heng Li, Lei Dong, Lifei Zhang, James N. Yang, Michael T. Gillin, and X. Ronald Zhu. Toward a better understanding of the gamma index: Investigation of parameters with a surface-based distance method. *Medical Physics*, 38(12):6730–6741, 2011.
- [66] Takashi Hanada, H Kojima, M Ishigami, S Katsuta, A Yorozu, T Otsuka, and K Maruyama.

Availability of a tool using ccd camera-plastic scintillator system in hdr for quality assurance. 2:1443–1446, 2007.

- [67] Halil KÜÇÜCÜK, Öznur ŞENKESEN, and Evren Ozan GÖKSEL. Quality assurance in brachytherapy. *TURKISH JOURNAL OF ONCOLOGY*, 34(1).
- [68] I. Gerardy, J. R?denas, M. van Dycke, S. Gallardo, and Elisa Ceccolini. Dosimetric characterization of a brachytherapy applicator using mcnp5 modelisation and in-phantom measurements. *Applied Radiation and Isotopes*, 68(4-5):735–737, 2010.
- [69] Grzegorz Zwierzchowski, Grzegorz Bielecki, Janusz Skowronek, and Magdalena Mazur. Film based verification of calculation algorithms used for brachytherapy planning-getting ready for upcoming challenges of mbdca. *Journal of Contemporary Brachytherapy*, 8(4):326, 2016.
- [70] T Nakano, N Suchowerska, MM Bilek, DR McKenzie, N Ng, and T Kron. High dose-rate brachytherapy source localization: positional resolution using a diamond detector. *Physics in Medicine & Biology*, 48(14):2133, 2003.
- [71] T Nakano, N Suchowerska, DR McKenzie, and MM Bilek. Real-time verification of hdr brachytherapy source location: implementation of detector redundancy. *Physics in Medicine & Biology*, 50(2):319, 2005.
- [72] P Guiral, J Ribouton, P Jalade, R Wang, J-M Galvan, G-N Lu, P Pittet, A Rivoire, and L Gindraux. Design and testing of a phantom and instrumented gynecological applicator based on gan dosimeter for use in high dose rate brachytherapy quality assurance. *Medical physics*, 43(9):5240–5251, 2016.
- [73] Matej Batič, Janez Burger, Vladimir Cindro, Gregor Kramberger, Igor Mandić, Marko Mikuž, Andrej Studen, and Marko Zavrtanik. A system for localization of high dose rate 192 ir source during brachytherapy treatment with silicon detectors. pages 3794–3800, 2009.

- [74] A Manikandan, Sarkar Biplab, Perianayagam A David, R Holla, TR Vivek, and N Sujatha. Relative dosimetrical verification in high dose rate brachytherapy using two-dimensional detector array imatrixx. *Journal of medical physics/Association of Medical Physicists of India*, 36(3):171, 2011.
- [75] AB Mohamed Yoosuf, Prakash Jeevanandam, Glenn Whitten, Geraldine Workman, and Conor K McGarry. Verification of high-dose-rate brachytherapy treatment planning dose distribution using liquid-filled ionization chamber array. *Journal of contemporary brachytherapy*, 10(2):142, 2018.
- [76] J. H. D. Wong, I. Fuduli, M. Carolan, M. Petasecca, M. L. F. Lerch, V. L. Perevertaylo, P. Metcalfe, and A. B. Rosenfeld. Characterization of a novel two dimensional diode array the magic plate as a radiation detector for radiation therapy treatment. *Medical Physics*, 39(5):2544–2558, 2012.
- [77] A Espinoza, B Beeksmma, Marco Petasecca, I Fuduli, C Porumb, D Cutajar, S Corde, M Jackson, MLF Lerch, and Anatoly B Rosenfeld. The feasibility study and characterization of a two-dimensional diode array in magic phantom for high dose rate brachytherapy quality assurance. *Medical physics*, 40(11):111702, 2013.
- [78] Gabriel P Fonseca, Mark Podesta, Murillo Bellezzo, Michiel R Van den Bosch, Ludy Lutgens, Ben GL Vanneste, Robert Voncken, Evert J Van Limbergen, Brigitte Reniers, and Frank Verhaegen. Online pretreatment verification of high-dose rate brachytherapy using an imaging panel. *Physics in Medicine & Biology*, 62(13):5440, 2017.
- [79] Ziyad A Alrowaili, Michael LF Lerch, Marco Petasecca, Martin G Carolan, Peter E Metcalfe, and Anatoly B Rosenfeld. Beam perturbation characteristics of a 2d transmission silicon diode array, magic plate. *Journal of applied clinical medical physics*, 17(2):85–98, 2016.
- [80] ZA Alrowaili, M Lerch, Marco Petasecca, M Carolan, and A Rosenfeld. Radiation response

and basic dosimetric characterisation of the magic plate. In *Journal of Physics: Conference Series*, volume 777, page 012034. IOP Publishing, 2017.


- [81] AH Aldosari, Marco Petasecca, A Espinoza, Matthew Newall, I Fuduli, C Porumb, Sami Alshaikh, ZA Alrowaili, Michael Weaver, P Metcalfe, et al. A two dimensional silicon detectors array for quality assurance in stereotactic radiotherapy: Magicplate-512. *Medical physics*, 41(9):091707, 2014.
- [82] M Petasecca, MK Newall, JT Booth, M Duncan, AH Aldosari, I Fuduli, AA Espinoza, CS Porumb, S Guatelli, Peter Metcalfe, et al. Magicplate-512: A 2d silicon detector array for quality assurance of stereotactic motion adaptive radiotherapy. *Medical physics*, 42(6Part1):2992–3004, 2015.
- [83] Joel Poder, Dean Cutajar, Susanna Guatelli, Marco Petasecca, Andrew Howie, Joseph Bucci, and Anatoly Rosenfeld. Hdr brachytherapy in vivo source position verification using a 2d diode array: A monte carlo study. *Journal of Applied Clinical Medical Physics*, 19(4):163–172, 2018.
- [84] Joel Poder, Dean Cutajar, Susanna Guatelli, Marco Petasecca, Andrew Howie, Joseph Bucci, Mauro Carrara, and Anatoly Rosenfeld. A monte carlo study on the feasibility of real-time in vivo source tracking during ultrasound based hdr prostate brachytherapy treatments. *Physica Medica*, 59:30–36, 2019.
- [85] Hiroyuki Okamoto, Satoshi Nakamura, Shie Nishioka, Kotaro Iijima, Akihisa Wakita, Yuki-nao Abe, Naoki Tohyama, Shinji Kawamura, Toshiyuki Minemura, and Jun Itami. Independent assessment of source position for gynecological applicator in high-dose-rate brachytherapy. *Journal of Contemporary Brachytherapy*, 5:477–486, 2017.
- [86] Antony L Palmer, Chris Lee, Ailsa J Ratcliffe, David Bradley, and Andrew Nisbet. Design and implementation of a film dosimetry audit tool for comparison of planned and delivered

- dose distributions in high dose rate (hdr) brachytherapy. *Physics in Medicine and Biology*, 58(19):6623–6640, 2013.
- [87] F. Attix C. Constantinou and B. Paliwal. "A solid water phantom material for radiotherapy x-ray and x-ray beam calibrations", volume 9. Medical Physics.
- [88] Fabian Krause, Franziska Riske, Susann Bohn, Marc Delaperriere, Jürgen Dunst, and Frank-André Siebert. End-to-end test for computed tomography-based high-dose-rate brachytherapy. *Journal of contemporary brachytherapy*, 10(6):551, 2018.
- [89] Gabriel P Fonseca, Mark Podesta, Murillo Bellezzo, Michiel R Van den Bosch, Ludy Lutgens, Ben GL Vanneste, Robert Voncken, Evert J Van Limbergen, Brigitte Reniers, and Frank Verhaegen. Online pretreatment verification of high-dose rate brachytherapy using an imaging panel. *Physics in Medicine & Biology*, 62(13):5440, 2017.
- [90] Alireza Nikoofar, Zohreh Hoseinpour, Seied Rabi Mahdavi, Hadi Hasanzadeh, and Mostafa Rezaei Tavirani. High-dose-rate 192ir brachytherapy dose verification: A phantom study. *Iranian journal of cancer prevention*, 8(3), 2015.
- [91] JG Holt. Aapm report no. 41: remote afterloading technology. *MEDICAL PHYSICS-LANCASTER PA-*, 20:1761–1761, 1993.
- [92] Joel Poder, Mauro Carrara, Andrew Howie, Dean Cutajar, Joseph Bucci, and Anatoly Rosenfeld. Derivation of in vivo source tracking error thresholds for trus-based hdr prostate brachytherapy through simulation of source positioning errors. *Brachytherapy*, 18(5):711–719, 2019.
- [93] Anthony A Espinoza. The development of a silicon detector quality assurance system for high dose rate brachytherapy. 2016.

- [94] David Crecraft and Stephen Gergely. *Analog Electronics: circuits, systems and signal processing*. Elsevier, 2002.
- [95] Iolanda Fuduli. Data acquisition systems design for quality assurance in advanced radiation dosimetry. 2016.
- [96] OL Dancewicz, SR Sylvander, TS Markwell, SB Crowe, and JV Trapp. Radiological properties of 3d printed materials in kilovoltage and megavoltage photon beams. *Physica Medica*, 38:111–118, 2017.
- [97] IEC BIPM, ILAC IFCC, IUPAC ISO, and OIML IUPAP. Evaluation of measurement data—guide to the expression of uncertainty in measurement (gum 1995 with minor corrections). *Joint Committee for Guides in Metrology, JCGM*, 100, 2008.
- [98] Ryan L Smith, Annette Haworth, Vanessa Panettieri, Jeremy L Millar, and Rick D Franich. A method for verification of treatment delivery in hdr prostate brachytherapy using a flat panel detector for both imaging and source tracking. *Medical physics*, 43(5):2435–2442, 2016.
- [99] Fabian Krause, Franziska Riske, Susann Bohn, Marc Delaperriere, Jürgen Dunst, and Frank-André Siebert. End-to-end test for computed tomography-based high-dose-rate brachytherapy. *Journal of contemporary brachytherapy*, 10(6):551, 2018.
- [100] Christian Kirisits, Mark J Rivard, Dimos Baltas, Facundo Ballester, Marisol De Brabandere, Rob van der Laarse, Yury Niatsetski, Panagiotis Papagiannis, Taran Paulsen Hellebust, Jose Perez-Calatayud, et al. Review of clinical brachytherapy uncertainties: analysis guidelines of gec-estro and the aapm. *Radiotherapy and oncology*, 110(1):199–212, 2014.

Appendix

Nelune Comprehensive Cancer Centre
Research led excellence in Cancer Care
Department of Radiation Oncology



The Prince of Wales Hospital
High Street Randwick NSW 2031
Sydney, Australia

RADIOTHERAPY CONSENT FORM

Contact details
Tel: (+61 2) 9382 2501
Fax: (+61 2) 9382 2500

I (name).....
DOB MRN.....

Of (address).....
Request radiotherapy to be given to (site).....

My condition and the treatment recommended have been explained to me. Alternative treatments have been discussed with me and I understand the consequences if no treatment is given.

I accept the professional opinion of Dr that radiotherapy is the appropriate treatment for my condition.

I understand that complications may occur with any medical treatment and I accept the possible risks associated with the proposed radiotherapy. The common acute and late side effects have been discussed with me.

I am aware that rarely, radiotherapy may cause severe late effects and/or a second cancer.

I have had the opportunity to ask questions about the radiotherapy and I am satisfied with the information I have received.

I understand that my records may be used for research or medical audit. My personal details will remain confidential.

FOR FEMALES ONLY: I am not pregnant now and have no reason to suspect I am pregnant. I understand if I become pregnant during my treatment, my baby may be harmed.

Signature of Patient	Name	Date
Signature of Doctor	Name	Date
Signature of Guardian/Interpreter	Name	Date

 Health
South Eastern Sydney
Local Health District

A Centre for Multidisciplinary Cancer Treatment and Research
South Eastern Sydney Local Health District

Figure 1: Radiotherapy consent form submitted NRA ethics application for retrospective treatment planning study with anonymised patient data.